# Load-dependent electrophysiological and structural cardiac remodelling studied in ultrathin myocardial slices.

**Samha Alayoubi (M.S.)**

Myocardial Function,

National Heart and Lung Institute,

Imperial College London

A thesis submitted to Imperial College for the degree of Doctor of Philosophy

August 2016

***Dedicated to the soul of my father, Dr. Zohair AlAyoubi.***

## Acknowledgements

First and foremost, praise and thanks goes to God Almighty for his blessings and the ability to complete my research successfully. You give me the power to believe in my passion and pursue my dreams. I could never have done this without the faith I have in you.

I would like to express my deepest gratitude to my supervisor, Professor Cesare Terracciano, for giving me the opportunity to join his laboratory and for his support, excellent guidance and contribution throughout my PhD. Furthermore, I would like to thank Dr Michael Ibrahim for his assistance with the surgical techniques, Dr James Cartledge for his help with the echocardiography and Dr Charanjit Singh for his help with imaging.

Very special thanks also goes to my best friend Dr Priyanthi Dias for her generous help with the western blotting, the final write up and for her constant support, friendship and help in making my stay in and outside of the lab an enjoyable experience. As well as this, I would like to thank all my colleagues in the lab for their help and support, and for being there when need. Therefore, making my time in the lab very enjoyable.

Additionally, I would like to thank Professor Nicholas Peters group for their help during my PhD, including Dr Junaid Zaman for supplying the SHR animals, Sayed Al-Aidarous for helping me with SHR experiments, and Mrs Paravina Patel and Dr Rasheda Chowdhury for their technical help.

I am also very grateful to King Saud University and their King Fahad Cardiac Centre for funding my PhD. I am also grateful to Professor Ahmed Alsaddique for his help and guidance during my PhD and I would like to specially thank the NHLI, particularly Dr Emma Watson.

You believed in me and without your support and understanding, I could not have finished my PhD.

I would like to dedicate this thesis exclusively to the soul of my father, Dr. Zohair, who I unfortunately lost quite recently. He was the person who encouraged me to be my best, to have high expectations and to fight for what I believe in. Daddy, you were waiting for this day to come but sadly you left us before. Only now, I know you are happy in your grave with my accomplishment.

Big thanks and love goes to my mom, without her love, continual prayers, confidence, willingness to look after my son when needed and her love for me, I would have not been able to complete this PhD. She shares in my success and this thesis is as much hers as it is mine. I must also thank my family, in particular my soul mate and sister Fakher and my brother Dr. Majed, for their support and love during my PhD.

Most of all, thanks to my husband Rakan for his constant encouragement, patience and being there when I needed him, especially during my write up. To my lovely boy, Talal: You are the best thing in my life! You were my constant inspiration and motivation. Thanks for tolerating mama being away from you.

Last but not least, to my sister and friend Dr. Felwah Al-Zaid, who I met during the hardest period of my PhD – the final write up. Without her, I could not have coped during this hard time. Thanks for being always there for me and listening to my many complaints. You always believed in me and you were sure that I could do it.

## Declaration of Originality

All the work in this thesis is my own work unless stated otherwise clearly within the text. All other externally utilised material has been referenced.

## Copyright Declaration

# Abstract

Introduction: Myocardial slices are becoming an established system to study cardiac electrophysiology and pharmacological research and development. Unlike other preparations, cardiac slices are a multicellular preparation that has an intermediate, adequate complexity required for this research. Previous studies have successfully obtained slices from human biopsies and animal models, where the electrical and structural parameters could be maintained for several hours – a process which is comparable to other preparation types. Therefore, we aimed to use left ventricular myocardial slices obtained from rat models of mechanical unloading (HAHLT) and from two models of overload (TAC and SHR), to investigate electrophysiological and structural alterations in these models.

Methods: Mechanical unloading was achieved by heterotopic abdominal heart and lung transplantation (HAHLT, 8 weeks) and overload was induced by thoracic aortic constriction (TAC, 10 and 20 weeks) in male Lewis rats. Spontaneous hypertensive rats (SHR) were also used as a second model of overload and were primarily induced by hypertension (3, 12 and 20 months). Brown Norway and Wistar Kyoto rats were used as the control groups for SHR. Myocardial slices from the left ventricle (LV) free wall were cut (300-350 µm thick) tangentially to the epicardial surface using a high-precision slow-advancing Vibratome and were point-stimulated using a multi-electrode array system (MEA), therefore, acquiring field potentials (FPs). Field potential duration (FPD) and conduction velocity (CV) were analysed locally and transmurally across the LV free wall. In addition, FPD heterogeneity within each slice was calculated. For the SHR group, the same slices used for the MEA recording were preserved and used subsequently to measure Cx43, Nav1.5 protein levels and fibrosis.

Results: Slices obtained from normal rat hearts that are chronically unloaded were found to develop atrophy at a whole heart level. They showed an increase in FPD and its heterogeneity with preserved conduction properties when compared to controls.

In TACs, an *in vivo* whole heart function assessment confirmed hypertrophy with no signs of cardiac dysfunction. Slices from TAC rats showed an increase in FPD at both 10 and 20 weeks after banding. FPD heterogeneity was increased at 10 weeks but normalised at 20 weeks. Changes in CV properties were observed in this group, showing a faster CV and longitudinal conduction velocity ($CV_L$) at 10 weeks and no change at 20 weeks. Transverse conduction velocity ($CV_T$) was unchanged in the TAC group.

In SHRs, however, hypertrophy was confirmed and signs of dysfunction in the aged group (20 months) were observed due to the decrease in EF by 18%, especially when compared to the 12 months group. FPD and its heterogeneity was unchanged in SHR when compared to controls. Disease and age-related abnormalities in CV properties were observed in SHR and these were associated with changes in Cx43, Nav1.5 protein level and fibrosis.

Conclusion: Myocardial slices are a suitable multicellular preparation to study electrophysiological remodelling obtained from different rat models of cardiovascular disease. In addition, it was possible to investigate the changes in CV and FPD transmurally in rats using this type of preparation method.

Thus, this study supports the use of this multicellular preparation in understanding the mechanisms of cardiac disease and the testing of new treatments and therapeutic targets.

# Table of contents

# List of figures

# List of tables

# Abbreviations

| | |
|---|---|
| AAO | Abdominal aorta |
| AO | Ascending aorta |
| AP | Action potential |
| APD | Action potential duration |
| AR | Anisotropic ratio |
| AVN | Atrioventricular node |
| BN | Brown Norway |
| CFBs | Cardiac fibroblasts |
| CICR | $Ca^{2+}$ induced $Ca^{2+}$ release |
| CR | Cardiac remodelling |
| $CT_L$ | Longitudinal conduction velocity |
| CV | Conduction velocity |
| $CV_T$ | Transvers conduction velocity |
| Cx43 | Connexin 43 |
| DADs | Delayed afterdepolarizations |
| EADs | Early afterdepolarization |
| EC coupling | Excitation-contraction coupling |
| ECM | Extra cellular matrix |
| EF | Ejection fraction |
| Endo | Endocardium |
| Epi | Epicardium |
| FP | Field potential |
| FPD | Field potential duration |

| | |
|---|---|
| GJ | Gap junction |
| HAHLT | Heterotopic abdominal heart-lung transplantation |
| HF | Heart failure |
| HFpEF | Heart failure with preserved ejection fraction |
| HFrEF | Heart failure with preserved ejection fraction |
| hHTx | Heterotopic heart transplantation |
| $I_{Ca,L}$ | L-type inward $Ca^{2+}$ current |
| $I_{Ca,T}$ | T-type $Ca^{2+}$ current |
| $I_f$ | hyperpolarisation-activated 'funny' current |
| $I_{K1}$ | Inward rectifier current |
| $I_{Kr}$ | Delayed outward rectifying K current,rapid |
| $I_{Ks}$ | Delayed outward rectifying K current,slow |
| $I_{Kur}$ | Delayed outward rectifying K current,ultra rapid |
| $I_{Na}$ | Inward $Na^+$ current |
| $I_{NaL}$ | late $Na^+$ current |
| $I_{to}$ | Transient outward K current |
| IVC | Inferior vena cava |
| $K_{Ach}$ | Acetylcholine-activated channel |
| $K_{ATP}$ | Adenosine-5'-triphosphate (ATP)-sensitive channels |
| LV | Left ventricle |
| LVAD | Left ventricle assist device |
| MEA | Multi electrode array system |
| MMPs | Matrix metalloproteinases |
| Myo | Midmyocardium |
| Nav1.5 | Cardiac sodium channel |

| | |
|---|---|
| NCX | $Na^{+}$-$Ca^{2+}$ exchanger |
| PA | Pulmonary artery |
| PLN | Phospholamban |
| PMCA | Plasma membrane $Ca^{2+}$ ATPase |
| RyR | Ryanodine receptor |
| SAN | Sinoatrial node |
| SCD | Sudden cardiac deaths |
| SDS | Sodium dodecyl sulphate |
| SDSP-AGE | Sodium dodecyl sulphate polyacrylamide gel electrophoresis |
| SERCA2a | Sarco-endoplasmic reticulum $Ca^{2+}$-ATPase |
| SHR | Spontaneous hypertensive rat |
| SR | Sarcoplasmic reticulum |
| TAC | Thoracic aortic constriction |
| TIMP | Tissue inhibitor of metalloproteinases |
| UL | Mechanical unloading group |
| WB | Western blotting |
| WKY | Wistar Kyoto |

# CHAPTER 1. Introduction

## 1.1. Normal electrical properties of the heart

The rate of the heart's electrical activity is regulated by the stimulation of the heart's pacemaker cells which are located in the sinoatrial node (SAN) of the right atrium. The excitation wave stimulates the atria by depolarising adjacent atrial myocytes, having traversed through intercellular gap junctions (GJ). Following this, the resulting activation of the ventricles is caused by the excitation wave travelling through the atrioventricular node (AVN) and the Purkinje fibers which, in turn, depolarises the ventricular myocytes (Amin et al. 2010).

## 1.2. Action potential

The difference of potential (voltage) between the interior and exterior of a cardiac cell, which rises and falls in a consistent manner, is known as the action potential (AP). Hodgkin and Huxley, for instance, were the first to observe AP's in a giant squid axon (Hodgkin & Huxley 1952) and described it as a voltage waveform resulting from numerous currents flowing across the membrane of excited cells (DiFrancesco & Noble 1985). The high conductance for $K^+$ of the $I_{K1}$ channels contributes to the stability of the resting membrane potential (approximately -85 mV) for both the atrial and ventricular myocytes during AP phase 4, the resting phase. The $Na^+$ channels are opened due to the stimulation of electrical impulses from neighbouring cells, allowing an inward $Na^+$ current ($I_{Na}$). This results in Phase 0 depolarisation which is essential for the rapid propagation of a cardiac impulse, known as conduction velocity (CV). Phase 1 (early repolarisation), however, is triggered by the transient outward $K^+$ current ($I_{to}$). The most prolonged and unique phase within excitable cells is labelled as phase 2, depicting an equilibrium between the depolarising L-type inward $Ca^{2+}$ current ($I_{Ca,L}$) and the repolarising delayed outward rectifying currents, $I_{Kur}$, (ultra rapid), $I_{Kr}$,(rapid) and $I_{Ks}$ (slow) (Grant 2009). The contractile machinery 'switches on' when a $Ca^{2+}$

influx occurs and raises the $[Ca^{2+}]i$ to a level where there is enough to bind to the myofilament protein troponin C. The process by which this occurs is known as $Ca^{2+}$ induced $Ca^{2+}$ release (CICR) and arises after membrane depolarisation; $Ca^{2+}$ entry through the L-type $Ca^{2+}$ channels prompts $Ca^{2+}$ release from the sarcoplasmic reticulum (SR) through the ryanodine receptor (RyR) (Bers 2002). During the final repolarisation phase (Phase 3), the L-type $Ca^{2+}$ channels are closed (inactive) due to the preponderance of the delayed outward rectifying currents. The decreasing levels of $[Ca^{2+}]i$ allow $Ca^{2+}$ to dissociate from troponin, resulting in an increased muscle relaxation. This elimination of $Ca^{2+}$ from the cytoplasm is made easier due to the following mechanisms: (1) The sarco-endoplasmic reticulum $Ca^{2+}$ - ATPase (SERCA2a) which forces $Ca^{2+}$ back into the SR; (2) $Na^{+}$-$Ca^{2+}$ exchanger (NCX) which forces $Ca^{2+}$ out of the cell in exchange for importing $Na^{+}$ into the cell at a ratio of 1:3; (3) plasma membrane $Ca^{2+}$ ATPase (PMCA) which eliminates $Ca^{2+}$ from the cell and (4) mitochondrial $Ca^{2+}$ uniport which imports $Ca^{2+}$ into the mitochondria (Bers 2002). Due to the lack of $I_{Na}$ and excitation caused by $Ca^{2+}$, the pace maker action potential upstroke is slow compared to the atrial and ventricular myocytes (Dobrzynski et al. 2007). Hence, the resting membrane potential is more depolarised (-50mV) when compared with those of the atrial and ventricular cells (~-80mV).

Nodal cells undergo periodic oscillations of their membrane potential, resulting in depolarisation, which has the ability to result in repolarisation towards the threshold potential when the next AP is initiated (Mangoni et al. 2006). The SA node's ability to spontaneously and rhythmically self-excite is, therefore, generated by this pacemaker potential. The slow diastolic depolarising current (Verkerk et al. 2007; Herrmann et al. 2007) is thought to be caused by the hyperpolarisation-activated 'funny' current ($I_f$), which activates at the termination of an action potential and deactivates during the upstroke of an action potential (Barbuti et al. 2007; DiFrancesco 2005; Bucchi et al. 2006). Automaticity can also be

triggered by T-type $Ca^{2+}$ channels which are evident in all cardiac tissue with the potential for automaticity, including the sinoatrial node. Figure 1.1 is a schematic diagram showing the ionic currents associated with action potential generation in the ventricle and sinoatrial node.

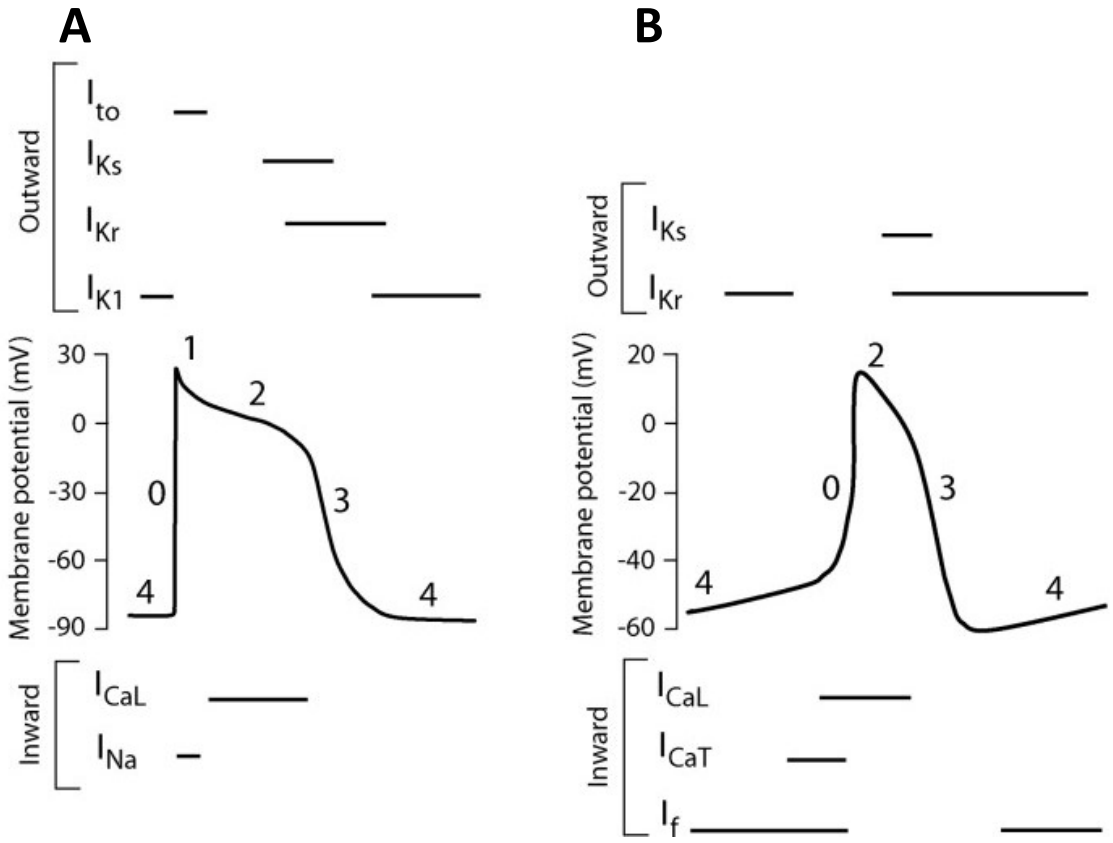


**Figure 1.1: Cardiac Action Potential**

This diagram demonstrates the various membrane currents which generate an action potential. It shows the different phases in the left ventricle A) and in the sinoatrial node B) myocytes. Adapted from (Amin et al. 2010).

## 1.3. Cardiac ion channels

The complex inter-relationship between the cardiac ion channels' two main properties, ion permeability and gating, is what initiates an AP. The movement of specific ions, such as $Na^+$, $K^+$ and $Ca^{2+}$, through their specific ion channels, is known as selective permeability – A process which allows certain molecules or ions to pass through the membrane. The opening and closing of ion channels, known as gating, is governed by three gating mechanisms - voltage dependent, ligand-dependent and mechano-sensitive gating. Most of these voltage gated channels open as a result of depolarisation and are found to be dependent on the divergence of membrane potentials (Grant 2009).

### 1.3.1. Sodium channels

The sodium channels govern cardiac excitability and electrical conduction velocity. Meaning, the influx of $Na^+$ through the $I_{Na}$ produces a substantial increase in membrane potential (depolarisation) and initiates the systolic period in phase 0 of an AP.

As $I_{Na}$ is the major ventricular current in phase 0, $(dV/dt)_{max}$ is used as an index of $I_{Na}$ in ventricular myocytes (King et al. 2013), whereby $(dV/dt)_{max}$ is the maximum rate of AP depolarisation and is directly proportional to the total ionic current across the cell membrane ($I_i$) (Hodgkin & Katz 1949).

The cardiac form of the main protein responsible for $I_{Na}$, $Na_v1.5$, plays a critical role in the production of a cardiac action potential and is encoded by the gene *SCN5A* (Fozzard & Hanck 1996; Yu & Catterall 2003). Four serially linked homologous domains (DI-DIV) folded around an ion-conducting pore form the α-subunit of $Na_v1.5$. As can be seen in Fig 1.2, each domain is made up of six transmembrane segments (S1-S6), with S4 controlling voltage-dependent activation. Most channels are inactive at the end of phase 0 and can only be reactivated after recovering from an inactive period during phase 4. During phases 2 and

3, on the other hand, some channels can remain open or reopen and are characterised by carrying a small late $Na^+$ current ($I_{NaL}$) (Amin et al. 2010). Despite its minor contribution in healthy hearts, $I_{NaL}$ may, as a result, play a major role in cardiovascular disease.

*SCN5A* is co-expressed with β-subunits and can have its gating properties accelerated due to the increase in $I_{Na}$ amplitude. In addition, the expression and/or function of $Na_v1.5$ can be affected or changed through the interaction with a number of regulatory proteins (Meregalli et al. 2005; Morita et al. 2008; Ueda et al. 2008).While the same gene is responsible for the encoding of the heart's $Na_v1.5$ channels, there are functional differences between the channels found in the atria and the ventricles. It has been found that the voltage for half-inactivation of $Na_v1.5$ channels is more negative in the atria compared to the ventricles in canines and guinea pigs, whereas the resting membrane potentials differ between the two regions, which impacts $Na^+$ channel availability and conduction velocity (Burashnikov et al. 2007; Li, Lau & Shrier 2002).

### 1.3.2. Calcium channels

Calcium channels are the primary route of entry for calcium to pass into the cells; a system of intracellular storage, the SR, and transporters such as the NCX, also play a significant role in $[Ca^{2+}]_i$ regulation. The L-type (low threshold type) inward $Ca^{2+}$ current ($I_{Ca,L}$) is also widely responsible for AP plateau, the longest phase in an AP. It is the gene *CACNA1C* which encodes the α-subunit ($Ca_v1.2$) of the L-type channels (Figure 1.2). During β-adrenergic stimulation, the amplitude of $I_{Ca,L}$ increased markedly in the presence of $Ca_vβ2$ β-subunit and the accessory protein $Ca_vα2δ1$. Beside the L-type there is the T-type (transient-type) $Ca^{2+}$ current ($I_{Ca,T}$ ) and is found principally in pacemakers, atrial and Purkinje cells and they found to be less important in exitation-contaction (EC) coupling. It is believed to contribute to the AP formation in pacemaker cells (Nerbonne & Kass 2005).

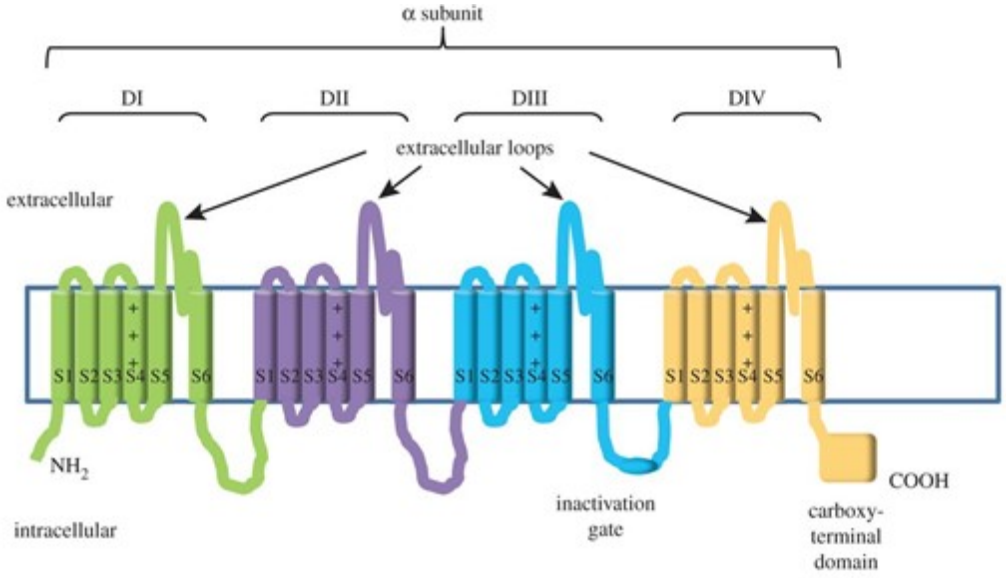


**Figure 1.2: α-subunit of $Na^+$ and $Ca^{2+}$ channels**

Four serially linked homologous domains (DI-DIV) containing six transmembrane segments (S1-S6) make up each α-subunit. S5 and S6 represent the extracellular region in each domain with S4 being the voltage sensor. Modified from (Namadurai et al. 2015).

### 1.3.3. Potassium channels

Cardiac potassium channels are responsible for repolarising excited cells and for reaching the resting membrane potential. As well as this, potassium channels are responsible for determining cardiac action potential morphology and overall duration.

According to the International Union of Pharmacology (Wei et al. 2005; Gutman et al. 2005; Goldstein et al. 2005; Kubo et al. 2005), $K^+$ channels can be classified into four main groups based on the structure of the unit making the (usually) four pore-forming α-subunit, which are: 1) The voltage-gated $K^+$ channels, including the $K_v4.3$, $K_v11.1$and $K_v7.1$ subunit to form channels that mediate the transient outward current ($I_{to1}$), the rapid delayed rectifier current ($I_{Kr}$) and the slow rapid delayed rectifier current ($I_{Ks}$) respectively.

2) The inwardly rectifying $K^+$ channels consist of the strong inwardly rectifying potassium channels ($K_{ir}2.x$) such as inward rectifier current ($I_{K1}$), the G protein–activated inwardly

rectifying potassium channels ($K_{ir}3.x$) such as acetylcholine-activated channels ($K_{Ach}$) and $K_{ir}$ 6.x forming adenosine-5'-triphosphate (ATP)-sensitive channels ($K_{ATP}$).

3) The tow-pore $K^+$ channels($K_{2P}$) which have four transmembrane domains and two pore (P) domains per subunit and are therefore referred to as "tandem" or "twin" pore $K^+$ channels such as TWIK ($K_{2P}1.1$) and TREK ($K_{2P}2.1$).

4) $Ca^{2+}$ activated $K^+$ channels. These channels share similar structure to the voltage-gated $K^+$ channels except for the additional extra transmembrane domain, named S0, which involved in regulation by β subunits. Small conductance $Ca^{2+}$-activated $K^+$ (SK) is an example for this type.

It is the variation in expression levels and the function of each channel which accounts for the regional differences in an action potential's configuration. Such differences may, therefore, be witnessed in the atria, ventricles, across the myocardial wall (endocardium (Endo), midmyocardium (Myo) and the epicardium (Epi)). Furthermore, they account mainly for the variances in AP's between different animal species. $K^+$ channels are also highly regulated and are the basis for the change in action potential configuration in response to the variation of heart rate (Amin et al. 2010; Grant 2009).

### 1.3.3.1. Transient outward $K^+$ current ($I_{to}$)

In large mammals, $I_{to}$ is responsible for the early rapid repolarisation in phase 1 of an AP, which represents a small downward deflection/notch that precedes the plateau phase. $I_{to}$ is the major repolarising current in adult rodents and is often used to explain the very short duration of an AP in support of faster resting heart rates (around 300/600 beats/min). As a result, $I_{to}$ has greater expression within the atria and Purkinje fibers than when compared to elsewhere. The ventricle also has a greater level of $I_{to}$ in the epicardium when compared to the endocardium (MacLeod et al. 2013).

Based on their individual kinetics to recover from inactivation, $Ca^{2+}$- independent $I_{to1}$ is the primary component of $I_{to}$ and has both fast and slow components, $I_{to1,s}$ and $I_{to1,f}$. The α-subunit (Figure1.3, A) of $I_{to1,f}$ are the $K_V4.2$ and $K_V4.3$ channels, encoded by the genes *KCND2* and *KCND3*, respectively; $K_V1.4$ (*KCNA4*), however, is a constitute of $I_{to1,s.}$ (Schmitt et al. 2014; Xu et al. 1999). Several regulatory subunits and pathways have been identified and found to modify the level and biophysical properties of cardiac $I_{to}$ (Wettwer et al. 1993). KChIP2 is one of these regulatory subunits which acts as a chaperone to increase $I_{to1,f}$ expression (An et al. 2000; Kuo et al. 2001) and modulates the inactivation and voltage dependence of the channel (Patel et al. 2002; Patel et al. 2004).

$I_{to1}$ is 4-aminopyridine (4-AP) sensitive. However, more specific blockers can be used to distinguish $I_{to1,f}$ from $I_{to1,s}$. Blocking or reducing $I_{to1}$ can result in notch disappearance by shifting the plateau into the positive range of potential. This will affect the activation, size and time course of the $I_{Ca,L}$ and results in the corresponding changes within CICR and the overall size of contraction (Niwa & Nerbonne 2010).

### 1.3.3.2. Delayed outward $K^+$ rectifying current ($I_K$)

$I_K$ is the major outward current responsible for ventricular repolarisation. There are two major types of $I_K$ ($I_{Kr}$ and $I_{Ks}$) in the heart with different biophysical properties and drug response (Sanguinetti & Jurkiewicz 1990), where the α-subunit (Figure 1.3, A) of $I_{Kr}$ is encoded by *KCNH2* and for $I_{Ks}$ it is encoded by *KCNQ1*. In most mammalian species, $I_{Kr}$ is the main outward $K^+$ current that contributes to repolarisation, whereas $I_{Ks}$ has a relatively small contribution to action potential repolarisation under normal conditions. $I_{Ks}$ importance rises as a "repolarisation reserve" when APD is abnormally prolonged (Cheng & Kodama 2004; Tinker & Harmer 2010). There are noticeable differences in $I_K$ between different species, meaning there are differences in the repolarisation duration and the morphology of an AP. For example, $I_{Kr}$ and $I_{Ks}$ are the major outward currents in humans whereas those two currents

are not prominent repolarising $I_K$ currents in rodents ($I_K$, $I_{Klate}$, and $I_{ss}$ account for repolarisation in rat). The nine to ten times faster heart rate in rodents and the relatively shorter AP is, therefore, an explanation for these differences in the current expression between the two species (Nerbonne & Kass 2005).

### 1.3.3.3. Inward rectifying current ($I_{K1}$)

$I_{K1}$ sets the resting membrane potential of atrial and ventricular cells during phase 4 and contributes to the terminal portion of phase 3 repolarisation. However, $I_{K1}$ is more expressed in the ventricles to protect them from pacemaker activity. Its α-subunit (kir2.1) (Figure 1.3,B) is encoded by *KCNJ2* and consists of one domain with two transmembrane segments (Tamargo et al. 2004).

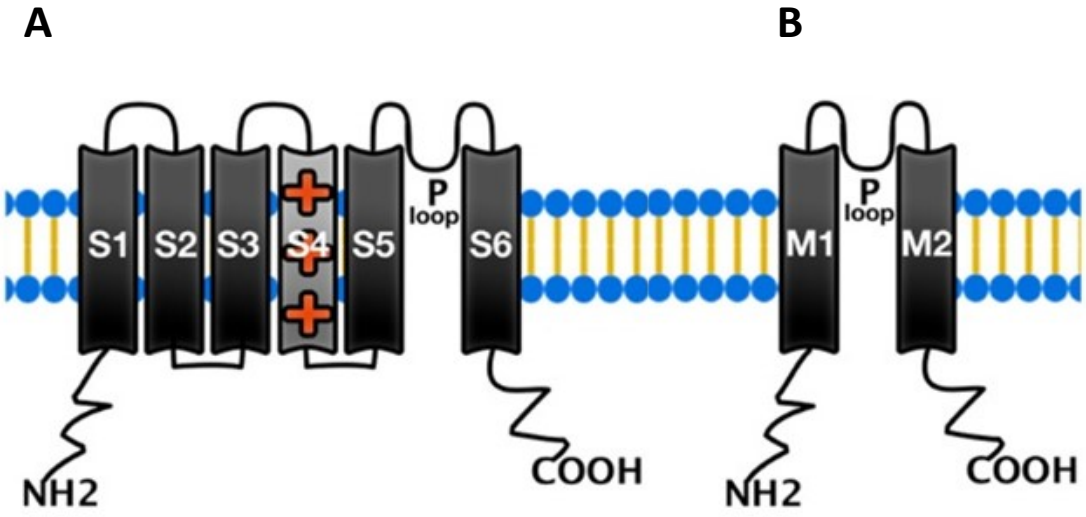


**Figure 1.3: Cartoon showing the structure of the voltage-gated $K^+$ channel α subunit**

A) showing the α -subunit of $I_{to}$, $I_K$ consist of one domain of six transmembrane segments (S1-S6) while B) showing the inward rectifying $K^+$ channel ($I_{K1}$) α -subunit consist of 2 transmembrane segments (M1-M2). Modified from (Mustroph et al. 2014).

## 1.4. AP heterogeneity in ventricular myocardium

AP shape and duration are varied in different regions of the ventricles (Fedida & Giles 1991; Litovsky & Antzelevitch 1989), with differences commonly found between the right and the

left and between the apex of the ventricles and transmurally across the ventricular walls (Carmeliet & Vereecke 2002).

AP differences spanning the ventricles have been identified in mammalian hearts and are shown to be responsible for the inscription of the T-wave in an ECG (Yan & Antzelevitch 1996; Yan & Antzelevitch 1998). These differences in AP provide protection against the retrograde propagation of an action potential during each cycle of activation, therefore, preventing abnormal conduction pathways. However, when these differences in AP are augmented as in pathological settings, they can contribute to the development of cardiac arrhythmias (Surawicz 1997; Burgess 1979).

The heterogeneity in the ventricular wall has been observed in both animal species and humans (Antzelevitch & Fish 2001). This is due at least to the presence of two main cell groups that are electrophysiologically and pharmacologically distinct: Endo and Epi myocytes with Epi cells exhibiting a shorter APD than Endo myocytes.

A third type of cell within discrete zones of the midmyocardium are called M-cells (Sicouri & Antzelevitch 1991). The principle feature of these cells is the ability of its AP to prolong more than that of Epi or Endo with a slowing rate or exposure to agents that prolong APD. This was, therefore, attributed to the weaker $I_{Ks}$ current with the stronger $I_{NaL}$ (Zygmunt et al. 2001; Liu & Antzelevitch 1995a) and NCX currents (Zygmunt et al. 2000). These cells have been identified mainly in canine and human ventricles in both isolated cells or slabs of tissue (Akar et al. 2002; Sicouri & Antzelevitch 1991; Glukhov et al. 2010; Glukhov et al. 2012) and has been found also in rabbits (Aslanidi et al. 2010; Idriss & Wolf 2004), guinea pigs (Sicouri et al. 1996) and pigs (Stankovicova 2000) but not in rats (Shipsey et al. 1997; McCrossan et al. 2004).

## 1.5. Propagation of action potential and its determinants

The speed of AP transmission from one myocyte to another through the low resistance GJ channels is known as the CV. Cellular propagation of an action potential involves local circuit currents consisting of four distinct elements that determine the CV, including 1) $Na^+$ channels mediating the excitatory inward current ($I_{Na}$,); 2) intracellular longitudinal resistance, $r_i$ ($r_i = r_c + r_j$; $r_c$, resistance of cytoplasm; $r_j$, resistance of GJ); 3) capacitance of the non-junctional membrane, $c_m$; and 4) extracellular longitudinal resistance, $r_o$ (Desplantez et al. 2007). Any change in these elements can, in turn, change the resulting CV (King et al. 2013).

GJs provide low-resistance electrical coupling between adjacent cardiac myocytes and allow for the movement of ions and small molecules between cells. GJs are expressed near the $Na^+$ channels at higher densities towards the end of the cells rather than their lateral margins, resulting in a lower $r_i$. (Kumar & Gilula 1996). Furthermore, a GJ consists of two connexons spanning the membranes of two opposing myocytes, whereby each connexon contains six connexin subunits with connexin 43 (Cx43) dominating in ventricular tissue (Severs 1990). However, changes in Cx43 expression, distribution, dephosphorylation and lateralisation can affect the ending CV result (Desplantez et al. 2007).

The myocardial fibre architecture of the heart is anisotropic, meaning the propagation of CV varies by direction, with CV being much greater longitudinally than transversely (Valderrábano 2007). Sano et al., more specifically, were the first to observe a discrepancy between $CV_L$ and $CV_T$ in paced isolated sheets or bundles of myocardium (Sano et al. 1959), and this was confirmed by a number of other researchers (Draper & Mya-tu 1959; Clerc 1976). The degree of anisotropy is defined by the anisotropy ratio (AR), AR= $CV_L$ / $CV_T$, which has the ability to be affected by the geometry, the size of the cells and the distribution of gap junctions. Thus, changes in CV have been recognised as a potential substrate for

abnormal rhythm and re-entry, in both normal and pathological conditions (Valderrábano 2007).

## 1.6. Heart failure

Heart failure (HF) is the most common final stage of cardiac disease and results in the ventricles being incapable of filling and generating an adequate cardiac output to meet the demands of cellular metabolism (Jessup & Brozena 2003; Coronel et al. 2001).

Multiple aetiologies are responsible for chronic heart failure and often more than one cause may co-exist. This includes systemic or pulmonary hypertension, myocardial infarction, coronary artery disease, genetic mutations in genes encoding sarcomeric proteins, diabetic and metabolic cardiomyopathy, viral and bacterial myocarditis, valvular insufficiency and congenital heart defects (Maillet et al. 2012).

HF is now broadly classified into two types with different entities: HF with reduced (HFrEF) and HF with preserved (HFpEF) systolic function. Among all HF patients, including female elderly patients, obese individuals and those with diabetes, 50% are HFpEF (De Keulenaer & Brutsaert 2011; Jessup & Brozena 2003). Interestingly, both types of HF have a similar clinical presentation, and appear to have shared neurohormonal and physiological disturbances. However, the underlying HFpEF pathophysiological mechanisms and the differences between HFrEF remain poorly defined, except for the diastolic dysfunction which is one of the main contributory components in HFpEF (Kitzman 2008).

## 1.7. Cardiac remodelling

Cardiac remodelling (CR) is the term used to describe the heart's adaptation in response to various stimuli. This adaptation can either be physiological due to exercise and pregnancy, or pathological in response to pathological events (Mihl et al. 2008).

In response to pathological insult, myocytes within the heart undergo a series of transcriptional, signaling, structural, electrophysiological and functional remodelling. Other non-myocyte cells, including fibroblasts, vascular smooth muscles cells, leukocytes and vascular endothelial cells also participate in this remodelling. These remodelling processes are manifested clinically as changes in size, shape and function of the heart after cardiac injury (Burchfield et al. 2013). Figure 1.4 shows the primary maladaptive stimulus that induces cardiac remodelling.

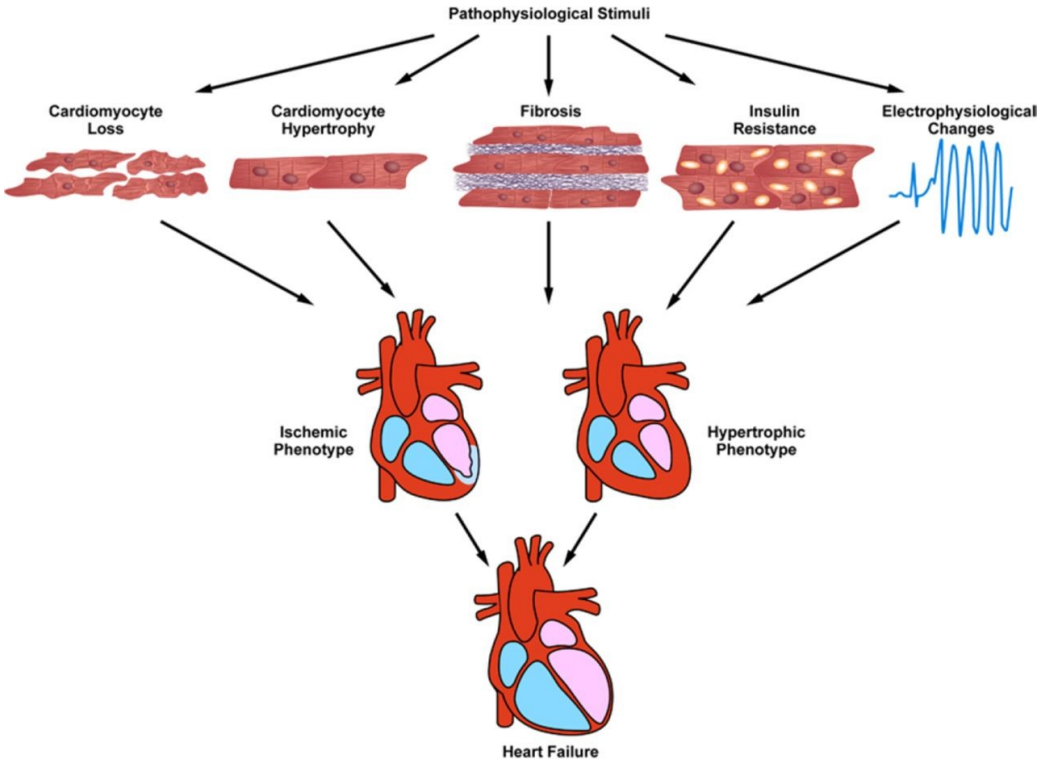


**Figure 1.4:Cardiac remodelling in response to pathological stimuli.**

Cardiac remodelling in response to pathological insult results in myocyte lost, hypertrophy, increase in fibrosis level and modulation in ion channels. This will lead to structural and functional changes of the heart and resulted in HF. Adapted from (Burchfield et al. 2013).

To be within the scope of the current study, we will focus on structural and electrophysiological remodelling which underlies changes in APD and CV in hypertrophy, and HF in the coming sections.

### 1.7.1. Cardiac hypertrophy

Cardiac hypertrophy, typically divided into physiological and pathological hypertrophy, is a type of cardiac remodelling which occurs when the heart experiences an increase in its workload. Unlike pathological hypertrophy, physiological hypertrophy does not induce fibrosis or reactivation of the fetal gene program, (Beisvag et al. 2009) and is not a risk factor for arrhythmia or the reduction in cardiac function leading to HF.

Functionally and geometrically, pathological hypertrophy can be concentric or eccentric (Grossman et al. 1975). Eccentric hypertrophy includes changes in the geometry of the heart, meaning it becomes more spherical with thinner walls. This type of hypertrophy is often observed after myocardial infarction and in volume overload, and can be characterised by the assembly of contractile-protein units, which causes an increase in the length of myocytes. In concentric hypertrophy, on the other hand, regarding pressure overload, the LV wall thickness increases with or without a change in chamber size. The contractile-protein units assemble in parallel leading to an increase in the myocytes width. Subsequently, with long-term pressure overload, this type may, as a result, progress to eccentric hypertrophy and HF (Kehat & Molkentin 2010). Figure 1.5 shows the ventricular remodelling patterns.

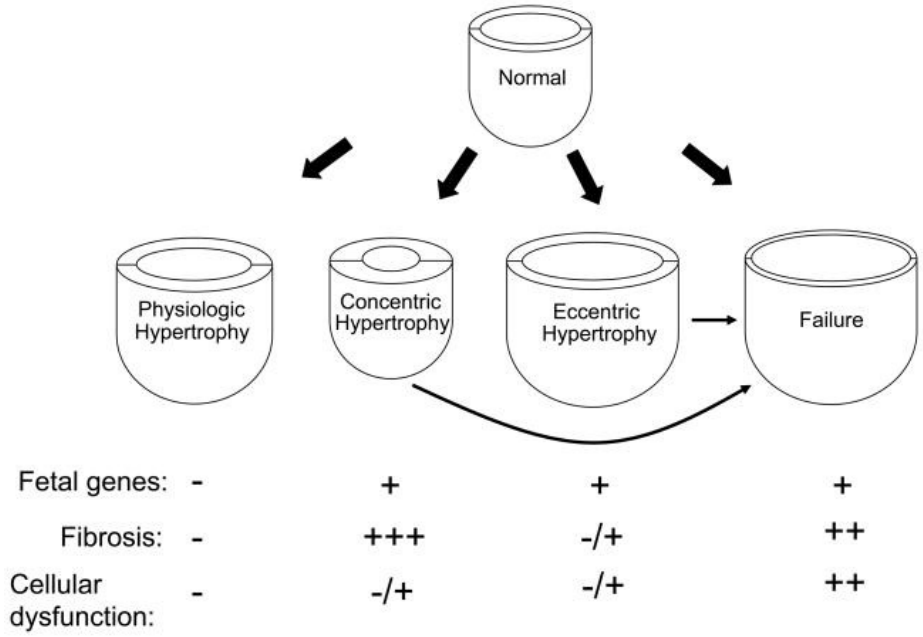


**Figure 1.5: Ventricular remodelling based on geometrical shape changes and the pathological and physiological stimuli that evoke these changes.**
Adapted from (Kehat & Molkentin 2010).

Despite previous research, multiple molecular signalling pathways have been identified to mediate cardiac hypertrophy and due to being complex, are yet to be fully understood (McMullen & Jennings 2007; Shah & Mann 2011). In physiological hypertrophy, molecular signaling pathways are widely mediated by signaling through insulin-like growth factor-1 and growth hormones, and can be transduced by phosphoinositide 3-kinase (PI3K)/Akt signaling; a process which is not associated with interstitial fibrosis or contractile dysfunction. As well as this, the induction of this pathway shows protection from ischemia-induced cell death and cardiac dysfunction (Dorn & Force 2005), while pathological hypertrophy is primarily mediated through the Gq protein family (Gαq and Gα11)(Wettschureck et al. 2001). Given this information, animal studies have shown that even brief exposure to pathological insults can induce different molecular cascades compared to the same duration of physiological exercise, therefore, suggesting that the response to pathological stress cannot be adaptive and

is mediated by different molecular mechanisms (Perrino et al. 2006). However, an overlap between the two mentioned mechanisms has been recognised. Pathological hypertrophy, for example, can be adaptive if the primary stimulus is eliminated before the development of intrinsic myocardial disease, while physiological hypertrophy is maladaptive if the insult becomes sustained and prolonged (Dorn et al. 2003; Dorn et al. 1999). This, therefore, denotes the complexity and crosstalk of the signaling pathways in both mechanisms (Iemitsu et al. 2001; Kong et al. 2005). Figure 1.6 represents a comparison between the molecular mechanisms underlying physiological and pathological hypertrophy.

Other important pathways that mediate cardiac remodelling through regulating cardiac and myocyte size include: Mechanosensitive signaling pathways which are activated at sarcolemmal and sarcomeric levels, and β-adrenergic mediated stimulation of adenyl cyclase (AC), protein kinase A (PKA) and $Ca^{2+}$ calmodulin-dependent kinase (CaMKII) (Shah & Mann 2011).

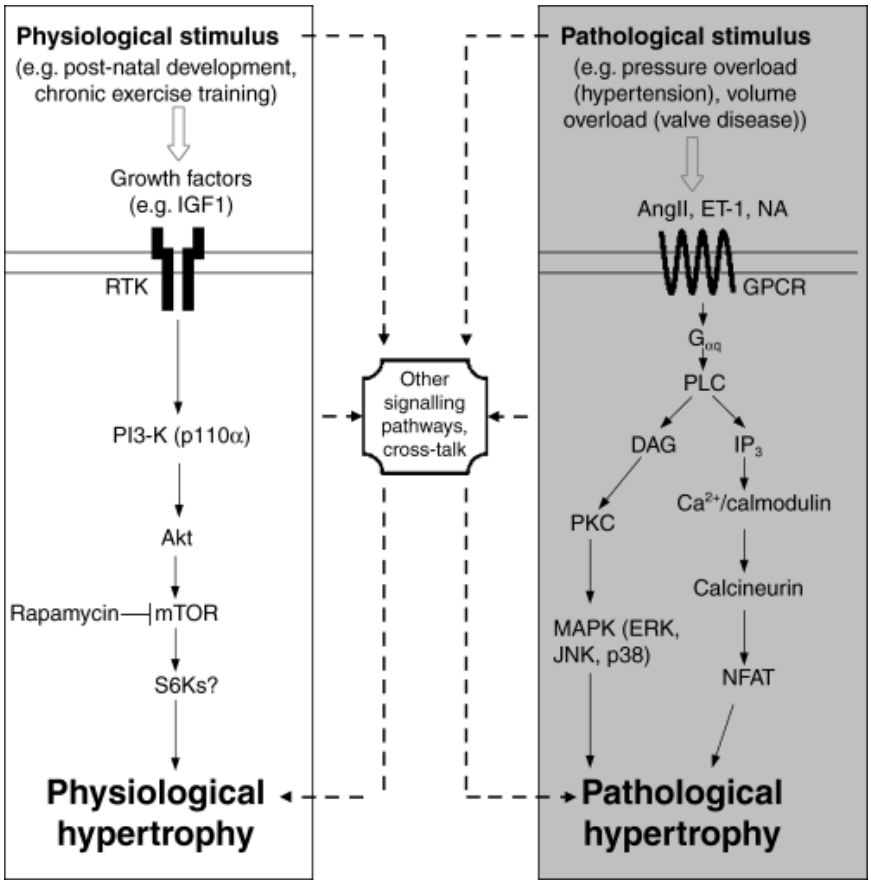


**Figure 1.6: The distinct signalling pathways in physiological and pathological hypertrophy**

(Abbreviations used: RTK, receptor tyrosine kinase; mTOR, mammalian target of rapamycin; NA, noradrenaline; PLC, phospholipase C; DAG, diacyl-glycerol; IP3, inositol 1,4,5-trisphosphate; MAPK, mitogen activated protein kinase; JNK, c-jun amino-terminal kinase; PKC, protein kinase C; PI3-K, phosphoinositide-3kinase; ERK, extracellular signal regulated kinase; AngII, angiotensin II; ET-1, endothelin 1; GPCR, G-protein coupled receptor; NFAT, nuclear factor of activated T cells; IGF1, insulin-like growth factor 1; S6Ks, ribosomal S6 kinases). This figure adapted from (McMullen & Jennings 2007).

### 1.7.2. Fibrosis and extra cellular matrix remodelling

Cardiac fibroblasts (CFBs) are one of the non-myocyte cell populations in the myocardium which are involved in many aspects of cardiac function, including cell-to-cell communication with cardiomyocytes, electrical activity, production of growth factors and cytokines. CFBs are also involved in intercellular signalling with other CFBs, endothelial or smooth muscle cells that can impact cellular events such as angiogenesis, cell proliferation, cardiomyocyte hypertrophy or apoptosis, and homeostasis and remodelling of the cardiac extra cellular

matrix (ECM) (Fan et al. 2012). Furthermore, CFBs produce ECM proteins, the enzymes that degraded these proteins (matrix metalloproteinases (MMPs)) and the inhibitors of these enzymes (tissue inhibitor of metalloproteinases (TIMPs)). Cardiac ECM is critical in mediating the mechanical connection among the cardiomyocytes, CFBs and the blood vessels within the myocardium (Eghbali 1992).

Therefore, cardiac ECM represents approximately 3% of the normal myocardium, and is largely made up of collagen, types 1 and 3 (Klotz et al. 2008; Krenning et al. 2010). Collagen plays a pivotal role in preserving myocardial properties through maintaining its structural composition. As well as this, it transmits forces with elastin, contributes to the elastic properties of the myocardium and acts as a ligand-binding protein affecting the function of myocardium components (Di Lullo et al. 2002). In clinical and experimental conditions, type 1 collagen, type 1:3 collagen ratio, collagen cross-linking and fibrosis are found to be elevated and have been associated with stiffer non-compliant ventricles, ventricular dilatation and detrimental effects on systolic and diastolic function (Jugdutt 2003; Janicki & Brower 2002).

Others which have a vital role in regulating ECM turnover and are involved in the remodelling process are MMPs and TIMPs. Although MMPs and TIMPs functions are tightly regulated under normal conditions, large changes often occur in the actions of HF, therefore, contributing to negative ECM remodelling (Li, Feng, McTiernan, Pei, Moravec, Wang, Rosenblum, Kormos & A. M. Feldman 2001; Spinale et al. 2000; Wilson & Spinale 2001).

### 1.7.3. Cardiac electrical remodelling in HF

Sudden cardiac deaths (SCD) from lethal arrhythmias (in particular, ventricular tachyarrhythmias) account for approximately 50% of HF patient lives with 350,000 events annually in the US (Thom et al. 2006). The mechanisms underlying ventricular arrhythmias are complex and not yet well understood. However, they are driven in part from the electrical

remodelling of the myocardium, involving the modification of numerous of ion channels, EC coupling and intercellular gap junctions (Cutler et al. 2011). Moreover, an increase in fibrosis deposition results in electrotonic coupling modification with a slow conduction between cells and the dispersion of refractoriness, therefore, intensifying arrhythmogenesis (Burchfield et al. 2013).

### 1.7.3.1. AP remodelling

One hallmark of HF that is independent of the etiology is AP prolongation (D J Beuckelmann et al. 1993; Kaab et al. 1996), a process which is highly arrythmogenic and results in triggering early afterdepolarisation events (EADs). The mechanisms underlying AP prolongation are complex. However, studies on humans and animal models, regarding HF, have revealed that changes in AP duration and profile results from alterations in the outward $K^+$ current (Kääb et al. 1998; Kaab et al. 1996), in the inward $Ca^{2+}$ current (Wang et al. 2008; Houser et al. 2000; O'Rourke et al. 1999) and the inward $Na^+$ current - Primarily in the late component $I_{Na,L}$ (Undrovinas et al. 1999). Prolongation of APD can cause $Ca^{2+}$ overload due to an increased calcium channel opening which can trigger abnormal impulses and perturbed signaling events. In addition, APD prolongation in HF is heterogeneous and has the ability to exaggerate the dispersion of APD within the heart, generating the substrate for re-entrant ventricular arrhythmias (Fadi G Akar & Rosenbaum 2003; Li, Lau, Ducharme, et al. 2002).

### 1.7.3.2. Sodium current remodelling

Under physiological conditions, activation and inactivation properties of sodium channels are under tight control to maintain cardiac excitability. In HF, $I_{Na}$ remodelling is variable with reports of increased, decreased and unchanged peaks. Thus, alterations in $I_{Na}$ have a limited effect on APD while they primarily alter conduction velocity. In contrast, $I_{Na,L}$ is increased in HF which can increase APD, therefore, promoting arrhythmias (Remme & Bezzina 2010; George 2005).

### 1.7.3.3. Calcium currents and calcium cycling remodelling

Defects in excitation-contraction coupling are common manifestation in HF and are characterised by decreased $Ca^{2+}$ transients, enhanced diastolic SR $Ca^{2+}$ "leak," and diminished SR $Ca^{2+}$ sequestration. Hence, these defects cause a reduction in contractile force, impaired relaxation and increased susceptibility to ventricular arrhythmias (Piacentino et al. 2003).

Chronic activation of beta adrenoreceptors (β-ARs) as seen in HF undelays alterations in $Ca^{2+}$ haemostasis, and therefore may trigger lethal arrhythmias. β-ARs stimulation modulate the activation of two intracellular regulatory kinase: cAMP-dependant protein kinase (PKA) and $Ca^{2+}$/calmodulin-dependent protein kinase II (CaMKII) which phosphorylate L-type $Ca^{2+}$channels, RyR and PLN. Therefore, excessive β-adrenergic stimulation can lead to SR $Ca^{2+}$ overload, spontaneous SR $Ca^{2+}$ release and delayed afterdepolarizations (DAD)(Xiao et al. 2006; Lohse et al. 2003; Rubart & Zipes 2005).

Calcium enters cardiac myocytes mainly through L-type calcium channels. The density of these channels has been reported to be altered in humans and animal models of hypertrophy and HF depending on the severity of the disease. In general, $I_{Ca,L}$ density is increased in mild to moderate hypertrophy and decreased in severe hypertrophy and heart failure (Kamp & Hell 2000; Pitt et al. 2006).

In normal conditions, the entry of $Ca^{2+}$ through $I_{Ca,L}$ induces $Ca^{2+}$ release from the SR through the large RyR complex and activates myocardial contraction. Impairment in RyR gating and alterations in its protein expression were observed in HF and resulted in SR $Ca^{2+}$ release defects. Furthermore, alterations in RyR release properties may increase diastolic $Ca^{2+}$ leak which, in turn, generates spontaneous $Ca^{2+}$ waves that triggers ventricular arrhythmias (Cutler et al. 2011).

SERCA2a and NCX are the main mediators of calcium removal from the cytoplasm of the myocyte and are found to be impaired in HF. Thus, SERCA2a expression and activity are often decreased in HF. Given this information, when PLN phosphorylation is decreased, it triggers an increase in the PLN inhibition of SERCA2a (Hasenfuss & Pieske 2002).

Furthermore, NCX function and expression are often increased in hypertrophy and HF to preserve the diastolic extrusion of cytosolic $Ca^{2+}$. At the same time, increased NCX activity may impair systolic function by favouring the extrusion of $Ca^{2+}$ out of the cell rather than back into intracellular stores (Wang & Hill 2010). As well as this, the up regulation of NCX with the reduction in a $I_{K1}$ current can give rise to DADs in HF (Pogwizd et al. 2001). As the forward-mode of the exchanger generates a depolarising current contributing to APD prolongation, NCX, therefore, could potentially play a significant role in shaping the overall AP profile. As a result, both the forward-mode of NCX and the delayed $I_{Ca,L}$ activation are believed to contribute to AP prolongation (Sipido et al. 2007). Moreover, $[Na]_i$ is an important determinant of NCX exchanger function, an increase in $[Na]_i$ induces $Ca^{2+}$ influx via the reverse-mode NCX model (Baartscheer 2003). The positive aspect of this effect is that reverse mode of NCX increases $Ca^{2+}$ load in the SR which works as positive inotrope. However, this enhances the susceptibility of spontaneous SR $Ca^{2+}$ release through the RyR, activation of the transient inward current and potential DADs development (Bers et al. 2002).

### 1.7.3.4. Potassium currents remodelling

$K^+$ channels are critical to restore cardiac excitability as they play an important role in AP repolarisation. Alterations in $I_{to}$, $I_K$ and $I_{K1}$ have been documented in HF and will be discussed in the following sections.

#### 1.7.3.4.1. $I_{to}$ alterations

$I_{to}$ is the main determinant in the early phase of AP repolarisation and its alteration can modulate AP plateau and repolarisation profiles. Because of this, the downregulation of $I_{to}$ is the most consistent ionic current change in failing hearts (Yue et al. 1997; Le Grand et al. 1994; Wang et al. 1997). Unlike in rodents, a reduction in $I_{to}$ has little influence on APD in large animal models and humans. However, it exerts an important influence on EC coupling and AP duration by modulating phase 1 and the plateau level which affects the currents that are active later in an AP (Wang et al. 2000).

In the normal LV, $I_{to}$ density is higher in the Epi than the Endo myocytes. This transmural gradient in $I_{to}$ contributes to the transmural gradient of APD, which enables Endo myocytes to provide more coupling current to depolarize adjacent cells. Therefore, this facilitates conduction in the physiological direction of Endo to Epi and prevents it in the opposite direction. In HF, the Endo to Epi physiological direction of conduction is diminished due to decline in the transmural gradient of $I_{to}$. Hence, this may enable arrhythmias from abnormal impulses originated in the epicardium (Medina-Ravell et al. 2003; Bristow et al. 2004).

#### 1.7.3.4.2. $I_K$ alterations

As was mentioned earlier in section 1.2.3.2, $I_K$ has different functional components which are species-specific. In large animals, $I_K$ is primarily responsible for initiating phase 3 repolarisation, thereby governing action potential duration and tissue refractoriness. $I_{Ks}$ and $I_{Kr}$, however, are the two main components of the $I_K$ current and each plays an important role in maintaining APD. Nonetheless, they function in a different way under physiological conditions, where $I_{Kr}$ predominates and $I_{Ks}$ becomes active during long APD in HF. Thus, both serve as a protective mechanism (Wang & Hill 2010).

#### 1.7.3.4.3. $I_{K1}$ alteration

As $I_{k1}$ is responsible for maintaining the resting membrane potential and contributes to AP termination, reduction in this current density may contribute to the prolongation of APD and enhances the susceptibility to spontaneous membrane depolarisation inducing delayed afterdepolarizations (DADs) (Pogwizd et al. 2001; Nuss et al. 1999; Rose et al. 2005). Changes in the functional expression of $I_{k1}$ are, therefore, more variable and controversial than $I_{to}$. However, the underlying basis of $I_{k1}$ downregulation in HF remains unknown as no consistent changes in the level of mRNA (Akar et al. 2005) or protein (Kääb et al. 1998) have been found.

### 1.7.3.5. Conduction remodelling

Slowed CV, which is associated with an increase in arrhythmia, is a prominent feature in both cardiovascular diseases and HF. Its reduction has been linked to alterations in membrane excitability by changes in $I_{Na}$ current, cell-to-cell coupling related to Cx43 alterations and the tissue architecture which can be affected by the level of fibrosis and cell size (Kléber & Rudy 2004; Coumel 1987).

$I_{Na}$ is a key determent of CV by providing the initial rapid depolarisation of an AP and electrical energy for impulse propagation (Amin et al. 2010). Abnormalities in the $I_{Na}$ gating function or its expression has, therefore, been described in HF human and animal models (Valdivia et al. 2005; Borlak & Thum 2003). However, little is known about the underlying mechanisms involved in these changes.

Changes in Cx43 including the reduction in density, lateralisation and post-translation modification, are prominent features in cardiac disease and HF (Akar et al. 2004). Thus, it is thought that HF increases $r_m$ and slows CV. As well as this, CV was found to be increased in the early stages of hypertrophy and this was associated with an increase in both cell size and Cx43 expression (Wiegerinck et al. 2006). However, prolonged periods of hypertrophy result

in a slower CV with a 25-50% decrease in Cx43 expression, as seen in HF (Kaprielian et al. 1998; Cooklin et al. 1997).

Fibroblast proliferation, migration and differentiation are enhanced in pathophysiological conditions (Manabe et al. 2002). This will, in turn, increase ECM deposition between cardiomyocytes and result in an altered cell-to-cell coupling. Hence, an increased $r_m$ and slow conduction (Spach et al. 1982; Mendez et al. 1970). Furthermore, fibroblasts were found to be electrically coupled with cardiomyocytes via Cx43 and Cx45 (Camelliti et al. 2004) and have a depolarising resting membrane potential (Kamkin et al. 1999). Therefore, this coupling can depolarise myocyte membrane potential and potentially inactivate the $Na^+$ channels. In addition, the coupling between fibroblasts and myocytes produces a net increase in cell capacitance (Miragoli et al. 2006) which results in a slowing conduction and triggers re-entry events (Xie et al. 2009; Maleckar et al. 2009).

### 1.7.3.6. Cardiac arrhythmia mechanisms

The mechanisms responsible for cardiac arrhythmia at cellular and tissue level can be classified as disorder of impulses formation, disorder of conduction/ propagation or a mix of both (Table 1.1). Regarding tachyarrhythmias, disorder of automaticity, triggered activity and re-entry are the most common mechanisms (Gaztan et al 2012).

**Table 1.1: Cardiac arrhythmias mechanisms.**

| **Disorder of impulses formation** | **Disorder of impulses conduction** |
|---|---|
| **Automaticity** | **Re-entry** |
| Altered normal automaticity | Anatomic re-entry |
| Abnormal automaticity | Functional re-entry |
| **Triggered activity** | |
| Delayed afterdepolarisation | |
| Early afterdepolarisation | |

List from (Gaztan et al 2012).

#### 1.7.3.6.1. Disorder of automaticity

Cells with intrinsic pacemaker activity are present in the SA node, atria, AV node and the His-Purkinje system. The firing rate of pace maker cells is determined by three factors: the maximum diastolic potential, the threshold potential at which the AP is initiated and the rate or slope of phase 4 depolarisation. Any change in these factors results in alterations in the frequency of AP generation and therefore, arrhythmia. Sinus tachycardia is an example of altered normal automaticity.

The atrial and ventricular non-intrinsic activity cells can exhibit abnormal automaticity under conditions that drive the maximum diastolic potential toward the threshold potential and become more positive. This can occur by the interplay of numerous currents that together results in a net inward depolarising current associated with decrease in potassium conductance. Atrial or ventricular tachycardia are examples of abnormal automaticity(Gaztan, Larraitznaga, Francis E. Marchlinski 2012; Tse 2016).

#### 1.7.3.6.2. Triggered activity

Triggered activity can result from premature activation by afterdepolarisations. Those afterdepolarisations are triggered by one or more preceding action potentials. It may take the form of either early afterdepolarizations (EAD) or delayed after depolarizations (DAD). EADs can occur at phase 2 or 3 of the cardiac action potential. They usually, but not exclusively, are associated with prolonged APD. The postulated mechanisms relate either to the increase in the $I_{NaL}$, $I_{Ca}$, or $I_{NCX}$, or to the decrease in the repolarising potassium currents ($I_{Kr}$,$I_{Ks}$,$I_{K1}$). EADs are observed in HF and long QT syndromes.

DADs usually occur during phase 4 of action potential, following completion of repolarisation. They can occur in conditions associated with intracellular calcium overload such as digitalis toxicity, hypercalcemia and HF(Shen et al. 1997; Cherry et al. 2012).

#### 1.7.3.6.3. Re-entry

Re-entry occurs when a propagated AP fails to die out after normal activation of the heart and persists to reactivates a region that has recovered from refractoriness. Such process is commonly denoted as re-entry, re-entrant excitation, circus movement, etc referring to the repetitive propagation of the wave of activation in circular path, returning to its site of origin to reactivate that site. This re-entrant activity can occur if a group of isolated fibres is not activated during the initial depolarisation wave. Re-entry has been divided into two main groups: anatomical re-entry, which is determined by anatomical structures, and functional re-entry. Myocardial tissue with the following electrophysiological properties are required for a re-entry to occur:

1) Myocardial tissue with different electrophysiological properties, conduction and refractoriness. 2) Unidirectional conduction block. 3) Area of block which the wavefront can circulate.4) Slow conduction velocity in the normal unblocked pathway than the refractoriness of the blocked pathway to allow recovery of the previously blocked pathway.5) Critical tissue mass. 6) Initiating trigger. (Gaztan, Larraitznaga, Francis E. Marchlinski 2012; Tse 2016).

## 1.8. Current therapy for heart failure

Depending on the stage of HF, non-pharmacologic, pharmacologic, and invasive strategies are considered to manage HF. Controlling the dietary sodium and fluid intake, appropriate physical activity and weight controls have been used and are considered to be the first line of therapy. However, when this fails, pharmacologic treatments including diuretics, vasodilators, inotropic agents, anticoagulants, beta-blockers, and digoxin are used. More advanced approaches to control HF include the use of more invasive therapies, such as cardiac resynchronisation therapy (CRT), pacemakers, implantable cardioverter-

defibrillators (ICDs), revascularisation procedures (coronary artery bypass grafting (CABG) and percutaneous coronary intervention (PCI)), valve replacement or repair and percutaneous ventricular restoration (PVR) therapy. Nonetheless, when HF progresses regardless of optimal medical therapy, heart transplantation is the most common standard treatment (Hunt et al. 2009). Ventricular assist devices are used to support HF patients who are waiting for a heart transplant or as a destination therapy which will be discussed in the following section. Experimental treatment strategies may, therefore, include gene and cell therapy, both of which are currently undergoing clinical trials (Abdel-Latif et al. 2007).

### 1.8.1. Left ventricular assist device (LVAD)

Although HF is one of the leading causes of death worldwide, the survival and prognosis of patients has been improved dramatically due to advancement in pharmacological treatments. However, a percentage of patients are not responsive to pharmacological treatments and often require more advanced interventional procedures (Jessup & Brozena 2003).

The most effective of such procedures is cardiac transplantation, but due to shortage of donors, it is not always the available choice (Dickstein et al. 2008). An alternative non-pharmacological choice is the use of a LVAD, which are found to be effective in the management and treatment of HF (Pruijsten et al. 2008).

In general, mechanical devices providing circulatory support are often classified into 1) LVAD which is a mechanical pump that provides active circulatory support and unloading of the ventricles, and 2) cardiac support devices which function by providing passive containment of the dilated ventricles (Terracciano et al. 2011). Furthermore, LVAD had been classified into extracorporeal devices, percutaneous short-term devices and long-term assist devices (Terracciano et al. 2010). Initially, LVAD were used to rescue the circulation in cardiogenic shock in post cardiotomy patients. Although this is not the case anymore, LVAD is still a substantial strategy for acute intervention in hemodynamically unstable patients

undergoing cardiac procedures and in post-myocardial infarction cardiogenic shock patients (Henriques & de Mol 2008). Nowadays, the major application of LVAD is the treatment of chronic HF. Subsequently, there are three major chronic indications for LVAD therapy: bridge-to-transplantation, destination therapy and bridge-to-recovery (Yacoub & Miller 2008). Currently, the most commonly applied therapy among these is the bridge-to-transplantation which improves circulatory function and quality of life in patients scheduled for transplantations (Terracciano et al. 2010). As well as this, it provides a better post-transplant prognosis (Christiansen et al. 2008). When a cardiac transplantation is contraindicated, patients can benefit from the permanent implantation of the LVAD as a therapeutic way to support circulation (Yacoub & Miller 2008). The most challenging but promising application is the use of LVAD as a bridge-to-recovery involves the temporary use of LVAD until the underlying myocardium pathology is recovered to the extent that the LVAD can be removed (Mancini, A. Beniaminovitz, et al. 1998; Maybaum, Mancini, Xydas, Randall C Starling, et al. 2007). More promising strategies, however, have suggested to use an LVAD in combination with pharmacological (Birks et al. 2006; Birks et al. 2011) and cell-based therapy (Ibrahim et al. 2012), in an attempt to prevent HF.

### 1.8.2. LVAD and cardiac reverse remodelling

Cardiac reverse remodelling is defined as any alteration in HF that is chronically reversed by a given therapy. It is this term which has been mainly linked to clinical, molecular and cellular studies with LVAD whereby the myocardial tissue was available before and after the unloading of the heart (Klotz et al. 2005; K. Dipla et al. 1998). Testing the hypothesis that eliminates pressure or volume overload in HF could, therefore, result in a regression of the pathological process (reverse remodelling). This is one of number major advantages provided by the use of LVAD. In human patients treated with LVAD, regression of ventricular dilatation and restoration of end-diastolic pressure and volume have been reported (Levin et

al. 1995; Scheinin et al. 1992; Rivello et al. 2001; De Jonge et al. 2001). Interestingly, this finding was associated with conformational changes in cardiac shape and size. As a result, changes in electrical activity of the heart were observed with rapid LVAD induced alterations of ventricular dimensions (Henein et al. 2002).

Changes in cardiac dimensions observed with LVAD are not only limited to organ level, but can be extended to a cellular level. Studies reported the normalisation of deranged structural proteins after chronic LVAD support (de Jonge et al. 2005; Aquila et al. 2004) and the chronic effect of using LVAD support, including ECM components, cell signalling pathways and fibrosis. The changes involved in reverse remodelling which underlie the improvements seen with LVAD, therefore, includes an increased expression of $Ca^{2+}$ handling genes that are downregulated in HF (SERCA2A, RyR and NCX) (Heerdt et al. 2000; Heerdt et al. 2002; Razeghi et al. 2002). In addition, this improvement was associated with changes in the electrical activity of the heart (Terracciano et al. 2004) and resulted in the reduction of APD, faster $ICa,_L$ inactivation and increased SR $Ca^{2+}$ content.

#### 1.8.2.1. Effects on action potential

LVAD insertion has shown both early and delayed effects on the heart's electrical system. APD and QTc were found to be prolonged after one week in experimental animal models and in humans, respectively; both of which saw an associated increase in the incidence of arrhythmia (Harding et al. 2001; Soppa, Lee, Stagg, Siedlecka, et al. 2008). In the long-term, regarding mechanical unloading, QTc was seen to decrease with an associated reduction in arrhythmic events. This finding was also confirmed in isolated myocytes as demonstrated by the reduction in APD (Ambardekar & Buttrick 2011). Furthermore, a reduction in APD was a characteristic feature of recovery in patients with LVAD support and hypotheses focused on these electrical changes have been established. Such hypotheses include: NCX upregulation, and a reduction in the level of Cx43 and potassium channel subunit Kv4.3. These changes

were, therefore, found to be predisposing and post-LVAD observed factors in ventricular arrhythmias (Lebeche et al. 2004; Lebeche et al. 2006; Poelzing & Rosenbaum 2004; Sáez et al. 1997; Refaat et al. 2008). Thus, $Ca^{+2}$ homeostasis plays an important role in the heart after mechanical unloading, a topic which will be discussed in the next section.

### 1.8.2.2. Effect on $Ca^{+2}$ handling

Changes in the $Ca^{+2}$ handling of myocytes may possibly contribute to the reduction in contractility and the negative force-frequency relationship observed in HF. Myocytes from LVAD-treated patients have shown calcium transients similar to non-failing myocytes with a greater systolic ratio peak and a faster rate of decay than myocytes from failing hearts (Chaudhary et al. 2004; K Dipla et al. 1998). This change in calcium transient morphology is associated with faster calcium entry through the $ICa,_L$, greater SR content and a shorter APD. In addition, changes in SERCA2, NCX and PLN have been observed (Terracciano et al. 2004; Terracciano et al. 2003; Heerdt et al. 2000). SERCA2 and NCX gene expression are often increased in response to mechanical unloading (Madigan et al. 2001; Terracciano et al. 2007). There is a controversy regarding SERCA2 protein levels as some studies show no change while others show increased levels, closer to non-failing levels (Chaudhary et al. 2004; Madigan et al. 2001; Ogletree et al. 2010; Heerdt et al. 2000). Thus, there is a lack of evidence to support this claim. NCX protein abundance and function has also been found to decrease comparably to non-failing heart values (Chaudhary et al. 2004). The protein levels of phosphlamban are not changed but the SERCA2/PLN ratio, which is an indicator of SR calcium uptake and diastolic relaxation, normalises after LVAD (Ogletree et al. 2010). Hence, the whole CICR undergoes reverse remodelling after LVAD support, a process which may explain partially whole heart function improvement leading to clinical recovery. However, these changes in CICR are duration-dependent as prolonged mechanical unloading was found to associate with cardiac dysfunction raising the question of optimal timing.

### 1.8.2.3. Effect on cardiac conduction

Effect of mechanical unloading on conduction and arrhythmogenesis has also been observed but the mechanisms underlying these changes remains largely un-investigated. In a study on patients undergoing LVAD insertion, it was shown that there was a reduction in the Cx43 level and this was observed mainly in the patient group which developed ventricular arrhythmias. In addition, an increased level of fibrosis in HF was associated with arrhythmia and increased electrical heterogeneity was linked to the setting up of re-entry circuits. However, the reported effects of mechanical unloading on fibrosis are conflicting as some reports show an increase in collagen (McCarthy et al. 1995b; Nakatani et al. 1996a; Li, Feng, McTiernan, Pei, Moravec, Wang, Rosenblum, Kormos & A. M. Feldman 2001) while others show reduced (B. A. Bruckner et al. 2000; B. A. Bruckner et al. 2001; Nakatani et al. 1996a) or unchanged levels (Navaratnarajah et al. 2013).

### 1.8.2.4. Factors involved in cardiac recovery.

Despite the beneficial effect of LVAD support, these benefits have been showed to be hindered by prolonged mechanical unloading. Three factors have been thought to oppose functional recovery after prolonged mechanical unloading, including myocardial atrophy, fibrosis and derangements in function and contractility. Cardiac recovery and device explantation was possible in selected patients treated with LVAD and with specific pharmacological therapies, which, in turn, may have reduced these detrimental effects (Birks et al. 2006; Birks et al. 2011). This suggests that LVAD implantation may be more feasible with adjunctive therapies such as pharmacologic or cell-based therapy (Soucy et al. 2015; Dandel et al. 2014). In addition, the degree and duration of the mechanical unloading has been suggested to be crucial for optimal recovery (Ibrahim, Kukadia, et al. 2012).

## 1.9. Animal models of cardiac disease

Human samples obtained from surgery or at the time of a heart transplant are an excellent tool for cardiovascular research. However, these samples can be rare and display considerable variability due to differences in factors such as genetics, medications, diet, environment and associated pathologies. Therefore, the development of animal models allows researchers to mimic different human cardiac diseases and provide valuable insights into pathophysiology. In addition, animal models are an essential tools to evaluate new therapeutic strategies and to predict and prevent complications in a more controlled manner (Milani-Nejad & Janssen 2014).

The commonly used animals in cardiovascular research are a mouse, rat, guinea pig, rabbit, dog, pig and sheep. As each animal has its unique cardiovascular system to meet the demand of that species, there is no ideal animal model of the human heart. Thus, each model has its own sets of advantages and disadvantages to use. Meaning, the choice of animal model depends mainly on the cardiovascular question of interest and whether the findings of the study can be reasonably translated to humans.

HF animal models have been induced in different species using numerous techniques which include pressure overload, volume overload, fast pacing, myocardial infarction or the administration of cardiotoxic drugs like isoproterenol. Furthermore, genetic models of cardiomyopathies have been produced in small animals, such as mice (Houser et al. 2012; Hasenfuss 1998). Animal models with combined procedures can, therefore, be generated to test particular aspects of interest. In the case of modelling mechanical unloading in rats, for example, TAC can be generated to induce heart failure and these failing hearts are then transplanted to the abdomen of a recipient rat to test the effect of mechanical unloading – A process which will be described in more detail in the next section (Schaefer et al. 2016).

Mice and rats are the most used animals in cardiovascular research. This is because they are easy to handle, have a shorter gestational time and have lower maintenance cost than when compared to bigger animals. In addition, genetic manipulation and drug testing in rodents is relatively easier and highly efficient (Patten & Hall-Porter 2009). However, the large differences between human and rodent hearts must be considered when a small rodent is used as a cardiac animal model. For example, rodents have a very fast heart rate (250/500 bpm) compared to humans (72 bpm). In addition, they have shorter APs with a short plateau phase (Nerbonne 2004). Furthermore, another example is with regards to calcium handling where SERCA2 accounts for 90-92% of calcium uptake in rodents (L. Li et al. 1998) and only 76% in humans (Piacentino et al. 2003), with NCX accounting for the majority of the rest in both groups. Although mouse and rat cardiovascular systems share many characteristics, there are distinct differences between the two species. For example, rats have more ability than mice to increase their heart rate during exercise with a more positive force-frequency relationship and slower kinetics of contraction and relaxation (Lujan et al. 2012).

Rat models of hypertrophy and heart failure have been extensively used to study long-term pharmacological interventions, including long-term survival studies and have been the most widely and successfully used models in basic and translational research. Thus, rats are preferred for HF models to mice mainly because surgical procedures and invasive hemodynamic assessments are far easier in rats than compared to mice. Moreover, further investigations can be conducted simultaneously in rats as they have a higher level of myocardial mass compared to mice (Patten & Hall-Porter 2009).

In the subsequent sections, We will talk about the three rat models we have used in this study. The first model used was the heterotrophic heart and lung transplantation (HAHLT). It is one of the heterotopic heart transplantation (hHTx) procedures which are used to mechanically unload the LV. The other two are models of pressure overload involved spontaneous

hypertension (SHR) and thoracic aortic constriction (TAC). SHR is a genetic model of systemic hypertension while TAC is a surgical model that is used to induce aortic stenosis.

### 1.9.1. Heterotopic heart transplantation

The heterotopic heart transplantation model in rodents was first described by Abbott et *al.* in 1964 (Abbott et al. 1965; Abbott et al. 1964). These authors used end-to-end anastomoses of the donor ascending aorta (AO) and pulmonary artery (PA) to the recipient abdominal aorta (AAO) and inferior vena cava (IVC) to produce a perfused, unloaded and non-working graft. This was improved later by Ono et al. who conducted side-to-end anastomoses instead and found a significant improvement in the level of survival rates (Ono et al. 1969; Ono & Lindsey 1969). Since then, many modifications and improvements on the technique have been described, including the "cuff technique" and the cervical and femoral technique (Gordon et al. 2007; Heron 1971; Rao & Lisitza 1985). This model was essentially developed to study immunological reaction, immunosuppressive therapy and organ protection after tissue grafting in transplantation investigations. However, after the rise of its use in LVAD patients and its substantial effects on cardiac recovery (Yacoub et al. 2001), this model has been used extensively to study the effect of mechanical unloading on the LV in an efficient way. In this procedure, the LV of normal or failed donor hearts is completely unloaded (since thebesian venous return is the only volume load) and this leads to severe myocardium atrophy and dysfunction. Therefore, adjustments to the procedure have been introduced to allow for partial unloading; for instance, transplanting the heart and the lungs (Campbell et al. 1986; Ibrahim et al. 2013; Liu et al. 2015). In this model, pulmonary blood flow returning through the pulmonary veins to the left atrium enters the left ventricle together with thebesian venous return, therefore, resulting in a partial unloading of the LV. Hence, this model provides a moderate and gradual level of mechanical unloading as it has been showed that the duration and the intensity of mechanical unloading is an important factor in cardiac recovery (Wang et

al. 2009; Liu et al. 2015; Ibrahim, Kukadia, et al. 2012). The mechanical unloading investigation has also been performed primarily on rats as hHTx in mice, compared to rat models, requires extensive microsurgical skills. On the other hand, large animal models (bovine, canine, porcine) are expensive and time-consuming. The main rat strain used in this procedure was the Lewis strain as these rats are syngeneic rats overcoming the problem of graft rejection and the need for immunosuppressive drugs.

This model has several limitations as it is a complex procedure and requires excellent surgical ability. In addition, there is a significant difference in the unloading achieved with this model compared with the LVAD support, as LVAD works on an intra-thoracic and innervated hearts, while the hHTx is deinnervated and subjected to intra-abdominal pressure. Finally, LVAD enhances coronary blood flow whereas there is evidence to suggest hHTx does not have a pronounced effect on coronary flow (Ibrahim et al. 2013).

### 1.9.2. TAC

Thoracic aortic construction in rats is a surgical model involving the banding or suturing of the thoracic aorta; a process which increases the afterload and leads progressively to LV hypertrophy and heart failure (Hasenfuss 1998). In this model, HF develops after 15-27 weeks of induction with around 30% of premature mortality (Suckau et al. 2009; Molina et al. 2009). Cardiac remodelling and HF development in this model, therefore, occurs more rapidly than with other models of pressure overload, such as abdominal aortic constriction or SHR. However, like any surgical model, this requires significant surgical skills as it can result in acute heart failure and a high mortality rate. Thus, obtaining a consistent level of aortic constriction to produce consistent cardiac remodelling can be challenging.

### 1.9.3. SHR

SHR is a genetic non-invasive model of primary hypertension which progresses to HF at around the age of 18-24 months. SHR serves as a model of human hypertension as hypertension starts at early age and advances with time. The cause of the rising blood pressure, however, remains unknown. SHR rats are the most studied model of hypertension, as indicated by the vast amount of publications that have used this strain (Pinto et al. 1998).

Due to mating with a female with a slightly elevated blood pressure, SHR are the offspring of an outbred Wistar Kyoto male rat with spontaneous hypertension from a colony in the Kyoto School of Medicine in Japan. Here, brothers and sisters are allowed to mate for spontaneous hypertension (characterized by systolic blood pressure over 150 mmHg persisting for more than one month) (Okamoto & Aoki 1963). At around 3 months of age, SHR already show a 24-hour mean arterial pressure of 135 mmHg which progresses to 150 mmHg at 7 months. SHR, therefore, develop concentric cardiac hypertrophy and overload-induced HF (Calhoun et al. 1994; Wichers et al. 2004; El-Mas & Abdel-Rahman 2005).

The Wistar Kyoto (WKY) controls were established as a normotensive control strain with inbred rats from the Wistar Kyoto colony. Although SHR were derived from WKY, there is a substantial degree of genetic variance between the two strains with only around 50% of common DNA fingerprint. (St Lezin et al. 1992). Thus, it has been suggested to use another normotensive strain in parallel to WKY as the strain in question could yield into new findings regarding the factors responsible for the elevation of SHR blood pressure, which would not appear if only WKY rats were used as a control. At the age of 18-24 month, 57% of the SHR males develop decompensated HF, with 13% surviving without HF and the remaining 30% dying from non-cardiac reasons (Bing et al. 1995). Although this model is non-invasive because it does not require any surgical procedures or toxic treatments to produce such

conditions, it does take a long time to develop hypertrophy and HF and this can be a limitation in some research studies.

## 1.10. Tissue slicing

The concept of live tissue slices that are used to investigate physiological properties goes back to the early 1920s (Krebs 1950). However, the rudimentary techniques used required massive manual intervention often resulting in a low viability and reproducibility which made it an unpopular method. Later on in the late 70s, the development of the Krumdieck automated slicer (Krumdieck et al. 1980) brought interest back to tissues slicing. It became widely adopted across a multitude of organs including the intestines, lungs, kidneys and the brain (Edwards et al. 1989; Freeman & O'Neil 1984; De Kanter et al. 2005; De Kanter et al. 2002).

### 1.10.1. Cardiac slices

Cardiac slices were initially used in metabolism research where oxygen consumption was measured (Yasuhara et al. 1996; Pincus 1933; WEBB et al. 1949) and ATP-sensitive potassium channel ($K_{ATP}$) properties in ischemic conditions were assessed (Han et al. 2002). Furthermore, Claycomb *et al* who used slices obtained from neonatal rat hearts found that DNA synthesis and cardiomyocytes differentiation could be regulated by adrenergic stimulation (Claycomb 1978). From 1990, slices have been used in direct cell electrophysiological investigations. For example, Burnashev and co-workers showed that cardiac slices from neonate rats are feasible, with similar characteristics of the $Na^+$ current and inward rectifying $K^+$ current to those recorded in isolated myocytes. However, the resting membrane potential in slices was less negative, therefore, suggesting that more optimisation was needed for this preparation (Burnashev et al. 1990).

In the past, tissue slices have received relatively little attention in cardiac research compared to other established myocardial model systems. This is possibly due to technical challenges in producing reliable cardiac slices. However, the advances in sectioning techniques with the increased knowledge of the myocardial architecture has played a significant role in being able to validate and optimise this preparation method. This was accomplished by using high precision vibratomes that can cut sections at a very slow speed (50 μm/s or less in case of very fibrotic tissue) with minimal z-axis blade deflection (<1 μm). As well as this, thin slices of 250-400 μM thickness were prepared to assure oxygen diffusion occurred to all the cells within each section. In addition, the tissue blocks were cut tangentially to the surface, providing the optimal alignment of the slices with locally prevailing cell orientation compared with transmural sections. This method was suggested by Yashura et al. (Yasuhara et al. 1996) and has been confirmed by Bussek et al. in histological sections (Bussek et al. 2009). Finally, minimising tissue contraction and energy consumption during slice preparation was achieved by adding excitation-contraction un-couplers, such as 2, 3-butanedione monoxime (BDM). All these modifications have, therefore, resulted in obtaining a relatively consistent, vital cardiac slice with uniform thickness and minimum tissue damage (de Boer et al. 2009; Meyer et al. 2010; Wang, Lee, Gary R. Mirams, et al. 2015; Bussek et al. 2009). Slices were mostly obtained from the ventricles of embryonic, neonate and adult donors, and were successfully prepared from different species including mice (Halbach et al. 2006; Pillekamp et al. 2005), rat, guinea pig (Bussek et al. 2009; Bussek et al. 2012b), dog (Camelliti et al. 2013; Camelliti et al. 2011), rabbit (Himmel et al. 2012; Wang, Lee, Gary R. Mirams, et al. 2015; Wang et al. 2014) and humans (Camelliti et al. 2014; Camelliti et al. 2011; Brandenburger et al. 2012; Kang et al. 2016).

Many model systems have been used for pharmacological and physiological investigations such as cardiomyocytes either isolated or cultured, tissue segments such as papillary muscle

or coronary-perfused wedges and Langendorff whole heart. However, there is controversy about which system is more representative of whole heart function (de Boer et al. 2009). Although isolated cardiomyocytes have been used extensively to study cardiac function, the lack of multicellularity and cell-to-cell electrical and mechanical connections make them inappropriate to study multicellular events, such as conduction. In addition, this preparation method lacks other important cell types, such as fibroblasts and endothelial cells, which are known to play an important role in cardiomyocytes function. The existing multicellular preparations, therefore, involve isolating entire sections from the heart, including the trabeculae (Jost et al. 2005), papillary muscles (Bavendiek et al. 1998; Toyama et al. 1997) and ventricular wedges (Glukhov et al. 2010). Trabeculae and papillary muscles are limited to the endocardial region of the heart and in large animals, they suffer from poor oxygenation and limited viability as they often exceed 400µm in diameter (Barclay 2005). On the other hand, ventricular wedges in large animals or humans requires a complex perfusion system to guarantee adequate oxygenation and the availability of large blocks of ventricular tissue. Finally, Langendorff-perfused whole heart studies are complex 3D preparations and are limited to surface recordings of the heart. Furthermore, studies of the whole heart obtained from animal models are costly as the entire heart is used per experiment and can be extremely rare with human hearts (Nanthakumar et al. 2007). Therefore, cardiac slices provide a unique balance between the simple isolated myocyte and the complex whole heart preparation, and overcomes the limitations of other multicellular preparation methods. In particular, tangential slices enable transmural mapping of APs across the LV, as the amplification of transmural dispersion for repolarisation has been associated with arrhythmias (Sicouri et al. 2010). In our group, we have successfully mapped the transmural gradient of AP repolarisation in the canine left ventricular free wall using slices (Camelliti et al. 2013). In addition, many slices

can be produced from a single heart or from biopsies. Therefore, a greater number of studies can be carried out with fewer animals or rare tissues like human samples.

Besides the acute use of these slices, myocardial tissue has been successfully cultured and maintained for several days (Habeler et al. 2009). Brandenburger *et al* have maintained human myocardial slices in a culture for 28 days (Brandenburger et al. 2012), which has opened up the possibility of maintaining human material for long-term investigations such as cell therapy and integration studies.

## 1.11. Hypothesis

Cardiac slices are a useful multicellular preparation to study electrical, structural and conduction remodelling in rat models of cardiac disease.

Therefore, we have set our aims as following:

1) To study FPD and CV changes in LV slices obtained from a rat model of mechanical unloading (Chapter 3).
2) To study FPD and CV changes in LV slices obtained from TAC – A model of aortic stenosis. (Chapter 4).
3) To study FPD and CV changes in LV slices obtained from SHR - A model of hypertension (Chapter 5).
4) To correlate the changes in conduction velocity to cellular substrates (Cx43, Nav1.5 protein levels and fibrosis) from the same slice preparation in the SHR model (Chapter 5).
5) To measure the FPD and CV transmural distribution of the LV in each animal model

# CHAPTER 2.General methods

## 2.1. Introduction

This chapter explains the general methodology used throughout this research, including animal models, myocardial slice preparations, multi-electrode array system (MEA) recordings and the analysis methods, western blotting and histology; all of which was undertaken to assess the function and structure of remodelling in myocardial slices. Dual optical mapping/MEA recordings were also used to assess the duration of the FP in rat slices.

## 2.2. Rat models of cardiac diseases

Despite the limitations regarding differences in myocardial function in rats compared to human hearts, rats have been extensively used as models of cardiac disease due to the relatively inexpensive and short gestation period (Patten & Hall-Porter 2009). In addition, it was also possible to produce models of disease using these animals as our lab had extensive experience with rat models of cardiovascular disease. In this study, we have, therefore, chosen to use two rat models of chronic pressure overload induced by hypertension or aortic stenosis. The two models are TAC and SHR. HAHLT was performed as a model of "partial" mechanical unloading of the LV. All operations were performed under licence by the UK Home Office, in accordance with the United Kingdom Animals (Scientific Procedures) Act 1986. All surgical procedures (TAC, HAHLT) were established in our lab (Ibrahim et al. 2013) and with my help were conducted by Dr. Michael Ibrahim.

### 2.2.1. Heterotopic abdominal heart transplantation

The heterotopic abdominal heart transplantation (HAHT) procedure in rats was first described by Abbot et al in 1964 (Abbott et al. 1964) and is a technique which has been used mainly to study the biology of transplanted cardiac grafts. This protocol was also used to study the effect of mechanical unloading on the myocardium. Two surgical techniques that

give either “complete” (HAHT) or “partial” HAHLT ventricular unloading in normal or failed rat hearts was adopted in our lab (Ibrahim et al., 2013).

In the complete mechanical unloading model, the donor heart is transplanted into the abdomen of the syngeneic recipient by anastomosing the donor’s ascending aorta and main pulmonary artery onto the recipient abdominal aorta and IVC, respectively. This method is known as a complete mechanical unloading of the LV as the donor aortic valve is competent and sees the recipient’s blood enters the donor aorta retrogradely, therefore, perfusing the coronaries without entering the LV (Figure 2.1, A).

In partial unloading, the heart and lungs of the donor are transplanted by a single anastomosis of the donor aorta to the abdominal aorta of the recipient. As in complete unloading, the transplanted heart is perfused through its coronary arteries by oxygenated blood from the recipient aorta, and this blood returns to the right atrium via the coronary sinus. However, in contrast to complete unloading, this blood is then ejected via the pulmonary artery into the donor lungs not the recipient IVC, and this subsequently returns to the LV via the pulmonary veins. Thus, this model produces a less profound degree of mechanical unloading than complete unloading, as blood entering the LV is a combination of that from thebesian veins, as well as blood returning from the donor pulmonary circulation (Figure 2.1, B).

In this study, more specifically, we have used the partial unloading model for two reasons. Firstly, this model produces a milder response that can better simulate clinical applications of mechanical unloading with LVADs. As well as this, the procedure requires only one surgical anastomosis as it is easier and more reliable to perform (Ibrahim et al., 2013). Hence, why it was chosen for the aforementioned study.

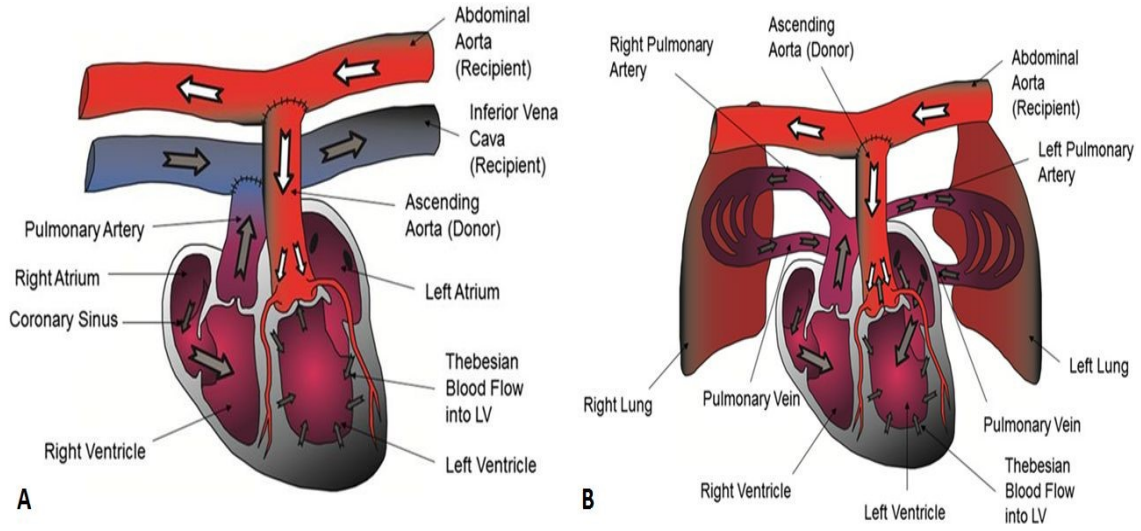


**Figure 2.1: Heterotopic abdominal heart transplantation.**

A) Complete and B) partial mechanical unloading models (reproduced from (Ibrahim et al., 2013)).

In this procedure, we have used 200-300 g of Lewis rats. This is a syngeneic strain, which allowed for better controls within experiments due to the lack of underlying genetic differences. Both donor and recipient rats were anaesthetised inside an anaesthetic chamber with 5% Isoflurane in pure oxygen, and were then shaved and weighed. The recipient was prepared first to reduce the ischemic time of the donor heart when harvested. The recipient was then transferred to a heated mat. 1.5% Isoflurane was administrated via a nose cone and a midline incision from the xiphisternum to above the pubic vein was made. The bowel was carefully retracted from the abdomen and wrapped in wet gauze and the retroperitoneal fascia was dissected to reveal the aorta and the IVC. The vessels were lifted and bluntly dissected free from surrounding structures. The IVC and aorta were then separated from one another by blunt dissection for greater access to the aorta and to reduce the risk of injuring the IVC during aorta suturing. Microclamps were applied to the top and bottom of the aorta leaving as much space between clamps as possible. Following this, a small hole using a 30-gauge needle was then made in the middle of the longitudinal section of the clamped aorta. Using straight microscissors with blades of a 5-mm length (World Precision Instruments, USA), the needle hole was extended to leave approximately 4 mm in length and was placed in the midline of

the vessels. The bowel was then returned to the abdomen and was made to be wet again using saline.

After preparing the recipient, the donor rat was prepared for heart harvesting for the transplantation. A cut was made from the jugular notch to the level of the pubic vein to expose the abdominal aorta and IVC. The sternum was then cut to expose the heart from the thorax side and a silk suture was tied around the abdominal aorta and IVC to help lifting them with ease. Heparin (4000 units, LEO Labs LTD, Bucks, UK) was then injected into the IVC via a 30-gauge needle and was allowed to circulate for 1 minute. Following this, a transverse cut was made over the anterior surface of the abdominal aorta, sufficient enough to ensure the introduction of a 25-mm radial artery cannula. The heart was then arrested by the administration of at least 50 ml of cold cardioplegic solution (St Thomas II) slowly through the abdominal aortic cannula. The IVC, and the left and right superior vena cava (SVC), were dissected and permanently ligated using a 4-0 Mersilk suture (World Precision Instruments, USA). Then, the aorta was cut with the PA and the pulmonary veins were left connected to the block. The heart-lung block was detached from the animal by cutting the trachea and oesophagus as high as possible. The heart-lung block was kept in ice cold saline until ready for re-implantation.

The donor heart-lung block was placed on cold saline-soaked swabs in the abdomen of the recipient for transplantation. End-to-side anastomosis of the donor aorta to the recipient abdominal aorta was performed using a continuous 8-0 Prolene suture with a 5-mm round-bodied needle (Ethicon, Johnson and Johnson, UK). The distal clamp was removed and the anastomosis was examined for any bleeding. The top clamp was then removed and the lungs rapidly became pink, with the donor heart starting to beat within 5 seconds. The abdomen was closed using a continuous 5-0 Vicryl (NHS Supply Chain, UK) suture and the animal was allowed to recover on its own before being returned to its original box.

### 2.2.2. Rat thoracic aortic constriction procedure

Rockman *et al.* were the first to validate a murine TAC model (Rockman et al. 1991). Since then, this procedure has been used and developed extensively in cardiovascular research to mimic human hypertrophy and HF development. In this procedure, a band was placed around the ascending aorta to induce stenosis and produce LV pressure overload. As noted previously, adult male Lewis rats were used for surgery (Harlan Laboratories, UK). We have chosen two time points to study cardiac remodelling which were 10 weeks after banding as an early stage and 20 weeks as a late stage, and the operations, themselves, were carried out on 8-10 week old rats (200-250 g). We were careful to use animals of the same weight at the time of the operation to make sure that aortic diameter was constant. The rat was anaesthetised inside an anaesthetic chamber with 5% Isoflurane (IsoFlor, Abbot,USA) in pure oxygen. The animal was weighed and the chest was shaved while sleeping. 10-15 mg/kg amoxicillin trihydrate (Clamoxyl LA®, Pfizer, USA) and 10-20 µg/kg buprenorphine hydrochloride (Vetergesic®, Reckitt & Colman, UK) was given subcutaneously for antibiotic prophylaxis and pain prevention.

The rat was intubated during the operation to allow for mechanical ventilation and anaesthesia was maintained with Isoflurane through a nose cone. A right lateral thoracotomy was performed to provide better exposure of the ascending aorta and following the dissection of the surrounding tissues, the ascending aorta was exposed. A 3-0 silk suture was then placed under it using curved forceps and a loose knot was made. The knot was tightened around a 0.9 mm external diameter needle placed adjacent to the aorta and the needle was then removed. By increasing alveolar pressure, end-expiratory pressure was increased to re-inflate the lungs and reduce any pulmonary oedema. The chest was then closed with 4-0 prolene suture (Ethicon®, Johnson and Johnson, UK). Overlying skin was closed using a continuous 2-0 silk suture. The rat was allowed to self-extubate as a clear signal of its

recovery from the anaesthesia and was then left to recuperate on its own before being placed into its original box.

### 2.2.3. Spontaneously hypertensive rat model

SHR is the most commonly used model in cardiovascular disease studies with a common use of WKY rats as the normotensive control group.

This model is suitable to monitor myocardial remodelling during transition from compensated LV hypertrophy to HF in aging. WKY and Brown Norway rats (BN) were used as the control "normotensive groups" and were all male. Rats used in this study were obtained from Charles River Laboratories, UK.

### 2.2.4. Controls

For HAHLT, the recipient's own heart was used as a control. For TAC, on the other hand, sham-operated sex and age-matched hearts were used. For the SHR group, we have used age and sex matched WKY and BN as a control.

## 2.3. Echocardiography

Echocardiography was performed to assess heart function *in vivo*. On the day of heart collection, the animal was anaesthetised with 95% O2/5% Isoflurane and anaesthesia was maintained light with 98.5% O2/1.5% Isoflurane. The level of anaesthesia was carefully controlled as this can affect the overall cardiac function. As well as this, the weight of the animal was recorded before conducting the echocardiography. The chest of the rat was shaved and ultrasound transmission gel was applied to the skin (Sonogel®, AnaWiz Ltd,UK). Data were acquired using a Visualsonics Vevo 770 echocardiography machine with a 15 MHz transducer (Visualsonics B.V., Netherlands). Using 2D parasternal long axis imaging, we obtained a left ventricular M-mode tracing of the end-diastolic and systolic

interventricular septum (IVSd and IVSs), the left ventricular internal diameter (LVIDd and LVIDs) and the left ventricular posterior wall (LVPWd and LVPWs). As a result of the research, each animal was sacrificed as described in the next section. Echocardiography for the SHR group was carried out by Benjamin Dyer and by me for the TAC group with help from Dr. James Cartledge.

## 2.4. Blood pressure monitoring

Blood pressure was monitored in the SHR animals and their normotensive control rats (WKY and BN). We obtained BP at 3,6 and 9 months which are not the same time point we use to do the functional and structural experiments and this was due to technical difficulties. However, this step was mainly to confirm the increase of BP in SHR animals at different time points compared to the normotensive control groups.

BP was measured using the tail-cuff plethysmography blood pressure monitoring system in restrained, warmed, conscious state.

The animals' BP was monitored in a singly-booked CBS small procedure room with restricted access to the room throughout the recordings to minimise the animal BP elevation from noise induced stress. The animals underwent training period of two sessions to acclimatise to the restrainer and the required temperature to minimise false effects on BP due to physical or thermal stress (McDougall et al. 2000).

A clear acrylic holder (Part no 81, IITC Life Science, USA) was used to restrained the animal while its tail placed through a tail cuff sensor (B60-7/16") inflated by an automatic amplifier (Part no 229) which recorded data onto a Windows XP laptop with IITC software. Tail cuff plethysmography has been validated to be within 5mmHg of invasive BP recordings but requires a degree of vasodilation to obtain accurate readings. Thus, the holder placed in a warming box with the temperature set to achieve an ambient air at 35 C° to minimise thermal stress.

All apparatus was manually calibrated using an external inflatable sphygmomanometer prior to each series of BP measurements, with intensity, pulse gain and filter settings optimised for each rat to achieve the best signal to noise ratio.

BP recording was conducted by Dr Junaid Zaman with the supervision of Phil Muckett, senior technician to Professor Stuart Cook, who kindly allowed the use of the equipment for these BP recordings. Each animal was marked on the tail at the start of the experimental run to identify serial BP measurement within the cohort. The initial BP recording was ignored until the training period of two sessions, total of eight BP measurements using the apparatus, was complete.

Data were obtained with 10-15s of cuff inflation, up to a maximum pressure of 300mmHg, with a pressure reduction trace showing the BP at which arterial pulsation occurred, which was taken as systolic BP. This was cross-checked with the heart rate to ensure it was not the result of noise of excess movement from the animal. The maximum width of the pulse waveform was taken as diastolic BP. The data were recorded in raw format in the CBC computer and then exported for offline BP trend analysis, which was performed manually. Each rat underwent two sets of three BP recordings per session, and the mean of the six values taken as the BP. In addition, these results were cross-checked with data from Charles River, who have much larger numbers of rats to monitor to ensure they were reflective of the population as a whole.

## 2.5. Rat heart harvesting

Harvesting the heart can be tricky as adhesions developed within the chest, abdomen and around the heart as a result of the surgeries. Therefore, special care was taken during this phase. After anaesthetising the animal with 5% Isoflurane and shaving the chest and abdomen, a central incision was made from the manubrium down to the mid abdomen, where

the skin was then opened for the following procedure. A small incision was then made in the abdomen muscles. This incision was followed by a median sternotomy with scissors to expose the heart. The heart was quickly excised and placed in a normal Tyrode (NT) solution containing 100 units of heparin (Monaparin™, CD Pharmaceuticals Ltd, UK) per ml (NT+H) at 37°C to prevent the blood from clotting. It was allowed to beat for approximately 10 seconds to remove the majority of the blood from within the heart and then was moved into NT+H at 4°C, a condition which caused the heart to stop beating in an attempt to preserve the tissue. This method was used on the operated animals (TAC, HAHLT) and SHR, but also in sham and control rat hearts to maintain consistency.

### 2.6. Morphometric measurements

At the point of animal sacrifice, the body weight was measured and the whole heart weight was recorded after harvesting from the animal. These measurements were used to calculate the heart weight to body weight ratio in order to normalise the size of the heart to the size of the animal in different experimental conditions.

### 2.7. Cardiac slice preparation

All extra tissue around the freshly excised heart (lung, thymus and excess fat) was cleaned to prepare the aorta for cannulation. This step was undertaken in cold NT+H to stop the heartbeat. The aorta was then cannulated with a 16-gauge cannula on a Langendorff perfusion system with a constant flow pump (MasterFlex® L/STM Economy Drive, Cole-Parmer Instrument Company Ltd., UK) (Figure 2.2) and a flow rate of approximately 12 ml per minute was used throughout. The heart was perfused with oxygenated NT at 37°C until the heart was cleared of blood and was contracting well (5-6 min).

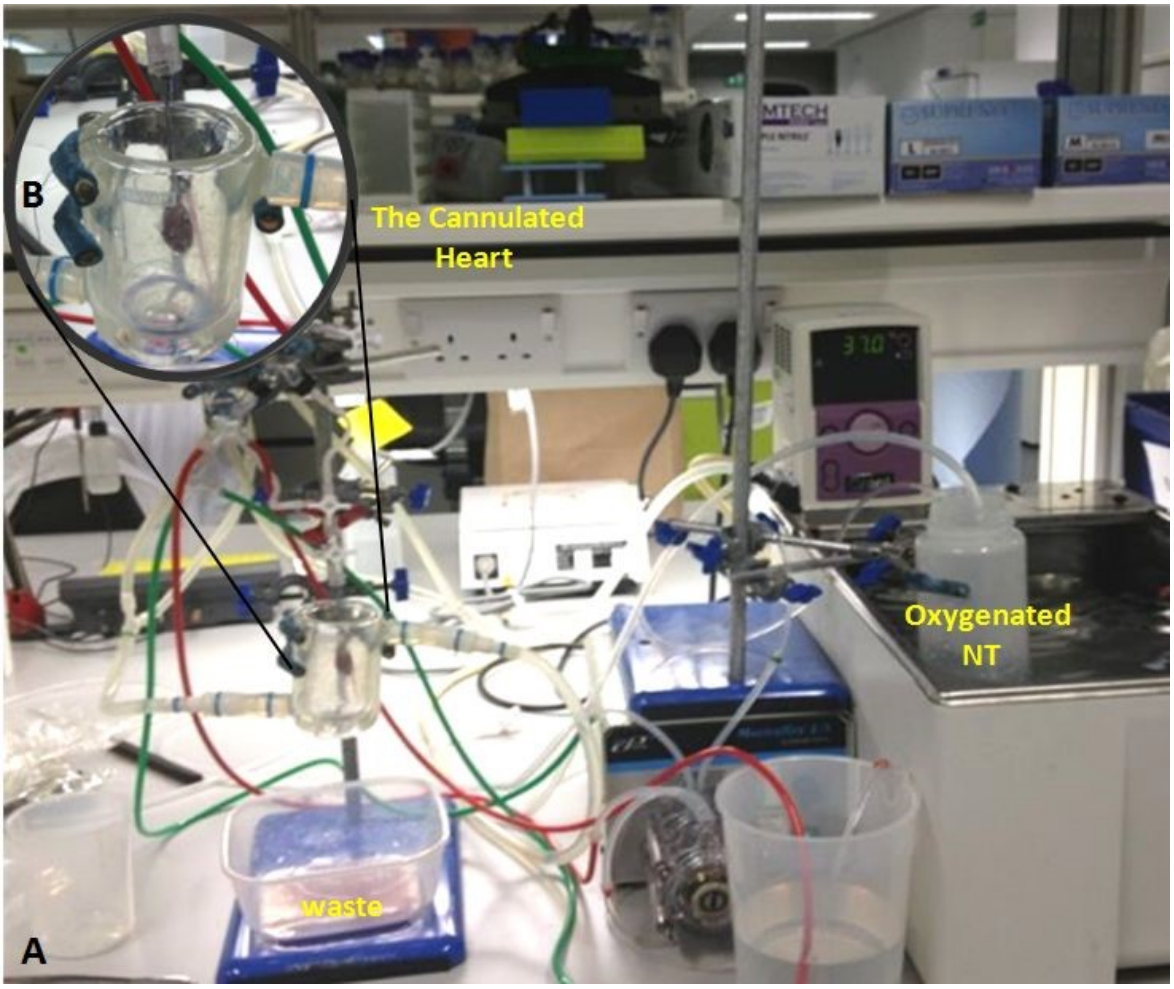


**Figure 2.2: Langendorff perfusion system.**

A) Water bath set at 37C° contains a bottle of NT solution with an output solution line to the Langendorff system and an oxygenation line. The input line is controlled by the pump. NT solution goes to a bubble trap to ensure that no air bubble enters the heart, which could cause air embolus in the coronaries. B) Zoomed image of the cannulated heart within the water jacket, which maintains physiological temperature.

The heart was removed from the perfusion system and placed in a Petri dish containing cold NT and the excitation–contraction uncoupler 2, 3-butanedione monoxime (NT+BDM). BDM was used to inhibit contractile activation. The heart was then dissected and a LV block from the free wall was obtained for slicing (Figure 2.3).

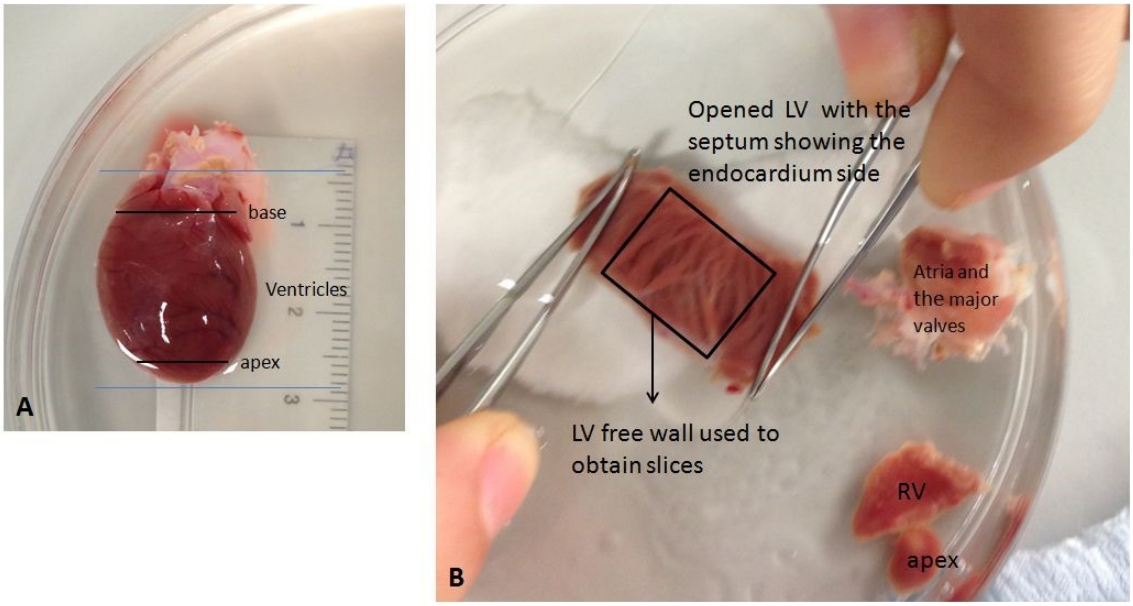


**Figure 2.3: Illustration of the method used to cut the left ventricle block for slicing.**
A) The heart (from 18 months old SHR rat) after Langendorff perfusion placed in cold NT+BDM solution. Black lines represent the area where two cuts were performed to obtain the ventricles block. First cut was from the apex and second cut was at the base of the heart. B) Shows the LV after taking out the RV and opening it by making one cut through the LV at the septum side. The LV block used to acquire slices was from the LV free wall.

The LV block was rapidly glued with the endocardium facing down using a surgical tissue adhesive (surgical glue- Histoacryl®, Braun, Germany) to a 4% agarose block. The agarose block was fixed by super glue to the metal cutting stage of a high precision vibratome (7000 smz, Campden Instruments Ltd., UK). The whole LV block-metal cutting stage was then rapidly attached to the vibratome bath which was filled with a cold (4°C) oxygenated NT+BDM solution. Slices (300-350 µm thick) were cut with a ceramic blade (Campden

Instruments limited, No.7550/1/C) in the tangent plane, at an advancement speed of 0.03 mm/s, amplitude of 2 mm, a vibration frequency of 75 Hz and a submicron blade Z deflection. Once cut, the slices were transferred gently from the bath of the vibratome to a glass tray containing an oxygenated NT+BDM solution at room temperature. A regular six-well tissue culture plate was immersed in this tray and used to hold the freshly cut slices after making a hole in each well to ensure proper oxygenation. In each well, the slice was placed on the top of a tissue culture cell strainer (EASYstrainer, greiner bio-one, USA) that ensured a fully oxygen diffusion to the inferior surface of the slice. To prevent the slice from curling after cutting, each slice was covered with a slice holder, which are metal rings (A4 Washers, No.51875) covered by fine mesh (Cadisch precision meshes ltd, No.0614). The whole LV block was then sliced and the order of the cut slices were kept starting from Epi to Endo to enable transmural analysis. Around 11 slices per LV block were obtained from each rat, however, the number of slices can be more or less depending on the size of the heart (hypertrophied or atrophied hearts). Figure 2.4 illustrate the slice cutting process and preservation.

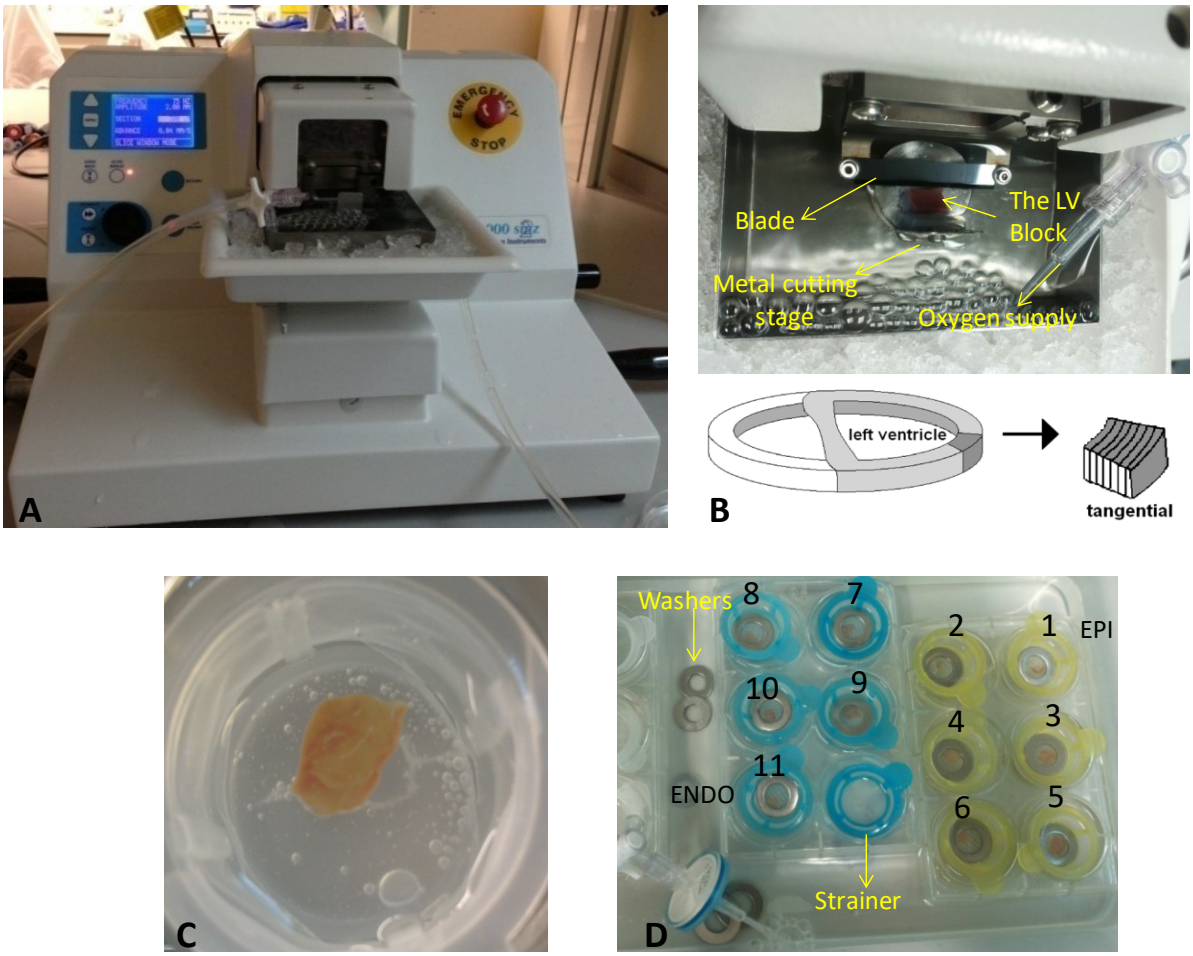


**Figure 2.4: Illustration of cutting left ventricle slices.**

A) The Vibratome used to cut cardiac slices. B) Slices of 300µm thickness were cut with a ceramic blade in the tangent plane. C) Freshly cut rat slice. D) Slices were placed on a nylon mesh surface to ensure fully oxygen diffusion to the inferior surface with metal rings covered by fine mesh to prevent the slice from curling. The numbers are illustrating the order of slices that cut from each LV block starting from the Epi.

## 2.8. Multi electrode array system

Electrophysiological activity in cardiac slices was assessed using a 60 electrode multi-electrode array (MEA) system (Multi Channel Systems, Germany). MEAs are dishes containing arrays of electrodes, each able to record voltage and to deliver stimulation. We used in this study the 60EcoMEA-Glass dishes with 8X8 array of embedded golden electrodes. These have a 100 µm diameter and are spaced at 700 µm. This system allows for

measuring the field potential at each electrode. Figure 2.5 shows the general workflow of MEA experiments.

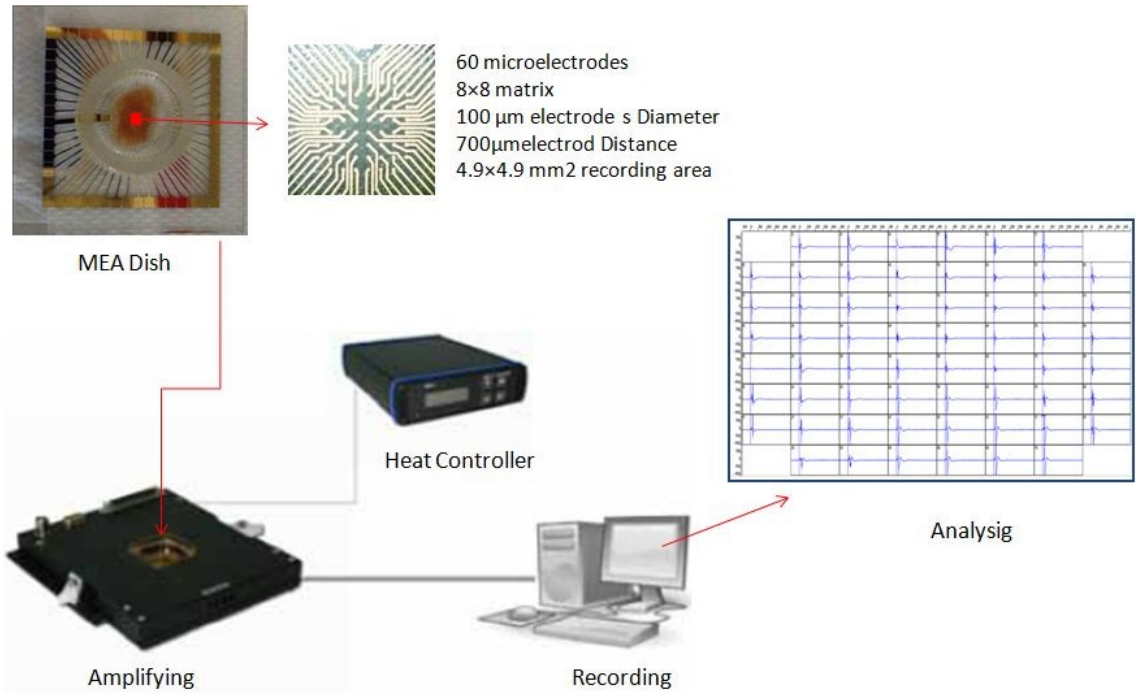


**Figure 2.5: General MEA workflow.**

A field potential (FP) is the extracellular electrical activity recorded from a number of cells and is used to represent the action potential. The most negative peak of the field potential corresponds to the upstroke peak of the action potential and the peak of the second wave form is used to mark the repolarisation of the cells (Halbach et al. 2003). The distance between these two peaks was used to calculate the FPD. The negative peak, however, was used to measure the activation time and the CV of each slice, as described previously (Camelliti et al. 2011; Bussek et al. 2012a; Bussek et al. 2009). Figure 2.6 demonstrates the output of an MEA recording and the main FP peaks used to calculate FPD and CV.

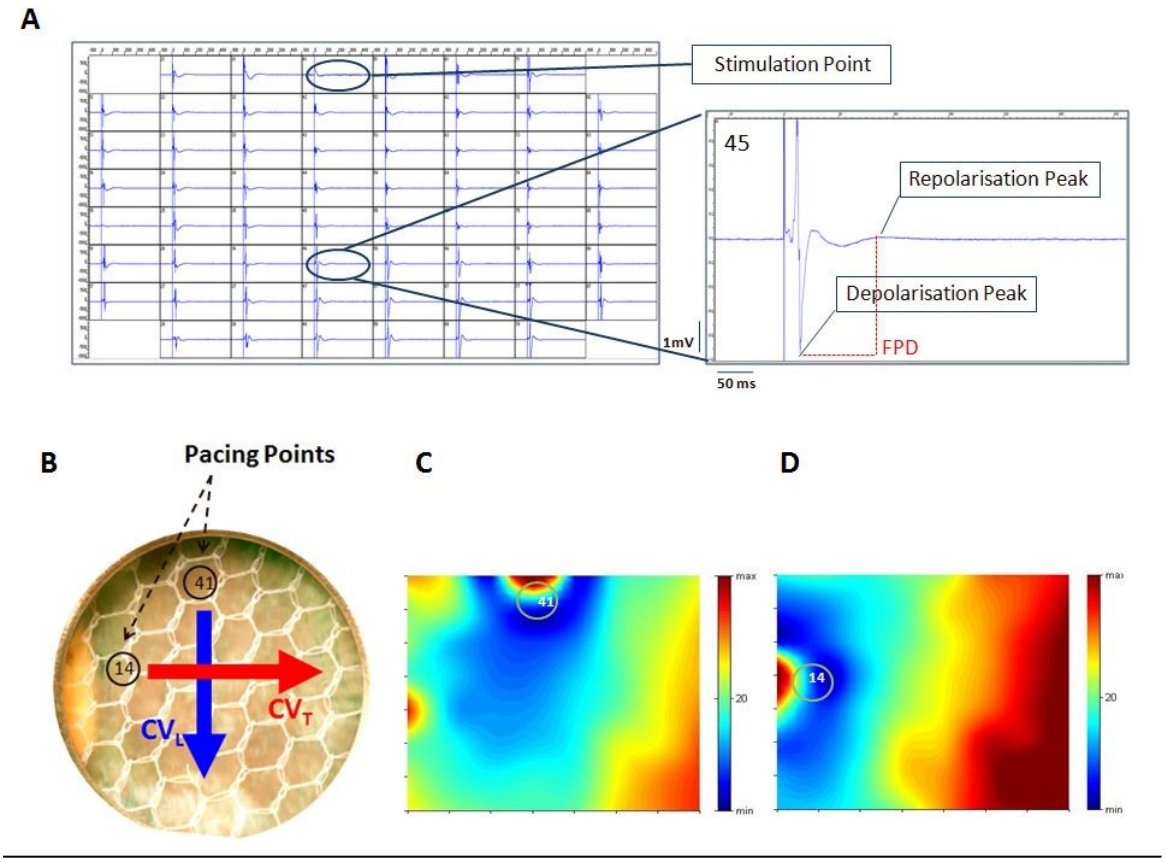


**Figure 2.6: Example of the output from an MEA.**

A) Overview of field potentials recorded simultaneously from the 60electrodes with enlarged image of field potential recorded from electrode 45. Depolarization and repolarization peaks were used to calculate FDP. The lower figures show the propagation of electrical activity in a slice paced within (B blue arrow; C activation map) or perpendicular to (B red arrow; D activation map) muscle fibre orientation. $CV_{L=}$longitudinal conduction velocity, $CV_{T=}$ transverse conduction velocity.

Slices were transferred from the NT+BDM solution into the glass MEA dish and were placed in the central area of the dish to ensure all electrodes were covered. A smaller holder with nylon mesh was put on the top of the slice to prevent it from floating and to keep it in contact with the electrodes during superfusion. The MEA dish was placed into an MEA 1060 amplifier and the temperature was controlled through a temperature controller (Multi Channel Systems, Germany). Slices were then perfused with an oxygenated recording solution (RS) at 37°C for 10 min to equilibrate before any actual recordings were made. Slices were point stimulated through an MC Stimulus (Multi Channel Systems) with a bipolar pulse of 500 µs

duration, 1-4 V and 1 Hz. The minimum voltage needed to stimulate the slice was used and this was between 0.5 and 1 V. It is important to use the minimum stimulation voltage to prevent field stimulation around the electrode and to reduce the overall number of artefacts produced, which may overlap with the stimulated FP. MC_Rack (Multi Channel Systems) was used to record FPs simultaneously from all 60 microelectrodes for approximately 25 seconds. Approximately six slices from the LV block, two or three from the sub-Epi, Myo and sub-Endo regions, were studied on the MEA system. We have used the Epi, Myo and Endo abbreviations in our experiments rather than sub-EPI and sub-Endo for simplicity.

The following protocol was used to record FPs from slices to calculate FPD and CV. The slice was point stimulated at any peripheral electrode and left to equilibrate for 10 minutes before any recording were taken. The slice was stimulated and recorded at deferent frequencies (0.5-4 Hz) starting from the lowest. The slice was then left to equilibrate for 5 min when changing the frequency before recording. Due to the anisotropy of cardiac tissue, slices were stimulated from four different directions and the concluding signal was recorded. Each direction was approximately 45$^{o}$ from each other and was used to assess the $CV_L$ which is the fastest CV running in the direction of the muscle fibres. This process also assessed $CV_T$ which is the slowest CV in the direction perpendicular to the muscle fibre orientation. The slice was then left to furtherly equilibrate for 5 min before recording when the direction of stimulation was changed. After MEA recordings were completed, slices were returned back to the glass tray of the NT/BDM solution for the subsequent experiments.

### 2.9. MEA analysis

Data was analysed using MC_Rack, MatLab with MEATools (University of Freiburg, Germany), MC_DataTool (Multi Channel Systems), Clampfit (Molecular Devices, USA) and Microsoft Excel (Microsoft, USA), as described below.

Using MC_Rack, a trigger was added to each trace. This aligned each field potential according to the stimulation artefact, which allowed the averaging of traces from the same electrode over the entire 25 seconds of recording.

### 2.9.1. Field potential duration

A minimum of 16 traces from different electrodes, were selected for FPD analysis (some recordings show fractionated depolarisation peak or absent repolarisation peak), however, only those with clear depolarisation and repolarisation peaks were chosen. The files were then converted to .abf files using MC_DataTool (Multi Channel Systems) to be opened in the Clampfit (Axon Instruments, USA) software. The FPD recordings over 25 s were averaged for each electrode. Then, two cursors were placed at the depolarisation peak and repolarisation peak and the time between the two cursors was calculated. The recordings of the 16 points were averaged to give the FPD of the slice and the standard deviation of the 16 points was used as a representation of FPD heterogeneity.

### 2.9.2. Conduction velocity

The data were analysed using MEATools within Matlab, and Extract LFP Features to obtain the change in delay between the stimulus artefact and the depolarisation peak of the field potential for each electrode recording over the slice. The values were put into a Microsoft Excel matrix which arranged them back into the 60-electrode configuration. Values were then checked visually to insure a correct acquisition.

The CV of each slice was calculated, using an Excel template sheet prepared by prof. Cesare Terracciano, based on the local method described by (Meiry et al. 2001). This involved the calculation of CV at each of the 60 electrodes using the maximum negative deflection of FPs recorded from the four surrounding electrodes (for the external electrodes, CV calculation was restricted by only three electrodes), using the following equations (1-5).

$$Tx_{a,b} = \left(t_{(a-1,b)} - t_{(a-1,b)}\right)/(\Delta X_L)) \quad (1)$$

$$Ty_{a,b} = \left(t_{(a,b-1)} - t_{(a,b+1)}\right) / (\Delta Y_L)) \quad (2)$$

$$CVx_{a,b} = Tx_{a,b}/(Tx_{a,b}{}^2 + Ty_{a,b}{}^2) \quad (3)$$

$$CVy_{a,b} = Ty_{a,b}/(Tx_{a,b}{}^2 + Ty_{a,b}{}^2) \quad (4)$$

$$CV_{a,b} = (CVx_{a,b}{}^2 + CVy_{a,b}{}^2) \quad (5)$$

where $t_{a,b}$ is the time of depolarisation of FPs at electrode (a,b), and $\Delta X_L$ and $\Delta Y_L$ are twice the distance between the electrodes (1.4mm).

The CV of the whole slice was calculated by averaging the CV of all the 60 electrodes (equation 6).

$$CV = [\Sigma_{a=1}^{8} \Sigma_{b=1}^{8} CV_{a,b}]/60 \quad (6)$$

Local CV was calculated four times from four directions for each slice to determine the faster and slower CV, corresponding to $CV_L$ and $CV_T$, respectively.

Transmural analysis of either FPD or CV was performed by subgrouping the FPD or CV values into three separate groups (Epi, Myo and Endo); all of which were based on the slice order in the LV block.

## 2.10. Dual optical mapping / MEA recordings

As we used slices from rat myocardium, which has a short, triangular action potential morphology, it was essential to define the depolarisation peak to calculate FPD. In order to do this, action potentials were optically mapped (OM) from slices at the same time MEA was acquired. Figure 2.7 illustrates the MEA/OM setup used here.

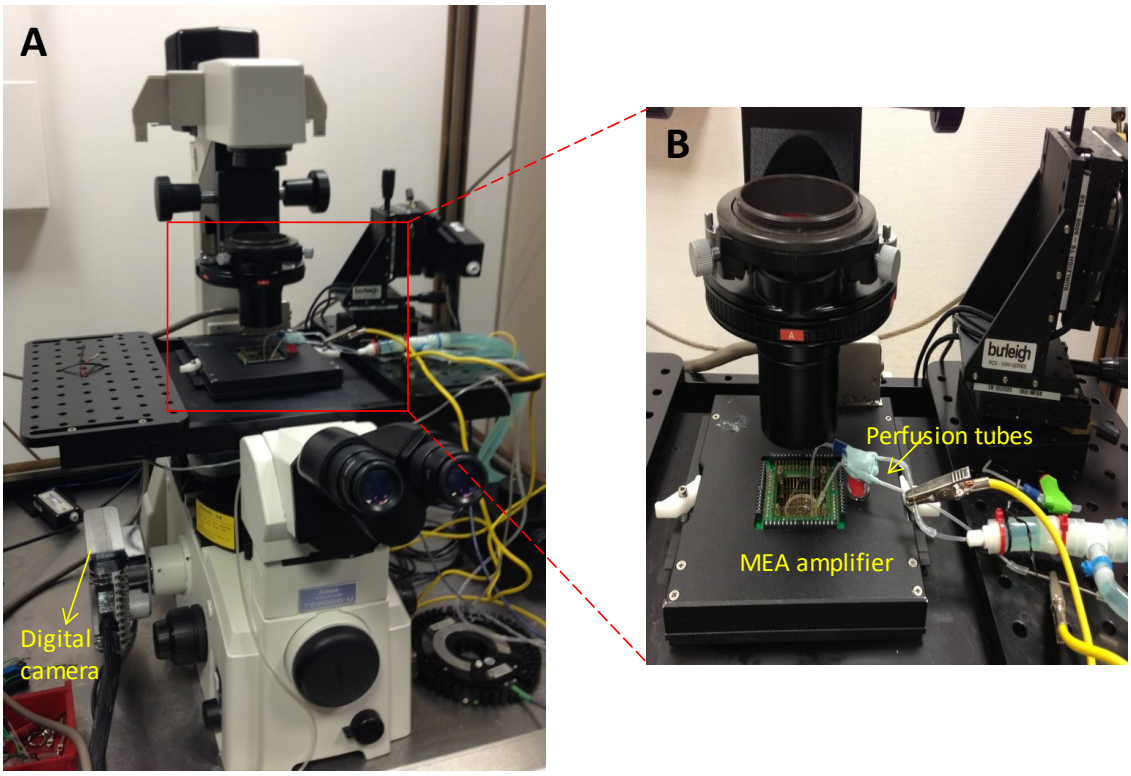


**Figure 2.7: Optical mapping / MEA setup.**

A) Image of the setup showing the MEA amplifier placed on the stage of an inverted fluorescence microscope which connected to a digital camera to acquire APs. B) Close up image to the MEA amplifier with the MEA dish connected to perfusion system.

As FPD is an index of AP duration at 90% of repolarisation (APD90%), the APD90% recorded was used to define the depolarisation peak in FP from the same area. Slices were loaded with 7 µM di-4-ANNEPS (Invitrogen) in 1ml NT and 10 µM blebbistatin (Sigma) (optical mapping recording solution), and were incubated for 5 minutes. Slices were then perfused at 37°C with an optical mapping recording solution throughout the recording. Blebbistatin is a mechanical un-coupler which inhibits myosin II. It is used widely in optical mapping experiments to reduce motion artefacts generated from myocardial contractions. Therefore, minimise the signal-to-noise ratio in AP recordings (Fedorov et al. 2007).

The slice was prepared for MEA as explained previously. The MEA amplifier was placed on the stage of an inverted fluorescence microscope and a 20x oil immersion objective was used to

focus the bottom of the MEA dish. The slice was superfused for 10 min and was point stimulated at 1 Hz with a 3±5V of 5 ms duration with the MEA system. After ensuring no contraction in the slice was present to prevent movement artefacts, MEA electrodes in the recorded view were noted and MEA was acquired. At the same time, Di-4-ANNEPS (Invitrogen) was excited using a 535 nm LED and emitted fluorescence collected through a 590 nm long-pass filter. A 10 second recording was captured using a NeuroCMOS camera (Redshirt) at 1 kHz (frame rate 1000/s) and dedicated Neuroplex software (IDL, Research Systems Inc.). Action potential analysis was, therefore, performed using Optiq software (Institute of Cardiovascular and Medical Sciences – University of Glasgow). Figure 2.8 shows an example of a dual AP/FP recorded from an LV slice.

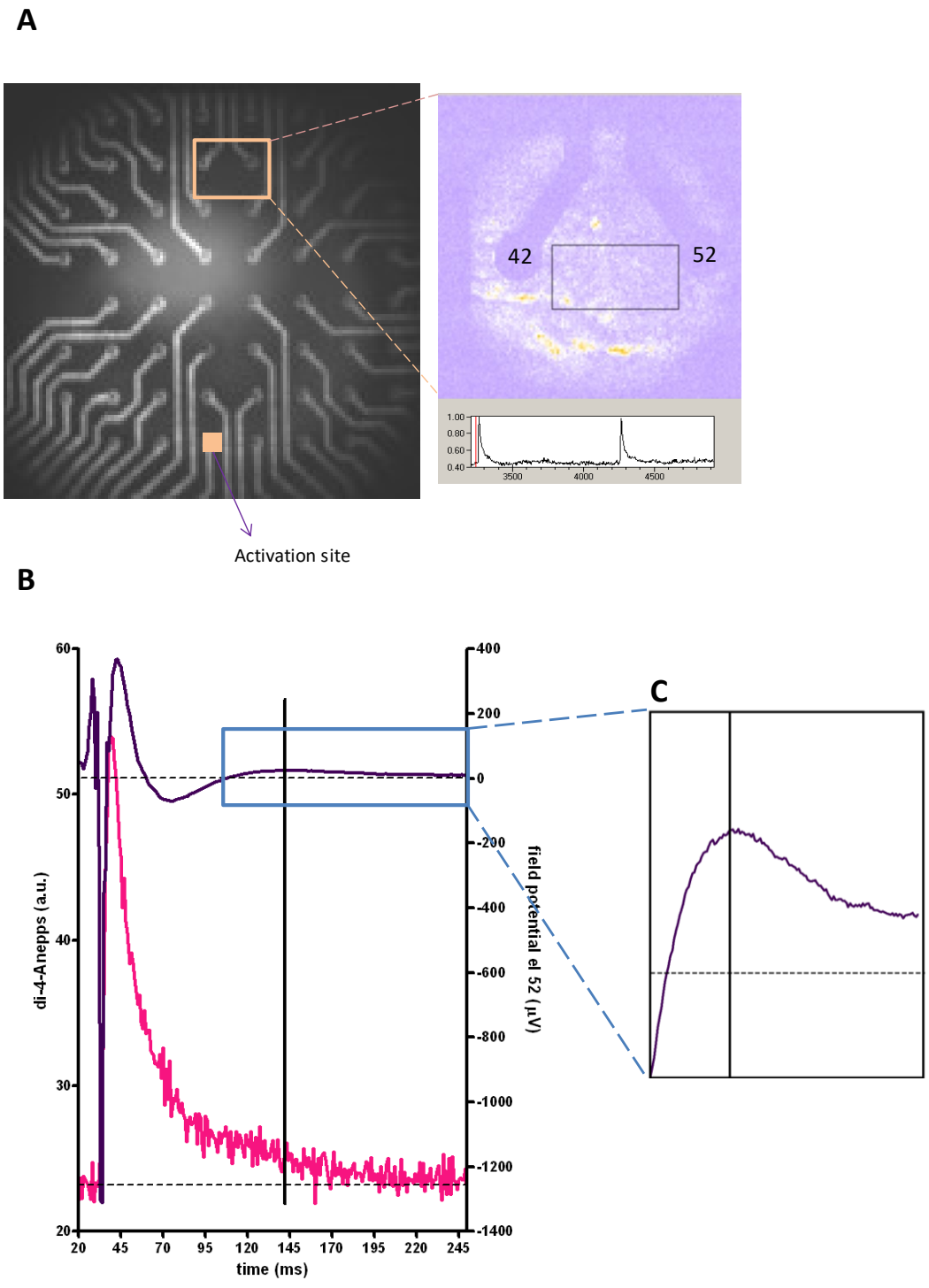


**Figure 2.8: Dual action and field potential recording in LV slice.**

A) Image of the 60 electrodes area of the MEA dish highlighting the area that optically mapped (between electrodes 42 and 52), to recorded APs. B) Representative trace showing AP at 90% repolarization is comparable to the repolarization peak in FP recorded at electrode 52. C) the inset shows a close up image of the FP repolarization peak.

## 2.11. Cryosectioning of slices for structural measurements

Following electrophysiological measurements, each slice was washed with a phosphate buffer saline (PBS) and was blotted with tissue. The slice was cut into two halves. One was rapidly frozen in liquid nitrogen for protein studies and the other half for histological experiments.

The slice was embedded in a Tissue-Tek® O.C.T compound (Sakura,Germany) between two microscopic slides forming a sandwich to flatten the slice. This sandwich was immersed in dry ice cold iso-pentane to allow slow freezing and was left for a total of 6 min. This technique, therefore, prevents the slice from cracking. Cryosections were cut using a cryostat (ThermoShandon) at -20°C. The frozen slice was then embedded onto the specimen holder using an OCT compound. The surface of the slice was then shaved to give a smooth surface and three sister sections were cut and mounted onto SuperFrost slides (Menzel-Glaser, Germany). Slides were then stored at −80 °C until use.

## 2.12. Staining to assess fibrosis in cardiac slices

In order to stain for fibrosis, 10 μm thick sections were washed with xylene and then with gradual concentrations of ethanol before being hydrated in water. Each section was then incubated with picrosirius red (PSR) for 35 min in order to determine the amount of interstitial myocardial fibrosis. Slides were washed briefly with distilled water and were rapidly dehydrated in an ascending series of ethanol, cleared in xylene and mounted in DPX (all from VWR).

Two sections were observed and the best one was entirely imaged using a light microscope (Nikon Eclipse, TE200) at a 10x magnification. Fibrosis was measured using Imagej software. For technical causes, a whole section analysis was not possible due to stain artefacts at the edges and holes within the section, which could, in turn, give positive false results. For that, a grid of about 12x12 mm was applied to the image. A minimum of 10 of the 12x12 squares were selected and analysed separately. The colour threshold tool in Imagej was used and the RGB filter was

selected to calculate the percentage of fibrosis in each square. The red and blue channels were set to zero and only the green channel was adjusted to represent the amount of fibrosis in each square. The percentage of fibrosis in each square was then fully recorded and the percentage of fibroses calculated from all small squares was averaged; therefore, providing an overall percentage of fibrosis in each section.

## 2.13. SDS-PAGE and western blotting to study protein expression

SDS-PAGE and western blotting were used to separate and quantify protein levels. The mixture of proteins carrying a negative charge travels to the positive site of the gel through gel electrophoresis, and the separation was based on the molecular weight and type. The separated molecules were then transferred to a membrane producing a band for each protein and were incubated with label antibodies specific to the protein of interest. The bound antibodies were then detected using several detection methods.

### 2.13.1. Sample preparation

One half of the slice was used to extract the protein for western blotting. The frozen slice was then weighted and homogenised in liquid nitrogen using a pestle and mortar, and the protein powder was rapidly transferred to an eppendorf tube containing a lysis buffer ($SB_{20}$). The sample was then mixed to ensure all the powder was contained within the lysis buffer. The sample was then left for 30 min at room temperature. Slice lysates were vortexed and then sonicated (LSL sonicator, Heat systems-Ultrasonics, Inc) at high power for approximately 10 seconds to shear the genomic DNA and reduce viscosity. The solution was then centrifuged at 15000 rpm for 30 minutes to remove any remaining tissue particles. To finish, supernatant was removed from the pellet and aliquoted to prevent several freeze-thaw cycles of the sample.

### 2.13.2. Protein quantification

Lysates were quantified for protein content using the Pierce$^{TM}$ BCA protein assay kit (Thermo Scientific, USA). This kit is based on the reduction of $Cu^{2+}$ to $Cu^{+}$ by proteins in an alkaline medium (the biuret reaction) and a colorimetric detection of $Cu^{+}$ using a reagent containing bicinchoninic acid. A standard curve prepared from series dilutions of a known protein concentration was then used to calculate the unknown protein concentration in the samples.

Samples were then diluted a ratio of 1:20 (v/v) with dH2O. For the standard curve, however, the standard provided with the kit for the 2 mg/ml BSA was used to prepare serial dilutions from 20-2000 µg/ml, including a blank of 0 µg/ml. As a result, all dilutions were prepared in the lysis buffer $SB_{20}$.

For each assay, a 25 µl sample or standard was added to 200 µl of the supplied working solution (mixing 50 part of reagent A with 1 part of reagent B) in a 96-well plate. Samples were mixed and incubated at 37°C for 30 min. Absorbance of each well was then read at 560 nm.

First, the standard curve was generated by plotting the protein concentration of the standard to the sample absorbance after subtracting the blank values from all absorbance values. Then, the protein concentration of each sample was measured from the standard curve.

### 2.13.3. Sample preparation for SDS- PAGE separation

Samples were prepared to a desired concentration into the loading buffer and incubated for 45 minutes at 37ºC to ensure complete protein denaturation. In addition to the SDS in the loading buffer, the bromophenol blue (Sigma) loading dye was added to enable visualisation of the migration of proteins while they move through the gel. A reducing agent (2-mercaptoethanol (Sigma)) was also added into the loading buffer to break all the disulphide bridges formed in the proteins.

### 2.13.4. Gels casting

In order to separate proteins in denaturing conditions, SDS-Polyacrylamide gels were prepared. Polyacrylamide gels are formed from the polymerisation of acrylamide and N,N-methylenebisacrylamide (Bis), which is a cross-linking agent for the gels. This polymerisation process is primarily initiated by the addition of ammonium persulfate (APS) along with N,N,N',N'-tetramethylethylenediamine (TEMED). SDS, on the other hand, was present in all gels and buffers to ensure the proteins retain a rod-like structure during migration. Furthermore, the molecular mass of the targeted protein determines the percentage of acrylamide and the degree of cross-linking needed. The top layer of the gel is a stacking layer which allows for the formation of a thin, sharply defined band to separate it from the lower level, which, in turn, improves the overall resolution.

Gels were prepared by pouring the mixture between two glasses using the Hoefer mini gel system. Approximately 3.5 cm at the top was left for the later addition of the stacking gel. The separating gel was layered with 1 ml of propan-2-ol on top of each gel to flatten it. The gel was left to set for 45 min and then propan-2-ol was washed with dH2O. A 4.5% stacking gel mixture was then poured on the top of the separating gel and an 18-well comb was inserted. Gels were then left to polymerise for 45 min before use.

Following this, the gels were transferred to the Hoefer gel running apparatus (Mighty Small II SE250/SE260) and the 18-well comb was carefully removed. A 1x running buffer was then poured into the gel running apparatus covering the loading area on the top of the gel. A 15 µl sample was loaded in to each well and the molecular weight was diluted into a 10 µl loading buffer (Precision Plus Protein Kaleidoscope standards, Bio-Rad). The remaining empty wells were then loaded with a loading buffer and the gel was run twice, one at 60V till the proteins reached the separate gel level and then at 180V. The running was stopped when the bromophenol blue reached the bottom of the gel.

### 2.13.5. Protein transfer

Polyvinylidene fluoride (PVDF) membranes (Millipore) were used for electrophoretical protein transfer. The membrane was cut exactly to the same size of the gel and was soaked with methanol for 5 min. Being shaken for 1 h, the membrane was then transferred into a buffer to activate it and furtherly transferred using the wet transfer method (Bio-Rad). The gel and membrane were then sandwiched between pre-wetted sponges and paper in a transfer buffer in the following order: Sponge/paper/gel/membrane/paper/sponge. This was done after ensuring that no air bubbles had formed between them. The sandwich was submerged in a transfer tank containing a pre-cooled transfer buffer with a cooling block, therefore, allowing for the protein transfer to be powered at 100V for 1.5 hours at 4°C.

### 2.13.6. Protein blotting

The PVDF membrane was removed from the transfer set up, rinsed in dH2O and then incubated for 1 hour at room temperature in blocking solution. The membrane was then incubated overnight at 4°C with the primary antibody diluted in a blocking solution. As well as this, the membrane was washed 5 times for 10 min each with a TBS-Tween buffer to remove any unbound primary antibody. Alkaline phosphatase-conjugated secondary antibodies were then added to the membranes and were incubated for 1 hour. Furthermore, washing the membrane also ensured that the tween was removed, therefore, preventing the smearing effect of the insoluble precipitate.

At room temperature, the protein bands were allowed to develop within 45 min of using an alkaline phosphatase buffer containing 165 µg/ml 5-bromo-4-chloro-3-indolyl-phosphate (Promega, USA) and 330 µg/ml nitro-blue-tetrazolium (Promega, USA). The reaction was terminated by washing the membranes in dH2O and dried between two sheets of tissue paper. Table 2.1 illustrates the primary and secondary antibodies specification used in this work.

**Table 2.1: Primary and secondary antibodies used in western blot studies**

| Targeted protein | Protein load | Primary antibody | Dilution | Secondary antibody | Dilution |
|---|---|---|---|---|---|
| Connexin 43 | 0.125µg | Polyclonal anti rabbit (Sigma, Cat. No. C6219) | 1:1500 | Alkaline phosphatase-conjugated donkey anti-rabbit (Pierce, Cat. No. 31345) | 1:1000 |
| $Na_v1.5$ | 5µg | Polyclonal anti rabbit (alomone, Cat. No. ASC-005) | 1:500 | Alkaline phosphatase-conjugated donkey anti-rabbit (Pierce, Cat. No. 31345) | 1:1000 |
| Actin | 0.25µg | Polyclonal anti Goat (Santa Cruz Biotechnology, Cat. No. sc-1616) | 1:1000 | Alkaline phosphatase-conjugated rabbit anti-goat (Pierce, Cat. No. 31300) | 1:1000 |

Membranes were scanned using a GENE Genius imager and Genesnap software (Syngene, UK), and digital images were recorded. The optical density of the bands was then measured using Sigma gel (Jandel Scientific).

## 2.14. Statistical analysis

Statistical analysis was carried out using GraphPad Prism 5 software (GraphPad Software Inc., USA). Data are represented as a mean ± standard error of the mean. Analysis of a pair of data sets was performed using unpaired t-tests. The one-way ANOVA, followed by the Tukey's post-hoc test, was used for comparisons between more than two groups.

$P<0.05$ was taken as significant and on graphical representation of data, one star indicates $p<0.05$, two stars indicates $p<0.01$ and three stars indicates $p<0.001$.

## 2.15. Solutions

The following solutions were used throughout this work. They are described in mM unless stated otherwise. All chemicals were provided by VWR international or Sigma Aldrich. The solutions were made up in dH2O. Fresh solutions were made when required and used for a maximum of 2 weeks.

**Normal Tyrode (NT):** 140 NaCl, 6 KCl, 10 glucose, 10 HEPES (free acid), 1 MgCl2, 1.8 CaCl2; pH 7.4

**Normal Tyrode + heparin (NT+H):** 140 NaCl, 6 KCl, 10 glucose, 10 HEPES (free acid), 1 MgCl2, 1.8 CaCl2, 100unit/ml heparin; pH 7.4

**Normal Tyrode +BDM (NT+BDM):** 140 NaCl, 6 KCl, 10 glucose, 10 HEPES (free acid), 1 MgCl2, 1.8 CaCl2, 10 2,3-butanedione monoxime; pH 7.4

**Recording solution:** 140 NaCl, 4.5 KCl, 10 glucose, 10 HEPES (free acid), 1 MgCl2, 1.8 CaCl2; pH 7.4.

**Optical mapping recording solution:** 140 NaCl, 4.5 KCl, 10 glucose, 10 HEPES (free acid), 1 MgCl2, 1.8 CaCl2, 10μM Blebbistatin; pH 7.4

**Solubilisation buffer (SB20):** 20% SDS w/v, 0.1M Tris, 10 ethylenediaminetetraacetic acid (EDTA); pH 6.8

**Loading buffer:** 96.5% SB20, 2.5% 2-mercaptoethanol, 1% bromophenol blue

**1X running buffer:** 0.192 glycine, 25 trizma base, 0.1% SDS.

**Transfer buffer:** 192 glycine, 25 trizma base, 10% methanol, 0.01% SDS

**Blocking solution:** 20 tris, 150 sodium chloride, 0.1% tween20, 4% non-fat dried milk; pH 7.6

**Tris-buffered saline Tween (TBS-Tween):** 20 tris, 150 sodium chloride, 0.1% tween20; pH 7.6

**Tris-buffered saline (TBS):** 20 tris, 150 sodium chloride; pH 7.6

**Alkaline phosphatase buffer:** 100 tris, 100 sodium chloride, 5 magnesium chloride; pH 9.5

# CHAPTER 3. Electrophysiological remodelling of myocardial slices from rat hearts undergoing mechanical unloading

## 3.1. Introduction

Cardiac electrophysiological remodelling has been studied extensively in human and animal models of cardiac disease, and aims to understand the mechanisms underlying these pathological changes. Thus, targets more specific therapeutic approaches. Many of these studies have mainly used cultured or isolated myocytes, but these are unsuitable for the investigation of multicellular events such as cardiac conduction and pharmacological responses. On the other hand, available multicellular preparations, such as Langendorff-perfused whole hearts or arterially-perfused tissue wedges, are limited to specific regions of the heart or suffer from poor oxygenation.

The development of the myocardial slice technique, however, overcomes many of these limitations and (Bussek et al. 2009; Bussek et al. 2012a; de Boer et al. 2009; Camelliti et al. 2011) enables the in-depth study of structural and functional interactions from the same preparation. In addition, they are becoming increasingly popular as model systems for cardiac electrophysiology and pharmacology research by showing more *in vivo*-like profiles than other 2D or single cell models (Wang et al. 2014; Wang, Lee, Gary R Mirams, et al. 2015).

In this part of the project, we have obtained slices from a HAHLT rat model, a model used in cardiovascular research to mimic the effect of left ventricular assist devices (LVAD). These devices are used in patients with end-stage heart failure to support heart function while waiting for a heart transplantation. A moderate degree of mechanical unloading, therefore, induces positive effects on the myocardium (Ibrahim & Yacoub 2014; Terracciano et al. 2010). However, prolonged mechanical unloading deteriorates cardiac function and is detrimental to cardiac recovery (Oriyanhan et al. 2007; Soppa et al. 2008; Ibrahim et al. 2010). Several studies have used isolated cardiac myocytes obtained from normal or failing hearts undergoing mechanical unloading in order to understand the effect of atrophy on cardiac function (Ibrahim, Kukadia, et al. 2012; Ibrahim, Navaratnarajah, et al. 2012; Navaratnarajah et al. 2013; Soppa, Barton, et al. 2008; Soppa, et al. 2008). These functional studies were primarily focused on

contractility and the $Ca^{2+}$ handling of isolated myocytes. However, little is known about the effect of mechanical unloading on myocardial excitability and conduction at a multicellular level. Here we aim to use slices obtained from normal hearts which underwent mechanical unloading for 8 weeks. This was done in order to study the effects of prolonged mechanical unloading and cardiac atrophy on FPD, CV and transmural changes within the LV wall.

## 3.2. Methods

### 3.2.1. Animal model

HAHLT was used to mechanically unload the heart. As a result, heart and lungs from donor rats were harvested and then transplanted by single anastomosis from the donor aorta to the abdominal aorta of the recipient, as described in chapter 2 section 2.2.3. After 8 weeks, the heart was harvested and the recipient heart was used as a control.

### 3.2.2. Morphometric analysis

The measurements of heart weight to body weight ratios were recorded to confirm atrophy, as described in chapter 2 section 2.1.

### 3.2.3. Slices preparation

Slices were prepared from each animal for each group, as described in chapter 2 section 2.5. The mechanically unloaded hearts were handled with care as they are relatively small and very fibrotic. Hence, cutting slices from them can be difficult.

### 3.2.4. MEA recording and analysis

Extracellular field potentials from slices were assessed during electrical stimulation using the MEA system as described in chapter 2 section 2.6 and 2.7. We have obtained MEA recordings from six slices at least per heart. The slices used in the MEA recordings were selected to cover

the different regions of the LV after knowing the total number of slices obtained. For transmural analysis, we have recorded at least from two slices from each region starting from Epi to Endo as described in chapter 2 section 2.7.3.

The MEA recording allowed analysis of:

- Field potential duration and heterogeneity in the field potential duration within each slice.
- Longitudinal and transverse conduction velocity and the heterogeneity in conduction velocity.
- The transmural distribution in the LV of field potential duration and conduction velocity.

Figure 3.1 is a schematic of the experimental protocol. The number of animals and slices used for each experiment is different and is detailed in each figure legend.

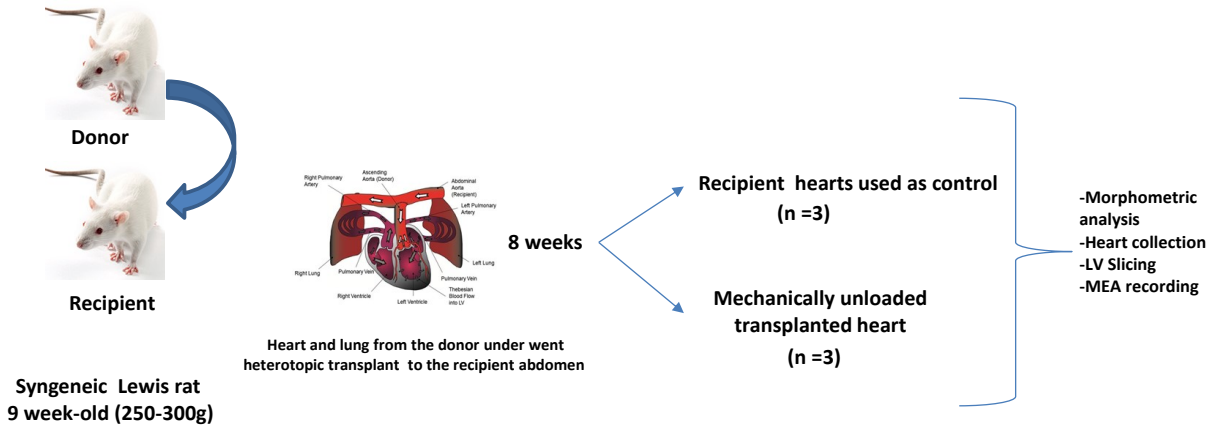


**Figure 3.1: Schematic representation of the experimental protocol used in this chapter.**

The heterotopic abdominal heart and lung transplantation (HAHLT) procedure was used to mechanically unload the left ventricle of Lewis rats.

## 3.3. Results

### 3.3.1. Mechanical unloaded rat hearts show atrophy

Heart weight to body weight ratio was measured in order to assess the effect of unloading on heart size. Hearts in UL were smaller at eight weeks compared to the control (Figure 3.2, A). Figure 3.2, B shows a representative image obtained from the UL, whereby the control heart demonstrated a reduced size of UL hearts compared to the control.

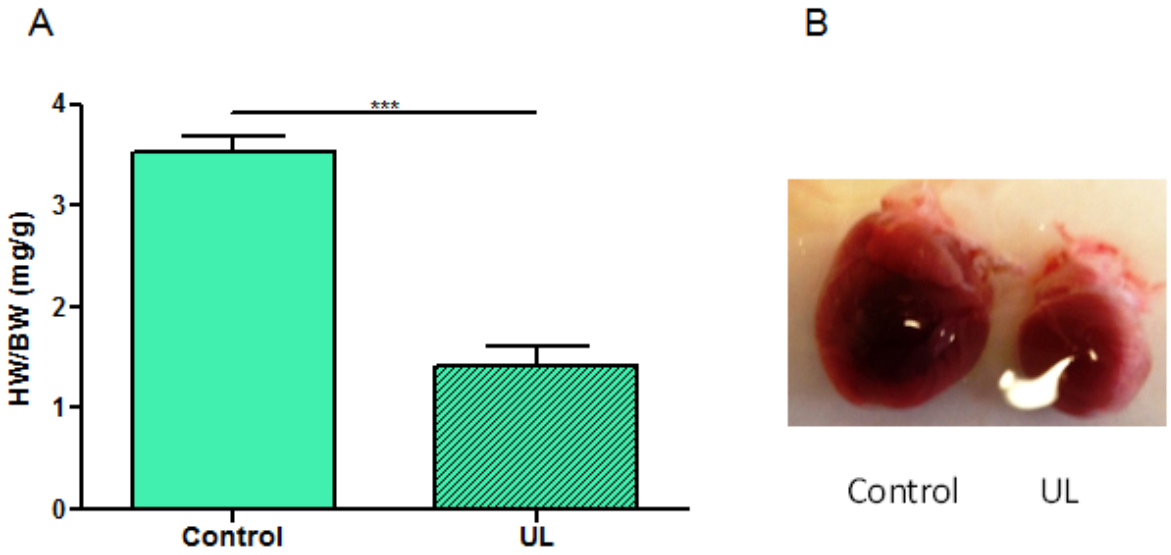


**Figure 3.2: Morphometric analysis of mechanical unloaded hearts.**

A) Heart weight to body weight ratio was decreased in 8 weeks mechanical unloaded hearts compared to control. B) Representative image showing mechanical unloaded heart is smaller in size than the control. (n=hearts): control n=3; UL n=3 (unpaired t-test).

### 3.3.2. Field potential duration changes in rat slices from mechanically unloaded hearts.

MEAs were used to evaluate the electrical properties within the myocardial slices and FPD was significantly prolonged in UL at eight weeks compared to the control (Figure 3.3, A). Hence, the standard deviation of the FPD was increased in UL compared to the control (Figure 3.3, B).

To assess the effect of stimulation frequency on FPD, slices from UL were paced at different pacing frequencies. FPD was also prolonged in UL compared to the control at all pacing frequencies. UL slices show a less negative response to a faster frequency and FPD was the shortest at fastest rate (Figure 3.3, C).

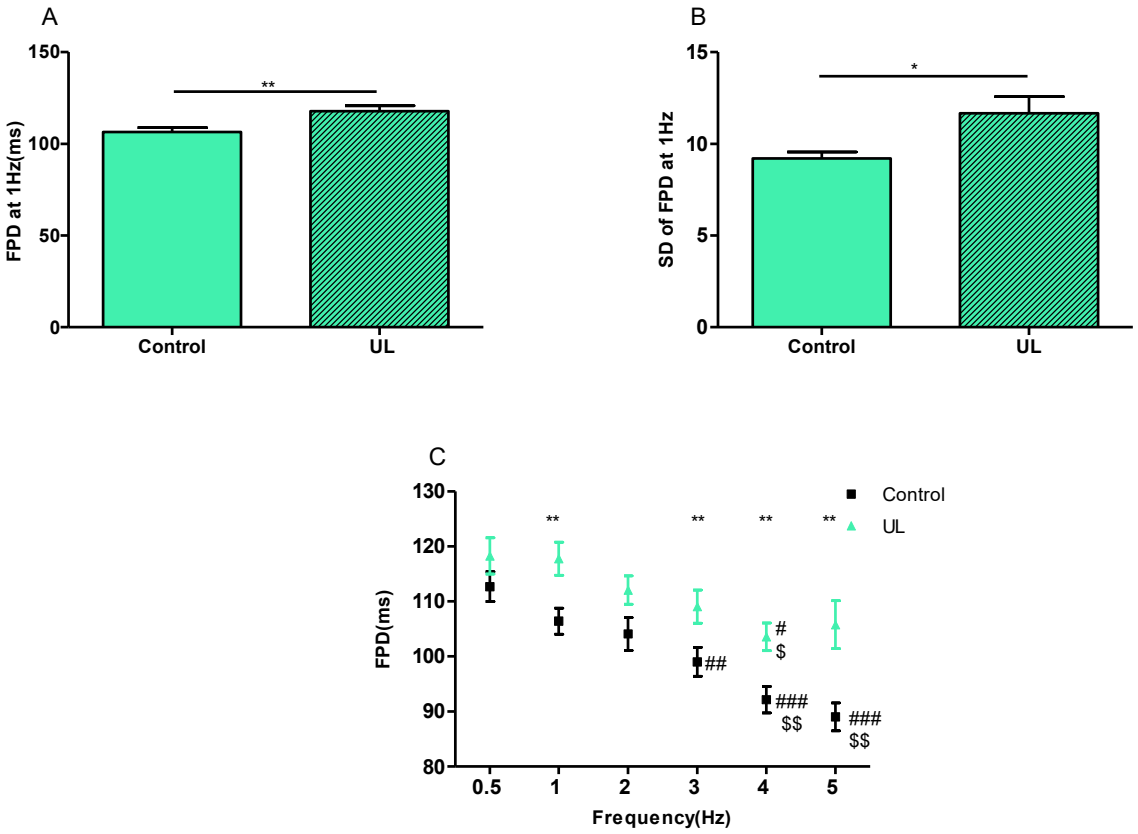


**Figure 3.3: Field potential duration measurements in mechanically unloaded slices.**

A) The FPD in UL was longer compared to control at 1 Hz. B) the standard deviation of field potential duration at 1 Hz within each slice was higher in UL compered to control. C) FPD in UL was longer as well at other pacing frequencies compared to control (using unpaired t-test). FPD was significantly shorter at 3,4,5Hz vs 0.5 and 1 Hz in control group and was significantly shorter at 4Hz vs 0.5 and 1Hz in mechanical unloading group (using one-way ANOVA,followed by Tukey's post hoc test). (n=slices/hearts) 8 weeks: Control n=13/2 ; UL n= 10/2. # vs 0.5Hz and $ vs 1 Hz within the same group.

### 3.3.3. Field potential duration transmural distribution in rat slices with mechanically unloading

FPD was measured from slices obtained from the epicardium, myocardium and endocardium to investigate the heterogeneity of FPD across the LV.

UL hearts show longer a FPD at the mid-myocardium and no change in FPD transmural within the control and UL groups (Figure 3.4).

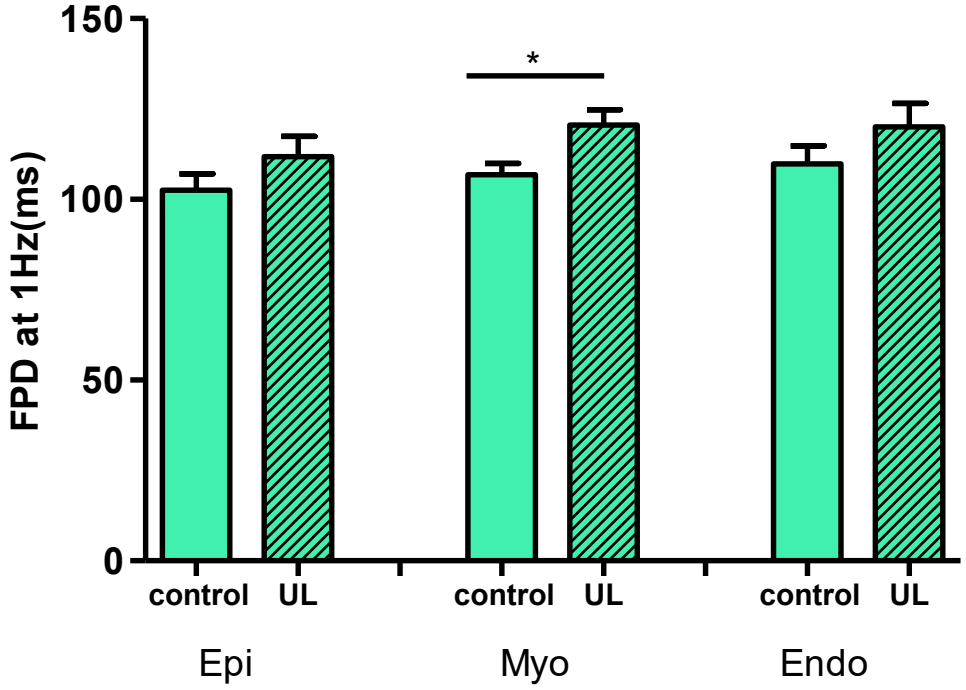


**Figure 3.4: Field potential duration in slices obtained from the Epi, Myo, and Endo regions of the left ventricular free wall in mechanical unloaded hearts.**

FPD was longer in 8 weeks of mechanical unloading in the myocardium compared to control (using unpaired t-test).

(n=Epi,Myo,Endo slices/hearts) 8 weeks: Control n= 4,5,4/2; UL n=3,4,3/2.

### 3.3.4. Conduction velocity changes in rat slices subjected to mechanical unloading

Total CV was determined by averaging the CV obtained from the four points of each slice recorded at 1 Hz. $CV_L$ was the CV along the fibre orientation of the myocardial slice which represent the highest conduction velocity. $CV_T$ is the CV perpendicular to the fibre orientation of the slice which represents the lowest CV.

There was no change in CV, $CV_L$, $CV_T$ and the anisotropic ratio (AR) = ($CV_L$ / $CV_T$) in the UL group compared to the controlled animals (Figure 3.5).

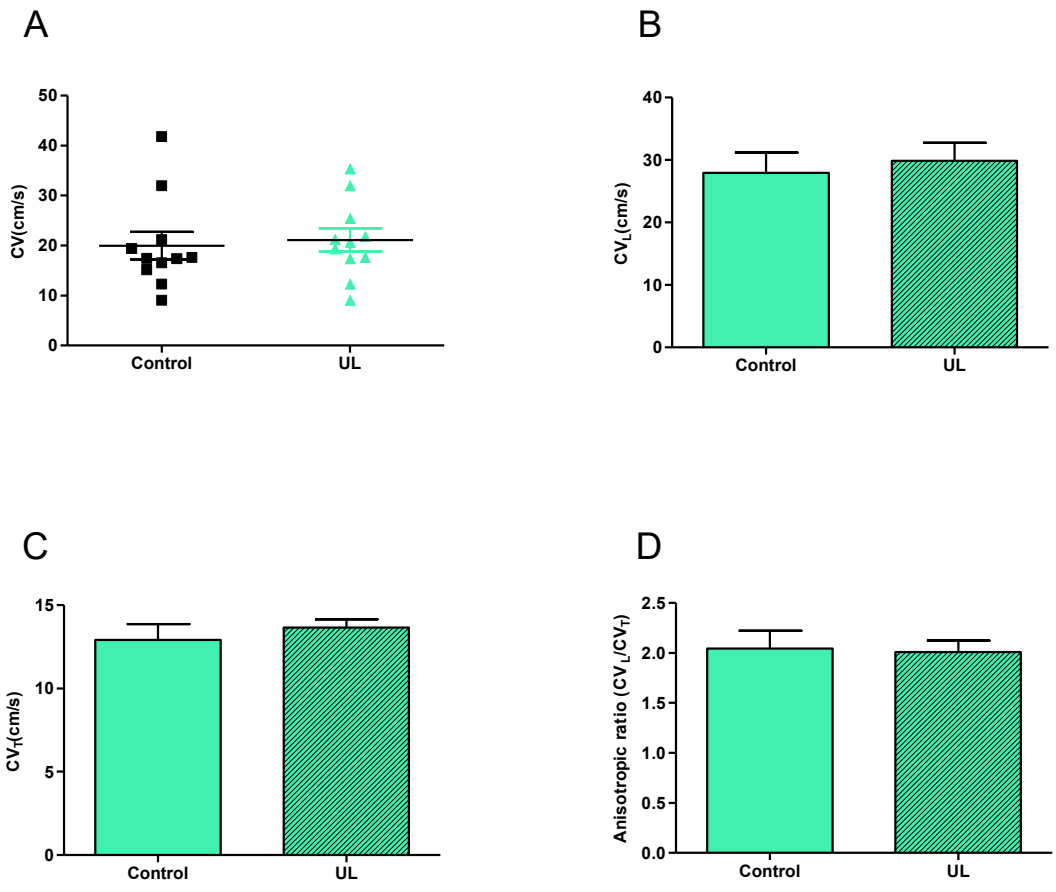


**Figure 3.5: Conduction velocity and Anisotropy in slices in mechanical unloaded rats.**

A) Scatter plot of CV from UL show no change in CV compared to control. B) $CV_L$ and $CV_T$ were not changed in UL compared to control. B, C). D) Anisotropic ratio was unchanged in UL compared to control. (n=slices/hearts) 8 weeks: control n= 13/2; UL n= 11/2 (unpaired t-test).

### 3.3.5. Conduction velocity transmural distribution in rat slices with mechanically unloaded

In order to test the changes in heterogeneity in conduction, conduction velocity was measured from slices at different transmural layers spanning from the epicardium to the endocardium. There were no significant changes in transmural CV in the UL group compared with control group (Figure 3.6).

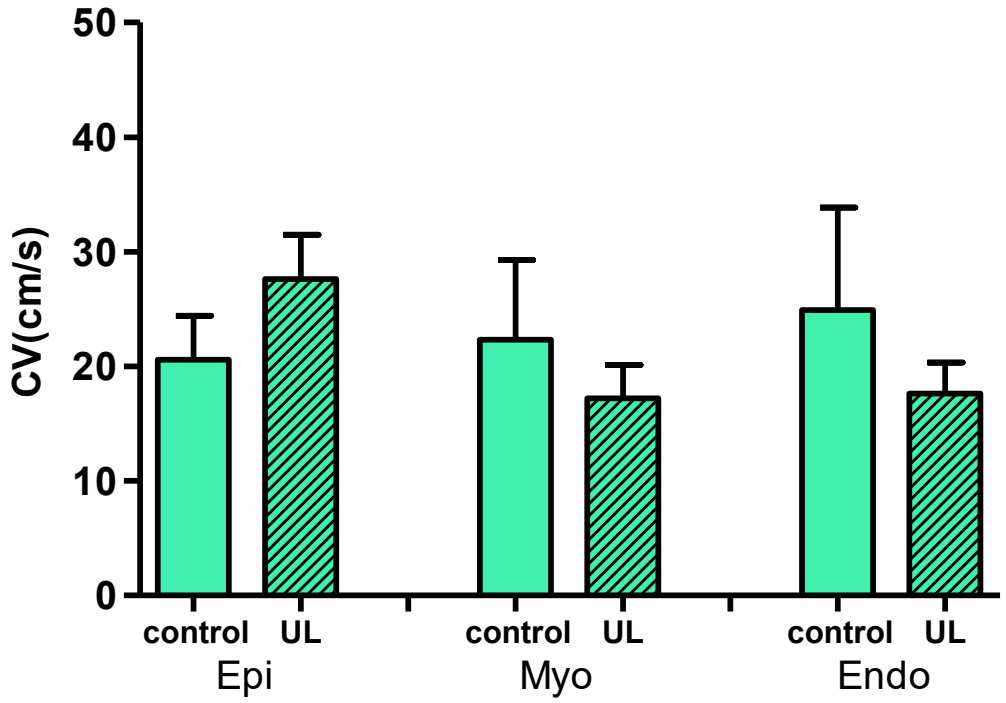


**Figure 3.6: Conduction velocity measured from slices of different transmural layers spanning from Epi to Endo in mechanical unloading hearts.**

No difference in CV transmural distribution was observed between mechanically unloaded and control slices. (n=Epi,Myo,Endo slices/hearts) 8 weeks: Control n= 4,4,4/2; UL n=4,4,3/2.

## 3.4. Discussion

This chapter has demonstrated that slices obtained from normal rat hearts, that are chronically unloaded, have developed atrophy at a whole heart level with disrupted action potential morphology and preserved conduction properties. In particular, we have shown that chronic mechanical unloading induces atrophy in normal hearts. As well as this, FPD was longer in the unloading group when compared to the control group at all different pacing frequencies. Furthermore, FPD was shorter with faster pacing in both the UL and control groups, and that FPD was heterogeneous within slices in the UL group. There was also a longer FPD at the mid-myocardium in the UL compared to control group. Finally, no changes in CV and transmural CV were observed.

### 3.4.1. Chronic mechanical unloading induced myocardial atrophy

Cardiac atrophy is generally defined as the reduction in size below the normal range or under the starting, pre-disease value. Unloading-induced cardiac atrophy is a common phenomenon in human patients during LVAD support (Terracciano et al. 2004) and in animal models of unloading (Ibrahim et al. 2010; Ibrahim, Kukadia, et al. 2012; Ibrahim, Navaratnarajah, et al. 2012; Ito et al. 2003; Soppa et al. 2008; Liu et al. 2015). This was, therefore, observed in both normal (Korecky & Masika 1991; Ibrahim et al. 2010; Soppa et al. 2008; Ibrahim, Kukadia, et al. 2012; Liu et al. 2015) and failed (Oriyanhan et al. 2007; Ibrahim et al. 2012) mechanically unloaded hearts.

Here, we have measured heart weight after partial unloading for 8 weeks and, in agreement with previous studies, we have demonstrated that chronic mechanical unloading in normal hearts is associated with myocardial atrophy (Brinks et al. 2009; Didié et al. 2013; Soppa et al. 2008; Tang-Quan et al. 2010; Ito et al. 2003; Ibrahim et al. 2010; Welsh et al. 2001; Muranaka et al. 2010). Although cell size has not been measured in this study, cell volume was measured

previously in our lab at the same time-point (8 weeks) and model and it show that there is a reduction in the cell volume after the process of unloading (Ibrahim, Kukadia et al. 2012).

Although the term suggests a functional deterioration, improvements in cardiac function after LVAD support were found to be independent to the overall degree of atrophy. This means that cells of a normal size can be dysfunctional, while slightly smaller cells do not always show dysfunction when associated with the functional improvement in failing hearts after unloading (Terracciano et al. 2004). Furthermore, Ibrahim et al. showed that the degree of reduction in LV weight and cell volume was linked to the level and duration of mechanical unloading with a maximum reduction at 8 weeks of complete mechanical unloading (Ibrahim, Kukadia, et al. 2012). Therefore, the degree of atrophy depends on the degree and duration of unloading and is not deterministic of cell function.

### 3.4.2. Prolonged mechanical unloading increases the duration and the dispersion of FPD in normal hearts

Clinical studies have shown that mechanical unloading of failing human hearts is of functional importance for the recovery of cardiac pump function (Menon et al. 1998; Müller et al. 1997). This functional improvement after unloading has been also been observed at a cellular level in failed cardiomyocytes from both human and animal models (Harding et al. 2001; Ibrahim, Kukadia, et al. 2012; Terracciano et al. 2009; Soppa et al. 2008). This includes cell excitability, $Ca^{2+}$ handling and contractility. However, this diminished after prolonged mechanical unloading and when the recovery was insufficient for the device explanation in most patients (Maybaum et al. 2007; Mancini et al. 1998).

Mechanical unloading in a failing myocardium has shown to be associated with electrical reverse remodelling in action potentials. In a study conducting ECG analysis before and after LVAD support, both early and delayed effects on the QT interval, a global measurement of repolarisation , have been observed (Harding et al. 2001). At the time of LVAD implantation, the

QT interval and the QTc were increased. In agreement, APD was also prolonged in failed cardiomyocytes after one week of mechanical unloading in a rat model (Soppa, Lee, Stagg, Felkin, et al. 2008). However, QTc did decrease after prolonged unloading. This was confirmed in isolated myocytes where a shortening in action potential duration after LVAD placement was observed (Harding et al. 2001). In another study, in patients with LVAD support, there was a strong correlation between QTc shortening and an increase in LV ejection fraction. As well as this, there was also a decrease in LV filling pressures suggesting that shortening of the action potential duration likely contributes to an improved cellular contractile performance observed after sustained LVAD support (Drakos et al. 2011). However, studies on mechanisms underlying changes in APD after prolonged mechanical unloading show a lacking contribution to impaired function. Thus, we have tested the effect of prolonged mechanical unloading (8 weeks) on myocardial excitability of normal hearts by measuring the duration of extra cellular field potential in myocardial slices. Primarily, we found a prolongation of FPD at all pacing frequencies. In an animal model of LVAD, Ibrahim et al showed no change in APD in normal isolated cardiomyocytes after 4 weeks of mechanical unloading (Ibrahim et al. 2010), despite both cardiomyocyte $Ca^{2+}$ handling and structural changes (Ibrahim et al. 2010; Ibrahim, Kukadia, et al. 2012). Additionally, they also showed that changes in the $Ca^{+2}$ handling and T-tubules structure are load and duration sensitive (Ibrahim, Kukadia, et al. 2012).

In another study, testing different intensities of mechanical unloading, Liu et al showed that changes in the structural and functional parameters are, in fact, load related (Liu et al. 2015). Therefore, we suggest that the changes we have observed in FPD are also due to the level and duration of unloading. Further investigations should be performed to test more time points and a wider variety of unloading levels.

Furthermore, ventricular arrhythmias (VAs) were found to be increased and this was thought to correlate to the prolongation of QT intervals at the time of LVAD implantation. It was also found that arrhythmias decreased in patients with a decreased QT after sustained LVAD (Harding et al. 2001; Bedi et al. 2007). Although we have not induced and measured arrhythmias, we have found that the dispersion in FPD (as a function of FPD standard deviation) was higher in the mechanically unloaded slices compared with the control. This, therefore, suggests that the mechanical unloading slices are possibly more susceptible to arrhythmias and that further studies are needed to elucidate any underlying mechanisms.

In physiological conditions, the epicardium has a shorter APD than the endocardium and mid-myocardium, whereby cells from the mid-myocardial region prolong more than other cell types in response to a slowing rate (Antzelevitch 2005).

Transmural dispersion of repolarisation across the ventricle wall has been suggested to play an important role in arrhythmogenesis of HF (Akar 2010). This heterogeneity creates an electrophysiological substrate to the intramural conduction block and the genesis of transmural re-entrant circuits results in polymorphic ventricular tachyarrhythmia (Fadi G. Akar & Rosenbaum 2003). Transmural dispersion of repolarisation has been tested in many animal and human models of heart failure. In humans, two studies have shown that transmural APD gradients were reduced in HF compared to non-failing hearts. This was because of APD prolongation in the epicardium and the midmyocardium (Ng et al. 2014; Glukhov et al. 2010). On the other hand, the transmural APD gradient was increased in the canine LV wedge with HF (Fadi G. Akar & Rosenbaum 2003).

Here, we have tested the transmural dispersion of FPD as there is little known about its role in enhancing arrhythmias after LVAD support. We have found that FPD at the mid-myocardium is longer when compared with the other regions. Further investigations are needed to understand

the mechanisms underlying this finding which includes testing transmural FPD dispersion at more time points with different levels of unloading in both normal and failing hearts.

### 3.4.3. Mechanical unloading does not affect conduction velocity.

As noted previously, the conduction velocity is seen to change after the LVAD but the mechanisms underlying these changes remain unknown. However, changes in the gap junctional protein Cx43 was found to correlate with changes in conduction and induce arrhythmias (Poelzing & Rosenbaum 2004). Studies in patients after the LVAD insertion show Cx43 was downregulated in the hearts of patients who had LVAD and who developed ventricular arrhythmias, whereas the expression of Cx43 was unchanged in patients who did not display ventricular arrhythmias (Refaat et al. 2008). In addition, to this, the increased level of fibrosis in HF has been shown to change conduction by blocking the normal electrical flow and set up re-entry circuits, therefore, resulting in arrhythmias (Massare et al. 2010). The effects of mechanical unloading on fibrosis are, however, commonly debated. Some reports have shown increased levels of fibrosis (Wohlschlaeger et al. 2005; B. a. Bruckner et al. 2001; B. a. Bruckner et al. 2000) while others have shown a reduction in fibrosis (McCarthy et al. 1995a; Nakatani et al. 1996b; Li, Feng, McTiernan, Pei, Moravec, Wang, Rosenblum, Kormos & a M. Feldman 2001). As a result, we have measured the speed and the transmural change of conduction in slices after mechanical unloading, and found there was no change in the conduction velocity compared with the control group. Thus, this suggests that the structural changes obtained by mechanical unloading in our setting may be insufficient to cause changes in CV. Meaning, further investigation is needed. For example, measuring the level of fibrosis and Cx43 expression and distribution may help to elucidate the underlying mechanisms.

## 3.5. Summary

In this chapter, we have studied changes in electrophysiological parameters and conduction velocity in rat slices after mechanical unloading. From our research, we have been able to produced slices from hearts after partial mechanical unloading which, when compared with total unloading, may be more clinically relevant. As well as this, we found this to simulate the modality of LVAD unloading in patients. Thus, we have shown an increase in FP duration and dispersion from normal rat hearts after chronic mechanical unloading.

# CHAPTER 4.Electrophysiological remodelling of myocardial slices from rat hearts undergoing thoracic aortic constriction

## 4.1. Introduction

To understand the mechanisms underlying structural and functional changes, cardiac electrophysiological remodelling in hypertrophy and heart failure has been studied intensively in human and animal models of cardiac disease. These changes are complex and includes ion channel remodelling, alterations in calcium handling, remodelling of the extracellular matrix and fibrosis, activation of the sympathetic nervous system and the renin–angiotensin–aldosterone-system, and dilatation and stretch (Coronel et al. 2013).

Studies in hypertrophy and heart failure have mostly been performed on single myocytes, which lack a multicellular level, or on whole animals; which do not provide detailed information on the cellular and molecular processes underlying hypertrophy and heart failure. Cardiac slices obtained from models of hypertrophy and heart failure have, therefore, not been used to investigate electrophysiological events such as conduction and transmural changes at a multicellular level. We have explained the benefit of using this method in detail in chapter 1, section 1.11.1.

In this chapter, we have used LV slices from a TAC model of chronic pressure overload to investigate: 1) FPD and changes in CV in early (10 weeks) and late (20 weeks) models of TAC; and 2) LV transmural changes in FPD and CV.

## 4.2. Methods

### 4.2.1. Animal model

The TAC procedure was used to produce chronic pressure overload in rats at defined time periods of 10 and 20 weeks, as described in chapter 2 section 2.2.2. The two-time points were used to address the effect of disease progression on electrophysiological parameters. Sham operated animals were used as controls for each time point.

### 4.2.2. Echocardiography and morphometric analysis

Heart function was assessed using echocardiography and the measurements of heart weight to body weight ratios were recorded to confirm hypertrophy, as described in chapter 2 section 2.3 and 2.5.

### 4.2.3. Slices preparation

Slices were prepared as described in chapter 2 section 2.6. Approximately eight slices were obtained from each rat left ventricle depending on the size and age of the animal, and each slice as cut at a 300 μM thickness.

### 4.2.4. MEA recordings and analysis

Extracellular field potentials from slices were assessed using an MEA system, as described in chapter 2 section 2.7. For practical reasons, we have obtained MEA recordings from around six slices per heart in order to possibly cover the different transmural regions of the sliced left ventricle. We have recorded at least two slices per Endo, Myo and Epi. This was explained in detail in chapter 2 section 2.10.

Following electrophysiological measurements, each slice was washed with a phosphate buffer saline (PBS), blotted with tissue and cut in half. One was rapidly frozen in liquid nitrogen for protein studies and the other half was used in histological experiments.

The MEA recording allowed analysis of:

- Field potential duration and the heterogeneity in the field potential duration within each slice.
- Longitudinal and transverse conduction velocity and the heterogeneity in conduction velocity.
- Transmural variations in CV and FPD.

Figure 4.1 is a schematic of the experimental protocol.

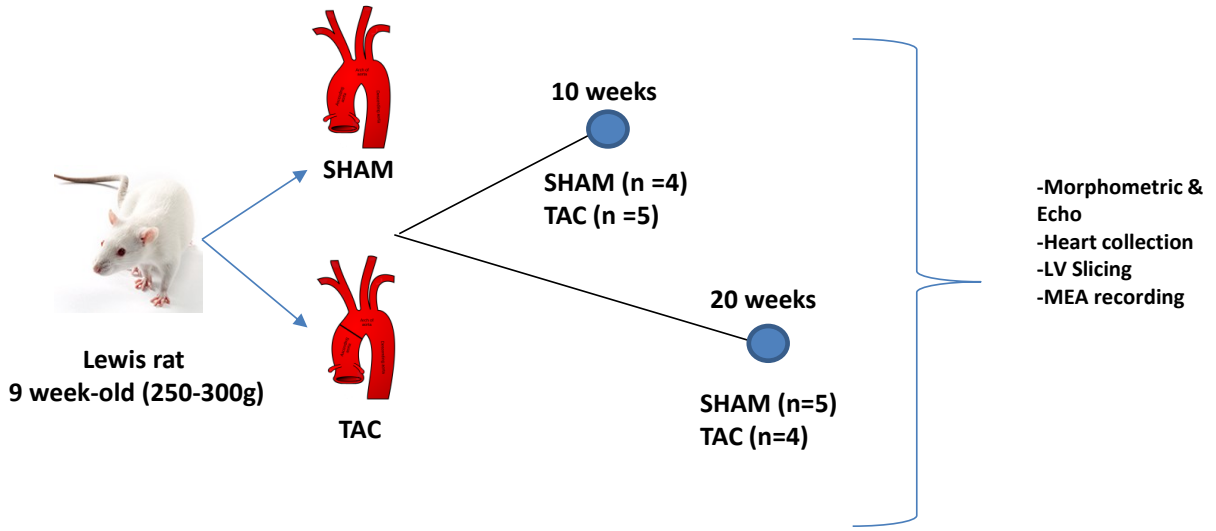


**Figure 4.1: Schematic representation of the experimental protocol used in this chapter.**
TAC was performed in Lewis rats to generate pressure overload of the LV.

## 4.3. Results

### 4.3.1. *In vivo* cardiac function assessment and morphometric analysis in the TAC group

Echocardiography and morphometric analysis was used to confirm cardiac hypertrophy in animal models. Left ventricular posterior wall thickness and ejection fraction were significantly higher in the TAC group compared to the sham group, at both 10 and 20 weeks (Figure 4.2 A, B).

Furthermore, TAC hearts showed a significant increase in the HW:BW ratio, compared to the sham group at 10 and 20 weeks confirming the hypertrophic response (Figure 4.3 C).

The results from the echocardiography and morphometric analysis indicated a compensated hypertrophy whereby the hearts have not yet begun to fail, explaining the maintained increased ejection fraction at 20 weeks compared to the 10 weeks TACs (Wei et al. 2010).

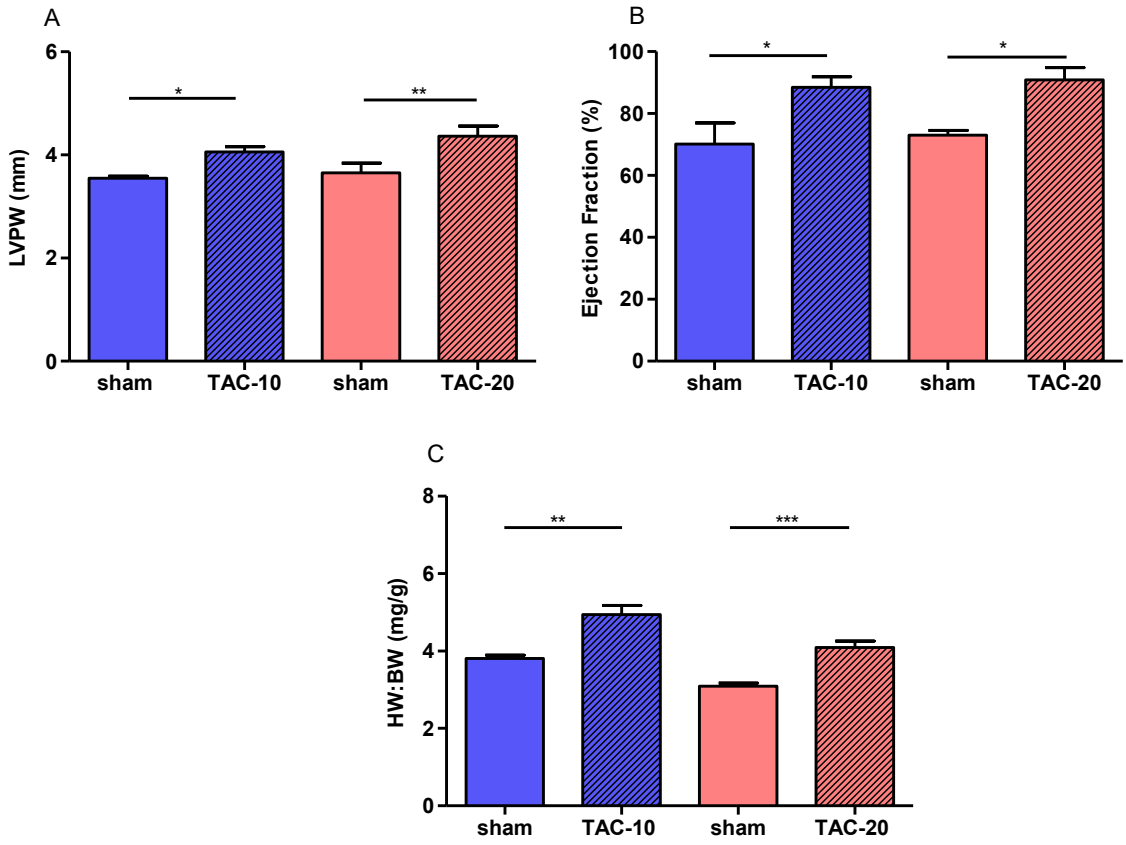


**Figure 4.2: *In vivo* functional and morphometric analysis of TAC model of hypertrophy.**

TAC animals showed an increase in all three parameters assessed at 10 and 20 weeks compared to sham: A) LVPW; B) Ejection fraction; C) Heart weight to body weight ratio. (n=hearts) 10 weeks: Sham n=4; TAC n=5, 20 weeks: Sham n=5; TAC n= 4 (using unpaired t-test).

### 4.3.2. Electrophysiological characterization: Field potential duration changes

Field potential duration was significantly prolonged at both the 10 and 20-week time points (Figure 4.3, A). FPD was also prolonged in TAC at 20 weeks compered to sham at all pacing frequencies. In addition, to this, TAC slices showed a positive response while FPD was shortest during a faster frequency (Figure 4.3, C). Heterogeneity in the action potential duration was calculated using the standard deviation of the field potential duration from 16 randomly selected electrodes per slice (for more details see method chapter 2 section 2.6.1.2). The standard deviation of the FPD was increased in the TAC group at 10 weeks but was unchanged at 20 weeks. FPD was also significantly more heterogeneous at 10 weeks compared with the 20-week time point (Figure 4.3, B).

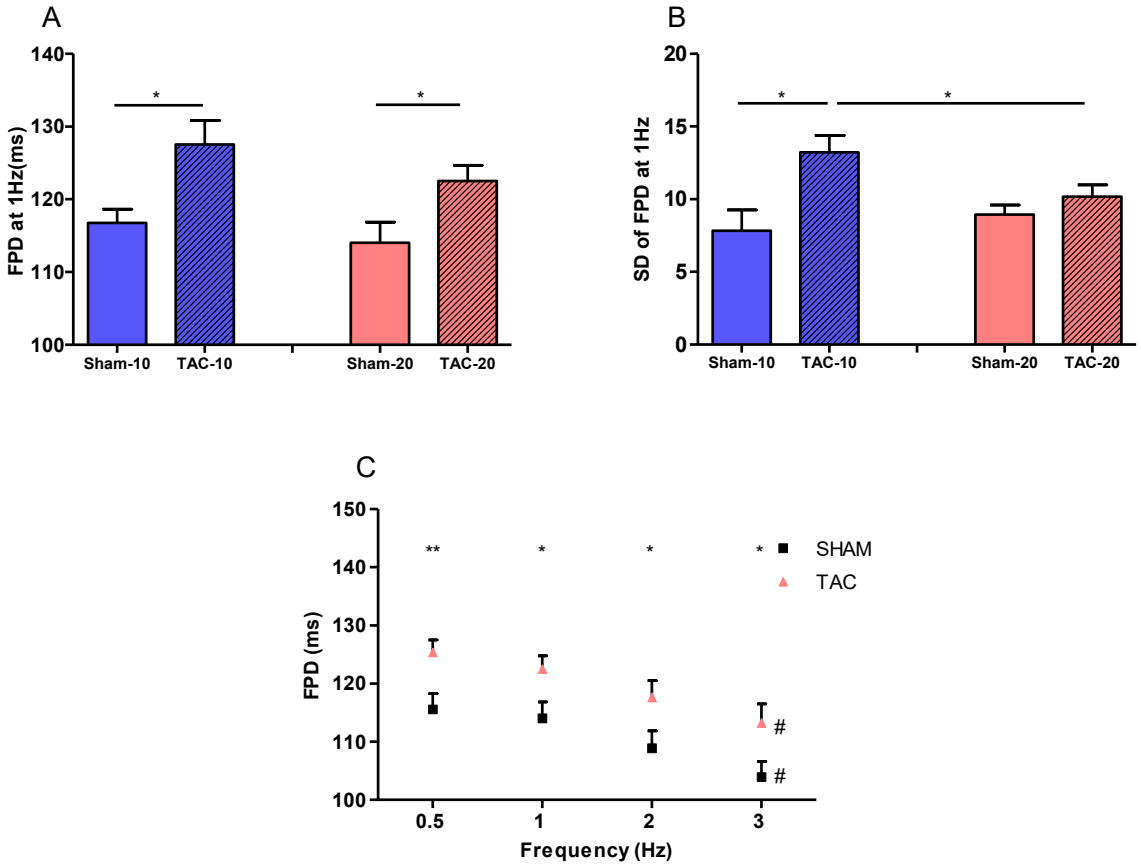


**Figure 4.3: Field potential duration measurements.**

A) The field potential duration measured at 1 Hz in TAC was longer compared to control at 10 and 20 weeks (using unpaired t-test). B) The standard deviation of field potential duration at 1 Hz within each slice was higher only at 10 weeks of TAC compared to control (using unpaired t-test). C) In response to changes in stimulation frequencies, field potential duration was significantly prolonged in TAC when compared to sham, which has been tested in the 20 weeks' group only (using unpaired t-test). Field potential duration was significantly shorter at 3Hz vs 0.5 in both Sham and TAC group (using one-way ANOVA, followed by Tukey's post hoc test). (n=slices/hearts) 20 weeks: Sham n=20/ 3; TAC n=18/4. # vs 0.5Hz within the same group.

### 4.3.3. Electrophysiology: changes in the transmural distribution of field potential duration

FPD was measured from slices obtained from Epi, Myo and Endo at the two time points to investigate the progression of heterogeneity overloading for FPD across the LV.

We observed prolongation in the FPD within the epicardium in the TAC group at 10 and 20 weeks compared to the corresponding sham. Furthermore, sham groups showed a shorter FPD at the Epi compared with both Myo and Endo (Figure 4.4 A, B).

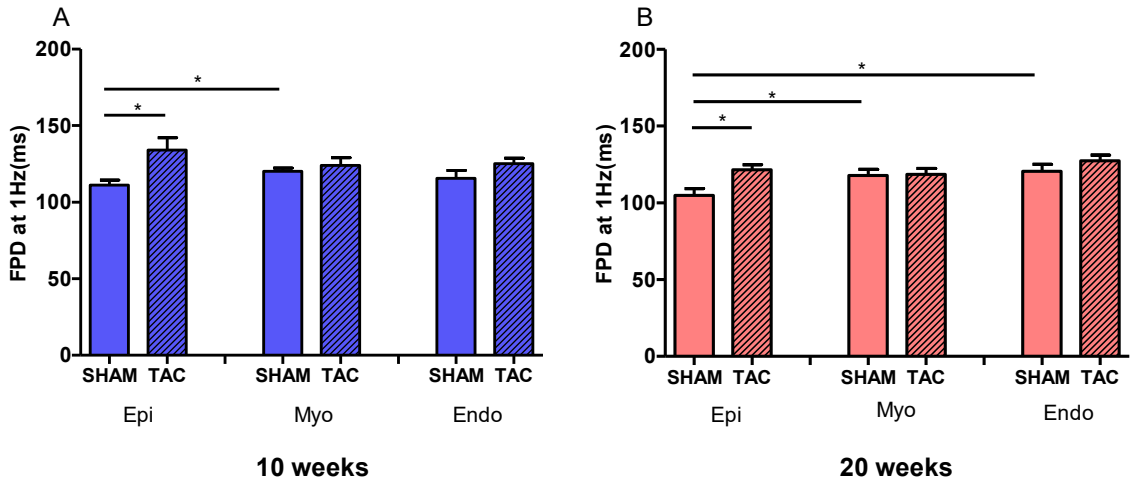


**Figure 4.4: Field potential duration in slices obtained from the Epi, Myo, and Endo regions of the left ventricular free wall of the TAC rats.**

A) FPD was longer in TAC compared to sham slices in the Epi (using unpaired t-test) and was shorter in the Epi compared to the Myo in the sham group at 10 weeks (using one-way ANOVA,followed by Tukey's post hoc test). B) FPD was longer in TAC compared to sham slices in the Epi (using unpaired t-test) and was shorter in the Epi compared to the Myo and Endo in sham group at 20 weeks (using one-way ANOVA,followed by Tukey's post hoc test).(n=Epi,Myo,Endo slices/hearts) 10 weeks: Sham n=4,7,2/3; TAC n=5,6,5/4, 20 weeks: Sham n=7,8,5/4; TAC n=6,6,6/3.

### 4.3.4. Electrophysiology: Conduction velocity

CV in TAC at 10 weeks was significantly faster compared to the age matched control group, therefore, suggesting compensatory mechanisms to increase conduction velocity; a parameter which was unchanged at 20 weeks (Figure 4.5, A). $CV_L$ was faster at 10 weeks and was normalised at 20 weeks (Figure 4.5, B). However, there was no significant change in $CV_T$ at both time points compared with the corresponding sham group (Figure 4.5, C). As a consequence, the anisotropic ratio ($CV_L/CV_T$) was higher in the TAC group compared to sham at 10 weeks and was unchanged at 20 weeks (Figure 4.5, D). These observations show that a faster $CV_L$ and an increase in the anisotropic ratio are present in the LV of a 10 weeks' rat model of aortic constriction.

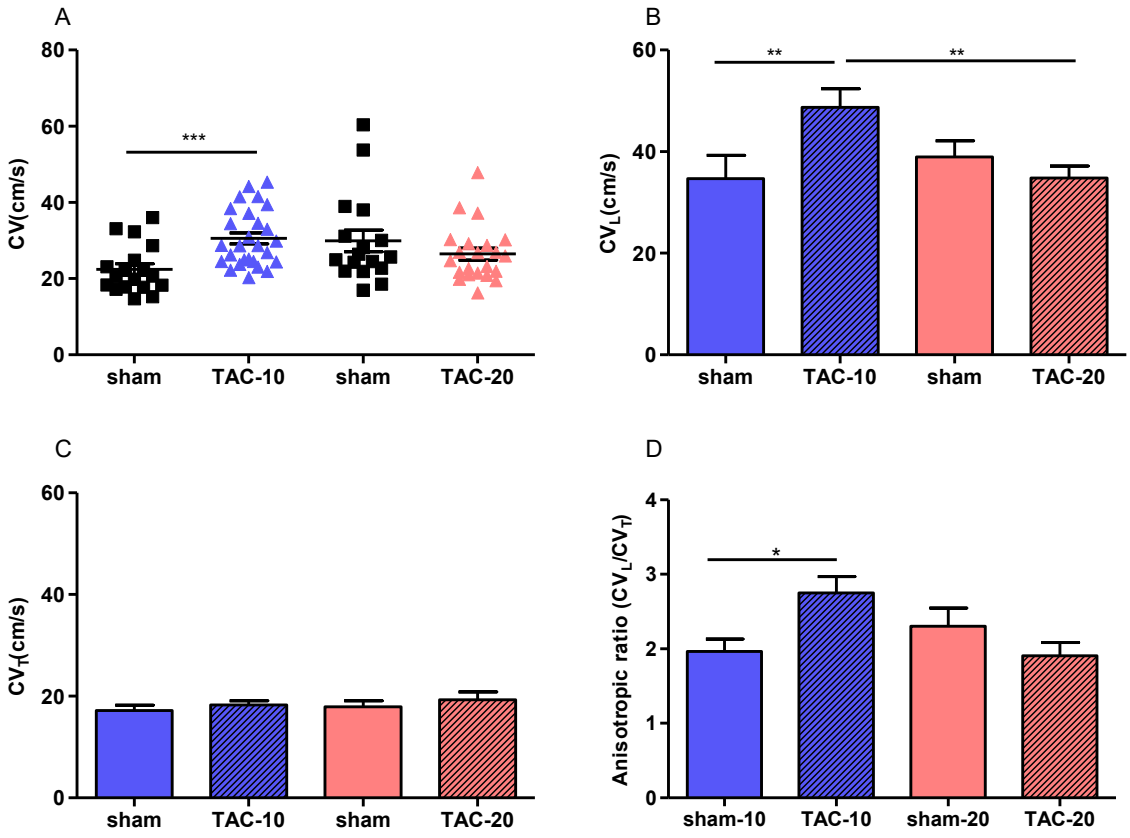


**Figure 4.5: Conduction velocity and anisotropy in slices from TAC groups.**

A) Scatter plot of CV from TAC group shows significantly faster CV in TAC group at 10 weeks and no change at 20 weeks. B) $CV_L$ was faster at 10 weeks and slower at 20 weeks. C) No change in $CV_T$ at both time points. D) Anisotropic ratio was higher in TAC at 10 weeks and unchanged at 20 weeks compared with sham. (n=slices/hearts) 10 weeks: Sham n=18/ 3; TAC n=27/4 h, 20 weeks: sham n=17/4; TAC n=22/3. (unpaired t-test)

### 4.3.5. Electrophysiology: Conduction velocity transmural distribution

To assess if changes in transmural distribution affected conduction, CV was measured in slices taken consecutively spanning from the Epi to Endo. CV was significantly faster in the myocardium in TAC at 10 weeks with no change at 20 weeks (Figure 4.6, A, B). As well as this, there was no change in conduction velocity transmural distribution within the TAC group at 10 and 20 weeks, respectively (Figure 4.6, C).

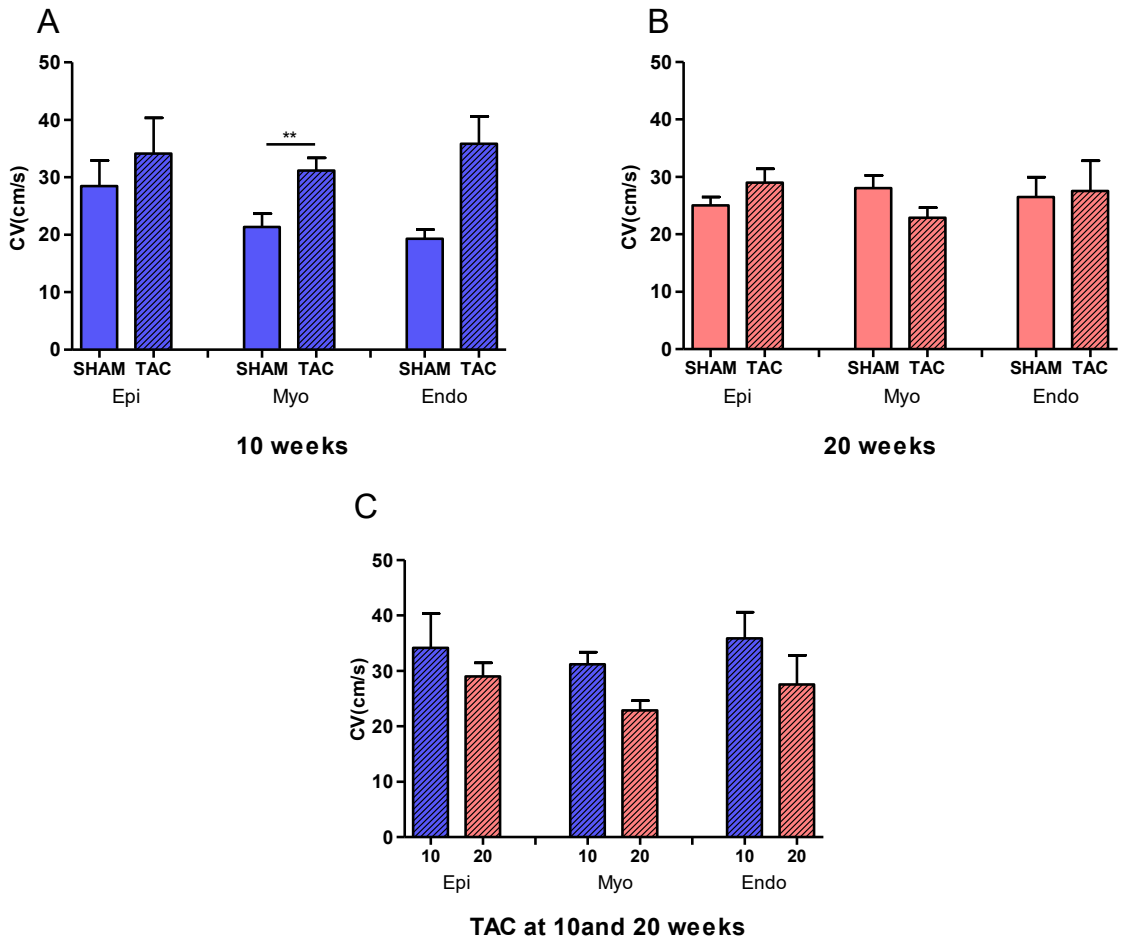


**Figure 4.6: Conduction velocity measured from slices at different transmural layers spanning from Epi to Endo in TAC groups.**

Transmural Conduction velocity in TAC at A) 10 weeks showing faster CV in TAC compared to sham slices in the Myo (using unpaired t-test). B) at 20 week and C) TAC at 10 and 20 weeks. (n=Epi,Myo,Endo slices/hearts) 10 weeks: Sham n= 7,8,3/3; TAC n=9,12,8/4, 20 weeks: Sham n=7,6,9/4; TAC n=6,6,3/3.

## 4.4. Discussion

This chapter describes the electrophysiological abnormalities at whole thickness and transmural levels in rat models of pressure over load using cardiac slices. The main findings in this chapter are: 1) TAC animals show cardiac hypertrophy without signs of dysfunction; 2) FPD was longer in the TAC group at 1 Hz in 10 and 20 weeks of overload; 3) FPD was longer in the group at different pacing frequencies in the 20-week group. Moreover, FPD was gradually shortened in both sham and TAC groups as the pacing rate increased at 20 weeks of overload; 4) FPD was also heterogeneous within slices at 10 weeks and normalised at 20 weeks; 6) there was a longer FPD in epicardial slices of the TAC hearts at 10 and 20 weeks, respectively; 7) finally, CV was faster in TAC at 10 weeks and normalised at 20 weeks, whereas $CV_L$ was faster in TAC at 10 weeks and there was no change in $CV_T$.

### 4.4.1. TAC shows LV hypertrophy

Cardiac hypertrophy is an important adapting mechanism that occurs as a response to chronic hemodynamic overload, therefore, allowing the heart to maintain its basic functions (Olivetti et al. 2000; Oka et al. 2014). TAC is a rat model of hypertrophy that produces chronic ventricular remodelling. In previous studies, TAC displayed a faster progression to LV dysfunction than other models of rat pressure overload (such as spontaneous hypertensive rat (SHR) which was measured and discussed later on in chapter 5) which may contribute to different responses in functional remodelling (Cantor et al. 2005; Halapas et al. 2008; Ward et al. 2011). To assess these changes during the development of pressure overload, we have chosen to measure electrophysiological parameters at two time points (10 and 20 weeks) in myocardial slices.

Prior to electrophysiological analysis, hypertrophy was confirmed by echocardiography to determine heart function. The increased heart weight to body weight ratio, along with a higher LV posterior wall thickness, indicates that hearts are experiencing concentric LV hypertrophy.

Concentric hypertrophy usually arises owing to pathological conditions such as chronic hypertension or valvular stenosis (Bernardo et al. 2010). The increased ejection fraction confirmed a compensatory hypertrophic response at 10 and 20 weeks, which is expected since cellular remodelling precedes whole heart dysfunction at approximately 24 weeks or more in this model (Del Monte et al. 2002). Some of the mechanisms mediating this compensatory phase and its transition to cardiac failure, therefore, includes the severity and duration of the onset of pressure overload (Frohlich & Susic 2012).

### 4.4.2. Field potential duration was prolonged in TAC at 10 and 20 weeks

APD/FPD values recorded in rats or other animals were found to vary significantly. The variations are primarily down to the species used, the different techniques applied for measuring APD/FPD, the preparations used (isolated single cell or whole tissue), the type and duration of hypertrophy, origin site of the myocytes within the ventricular wall and the final solutions used. However, the sham FPD data are comparable to slices obtained from normal rat slices measured previously in our lab.

Prolongation in APD/FPD is a common electrophysiological manifestation of hypertrophy and heart failure (Marbán 1999; Tomaselli 1999; Hart 1994; Pye & Cobbe 1992). This has been studied in humans and animal models in both isolated myocyte or intact tissue. Nonetheless, this has yet to be studied in slices obtained from a rat TAC model. In accordance with several models of hypertrophy, we have shown a prolongation of FPD in both 10 and 20 week models at 1 Hz when compared to the age matched group (Ahmmed et al. 2000; Marionneau et al. 2008; McIntosh et al. 1998; Mitsuyama et al. 2014; Kaab et al. 1996).

Beside changes in $Ca^{2+}$ handling, FPD prolongation in hypertrophy is caused primarily by alterations in the $K^{+}$ currents and this has been demonstrated in both human and animal models of cardiac hypertrophy and HF (D. J. Beuckelmann et al. 1993; Brooksby et al. 1993b; Cerbai et al. 1994; Wickenden 1998; Kaab et al. 1996; Kleiman & Houser 1989; Lue & Boyden 1992;

Potreau et al. 1995; Ryder et al. 1993; Thuringer et al. 1996). It is well known that $I_{to}$ underlies the initial, rapid repolarisation phase of an action potential, and that $I_K$ is responsible for the subsequent, slower phase of AP repolarisation back to the resting membrane potential (Apkon & Nerbonne 1991).

However, the mechanisms responsible for the prolongation of APD may be different between large and small animals as they have a different subtype expression for the $K^+$ channels. Furthermore, in adult rat ventricles, $I_{to}$ is responsible for the rectangular morphology of an action potential and the delayed rectifier potassium current $I_{Kr.}$ The inward rectifier potassium current $I_{K1,}$ however, is relatively small (Nerbonne 2000; Sun & Wang 2005). Therefore, $I_{to}$ would appear to be the main significant contributor to action potential prolongation in cardiac hypertrophy and failure in rats.

### 4.4.3. TAC show longer FPD at different pacing rate

Adaptation of APD to heart rate also varies among different species. For example, in diseased human cardiomyocytes, it has been shown that APD shortens with an increase in frequency (Attwell et al. 1981; Li et al. 1999; Ravens & Wettwer 1998; Sipido 1998), whereas rat ventricular myocytes experienced prolongation in APD (Shimoni et al. 1994; S Shigematsu et al. 1997; Schouten & ter Keurs 1991; Schouten 1986; Babuty et al. 1998). This phenomenon in rats was believed to be due to the large amount of $I_{to}$ compared with other species, which produces the reduced/absent plateau phase of an AP. This current is known to be depressed as the rate of stimulation is increased, therefore, predicting the prolongation of APD (Payet 1981; Mitchell et al. 1984; Kukushkin et al. 1983; Josephson et al. 1984). In addition, to this, $I_{Na}^+$ and $I_{Ca}^{+2}$ currents have also been shown to play a significant role in the adaptation of APD at different pacing rates in rats (Fauconnier 2003; S. Shigematsu et al. 1997; Carmeliet 2004) and these should also be considered in the observations reported here.

In this study, more specifically, we show that FPD was gradually shortened in both sham and TAC as pacing rate was increased. Mitsuyama and co-workers, for example, showed a shortening of APD at high pacing rates in SHR and WKY rats, respectively, which is in agreement with our findings regardless of the higher pacing rate used in their study (Mitsuyama et al. 2014). In contrast, APD was prolonged in normal isolated rat ventricular myocytes with a faster pace (Fauconnier 2003). This discrepancy of APD in response to higher pacing rates may arise from the differences in experimental conditions, such as $Ca^{2+}$ concentration and/or the method used for APD measurements (MEA or patch-clamp technique). Furthermore, we have measured the FPD where K, Ca and Na currents play an important role in both FPD shape and duration. This can be affected at different pacing rates which has not been tested in this study. However, we have demonstrated the prolongation of FPD under different pacing rates in TAC slices compared to sham at 20 weeks, which is in agreement with previous studies showing the prolongation of APD in hypertrophy (Hart 1994; Pye & Cobbe 1992; Mitsuyama et al. 2014).

As well as this, we have measured the standard deviation (SD) of FPD from at least 16 electrodes of each slice in order to examine the overall FPD dispersion. Increased dispersion of repolarisation and refractoriness within the left ventricle of hypertrophied hearts has been reported *in vivo* and *in vitro,* and may, therefore, be associated with an increased inducibility of polymorphic ventricular tachycardia or ventricular fibrillation (Kowey et al. 1991; Kowey et al. 1992; C S Kuo et al. 1983; Rials et al. 1995). Here, TAC was more heterogeneous during the early stage of hypertrophy in the $10^{th}$ week but this was not observed at 20 weeks when the disease was seen to progress.

### 4.4.4. TAC hearts show changes in transmural dispersion of FPD

Heterogeneity of repolarisation is a well-established characteristic in cardiac physiology and can be identified between cells that span the transmural ventricular wall allowing efficient contraction and relaxation. Transmural dispersion of repolarisation has been reported in canines,

felines, rabbits, rats and humans using normal ventricular myocytes or tissue slabs (Antzelevitch & Dumaine 2011). In addition, this was reported in canine LV slices (Camelliti et al. 2013). It is important to study the changes in the heterogeneity of repolarisation as it can be a potential source of arrhythmia (C S Kuo et al. 1983) and this was an imperative factor considered in our study. Hence, we have showed shorter FPD in the epicardium compared to the other regions for the sham group and prolonged in the TAC group at both time-points. Furthermore, this was in agreement with previous studies using myocytes obtained from rats and a number of other species (Antzelevitch et al. 1991; Casis et al. 1998; Clark et al. 1993). Although this has not been tested here, this effect may be due to the higher density of $I_{to}$ in Epi cells and how it changes in cardiac remodelling as the current density decreases. However, a point should be taken into consideration when testing the FPD transmural obtained from rats. This states that previous studies on rat transmural heterogeneity of repolarisation have used mainly isolated myocytes, whereas we have used multicellular preparations. This phenomenon may, therefore, be less pronounced in multicellular preparations compared to isolated myocytes due to the adjacent myocytes that are electrically coupled by gap junctions. Thus, electrical coupling has the ability to reduce action potential differences throughout the heart (Boukens et al. 2009; Taggart et al. 1995). Nonetheless, large animals, such as dogs, often show pronounced transmural heterogeneity of repolarisation in multicellular preparations (Camelliti et al. 2013; Fadi G Akar & Rosenbaum 2003; Ueda et al. 2004). As well as this, rats have a relatively smaller heart when compared to larger animals with thicker and well defined layers within the LV. Hence, this makes it difficult to distinguish the different LV layers in rats. A rat's heart is also more curved, meaning the whole LV needs to be cut to obtain efficient slices. As a result, the curvature of the LV makes it difficult to cut slices in parallel of the cutting blade, which can introduce cutting at an angle. This can, therefore, generate slices with mixed LV layers. It should also be mentioned that FPD is shorter in rats compared to larger animals and changes in FPD within the LV can be

too small to detect; something which may be due to the endocardium being the biggest portion of the left ventricle and the epicardium being the smallest (Komukai et al. 2002).

### 4.4.5. TAC hearts show changes in CV

CV in hypertrophied myocardium was shown to be altered in animal experiments and clinical studies, however, there is no consistent pattern in these changes. CV can be accounted for by several structural and functional changes which includes cell size, gap junction Cx43 expression, fibrosis, ion channel density and their electrical excitability (mainly $I_{Na}$). Discrepancies could arise due to the type of LVH experimental model used, the severity of the hypertrophy and other methodological aspects (Bacharova 2007).

Furthermore, we have also observed a faster CV at 10 weeks but no change at 20 weeks when compared to the control. This increase in CV is mainly observed in the early stage of hypertrophy, however, CV does gradually decrease with the increasing severity of hypertrophy. In a guinea pig model of HF, CV only increased after 50 days and then furtherly decreased after 150 days in aortic banding (Cooklin et al. 1998). This is similar to our findings despite that we could not see a difference at 20 weeks. Conversely, CV at 20 weeks is reduced by 13% which indicates a change in CV with the progression of hypertrophy. It is possible that the increase in cell size (hypertrophy) is the predominant feature in this model as the other electrical and structural remodelling processes are not pronounced. Wiegerinck et al., for instance, found larger cell size increases for CV in rabbit models of HF (Waiegerinck et al. 2006). In two other studies, however, that included patients with HF, an increased CV was measured as well (Anderson et al., 1993; Toyoshima et al., 1982). Meaning, $CV_L$ was faster at 10 weeks and was not changed at 20 weeks, as found in our study. Furthermore, changes in Cx43 level and its localisation have previously been associated with a decreased longitudinal CV (Cabo et al. 2006). Thus, changes in $I_{Na}$ can also alter $CV_L$ (Parikh et al. 2013). The accumulated collagen, or fibrosis, transverse to muscle fibres can significantly affect $CV_T$ (Assayag et al. 1997). Therefore, there was no change

in $CV_T$ at all-time points which suggests no change in the fibrosis level; unfortunately, this has not been investigated in the aforementioned research study and requires further investigation to strongly conclude this result.

### 4.4.6. TAC show no changes in transmural dispersion of CV

CV depends on the availability of $Na^+$ channels and intercellular electric coupling by gap junctions. Therefore, heterogeneity in the expression of $Na^+$ channels or/and connexins may lead to regional differences in CV, which makes some parts of the heart more vulnerable to arrhythmias (Allessie et al. 1977). For that, we have measured the changes in transmural CV in this model. Although previous reports show changes in transmural CV (Glukhov et al. 2012; Poelzing et al. 2004; Poelzing & Rosenbaum 2004) at Epi than Endo, we were unable to detect a specific changes in CV transmurally.

## 4.5. Summary

The work described in this chapter demonstrated electrophysiological left ventricular remodelling in TAC rat models of pressure overload using myocardial slices.

# CHAPTER 5.Cardiac remodelling of myocardial slices from rat hearts with chronic hypertension

## 5.1. Introduction

Hypertension is a major public health problem, associated with an increased morbidity and mortality worldwide (Joffres et al. 2013). Typically, it is defined by blood pressure persistently at, or above, 140/90 mm/Hg which is commonly followed by hypertensive cardiomyopathy. Sustained elevated blood pressure may, therefore, lead to an increased LV wall thickness, a mechanism that overcomes LV wall stress. As such, one of the first characteristics of hypertensive heart disease is LV hypertrophy (Nadruz 2015). As noted previously, hypertension is the most common cause of left ventricular hypertrophy which increases the risk of coronary heart disease and heart failure, and, in turn, can increase the susceptibility to ventricular arrhythmias (Levy et al. 1996).

SHR is a widely used genetic model of hypertension in cardiovascular research to study cardiac remodelling and has been used extensively as a model of primary and secondary hypertension. As rats can progressively develop myocardial hypertrophy, whereby the severity increases with age, the ending result can lead to complete heart failure (Bing et al. 1995). At around 3 months of age, male SHRs start to show hypertension-induced compensated hypertrophy, which is followed by decompensated heart failure in 57% of SHRs at 18–24 months of age; especially when compared to a control (Carll et al. 2011).

Structural and electrophysiological remodelling has been studied extensively in this model. Myocytes isolated from SHR, for instance, can show hypertrophy (Tsutsui et al. 1999; Brooksby et al. 1992), APD prolongation and heterogeneity associated with ionic current alterations (Barbieri et al. 1994; Cerbai 2000; McCrossan et al. 2004). Additionally, to this, increased levels of fibrosis were documented in SHR animals (Herrmann et al. 1995; Brilla et al. 1996). Hence, these alterations are likely to contribute to the increased propensity to arrhythmias. The electrical and structural alterations in SHR, however, have been mainly studied in isolated myocytes which is not truly representative of the myocardium, as other non-myocyte cells such as fibroblasts

have also showed to contribute vastly to cardiomyocytes remodelling. Therefore, this chapter aims to use LV slices from the SHR model to investigate the mechanisms behind the LV electrophysiological and conduction abnormalities during hypertension from a multicellular perspective. Thus, we are investigating changes in:

1- FPD and CV over time.
2- FPD and CV transmural changes within the LV wall.
3- Cx43, $Na^+$ channel protein expression and fibrosis level in order to investigate mechanisms underlying AP and alterations in conduction.

## 5.2. Methods

### 5.2.1. Animal models

SHR animals were recruited at three time points, 3, 10-12 and 18-20 months as shown in Figure 5.1. For simplicity, we named the groups 3, 12 and 20 months. Brown Norway (BN) and Wistar Kyoto (WKY) rats were recruited as normotensive groups in this study. The BN animals were the only normotensive group used to compare functional parameters to SHR in the echocardiography experiments. For the electrophysiological assessment at 20 months, BN animals were the only normotensive group used.

### 5.2.2. Echocardiography and morphometric analysis

Heart function was assessed using echocardiography and the measurements of heart weight to body weight ratios were recorded to confirm hypertrophy, as described in chapter 2 section 2.3 and section 2.5, respectively.

### 5.2.3. Slices preparation

Slices were also prepared from each animal for each group, as described in chapter 2 section 2.6.

### 5.2.4. MEA recordings and analysis

MEA recordings were used to analyse: FPD and its heterogeneity within each slice, $CV_L$ and $CV_T$, and FPD and CV transmural distribution in the LV, as described in chapter 2 section 2.7. We obtained MEA recordings from approximately six slices per heart, and two slices per endocardium, mid-myocardium and epicardium to cover the different transmural regions.

Following electrophysiological measurements, each slice was washed with a phosphate buffer saline (PBS) and was blotted with tissue. The slice was then cut into two halves. One was rapidly frozen in liquid nitrogen for protein studies and the other half for histological experiments, as described in details in chapter 2 section 2.6.

### 5.2.5. SDS PAGE and western blot analysis of connexin 43 and sodium channel $Na_v1.5$.

The protein levels of Cx43 and $Na_v1.5$ in the slices were quantified by SDS-PAGE and a western blot, as described in details in chapter 2 section 2.14.

### 5.2.6. Picrosirius red staining to assess interstitial fibrosis in cardiac slices.

10 μm thick cryosections from frozen LV slices were cut and stained with PSR to quantify the amount of fibrosis as described in chapter 2 section 2.12 and 2.13.

Figure 5.1 is a schematic of the experimental protocol.

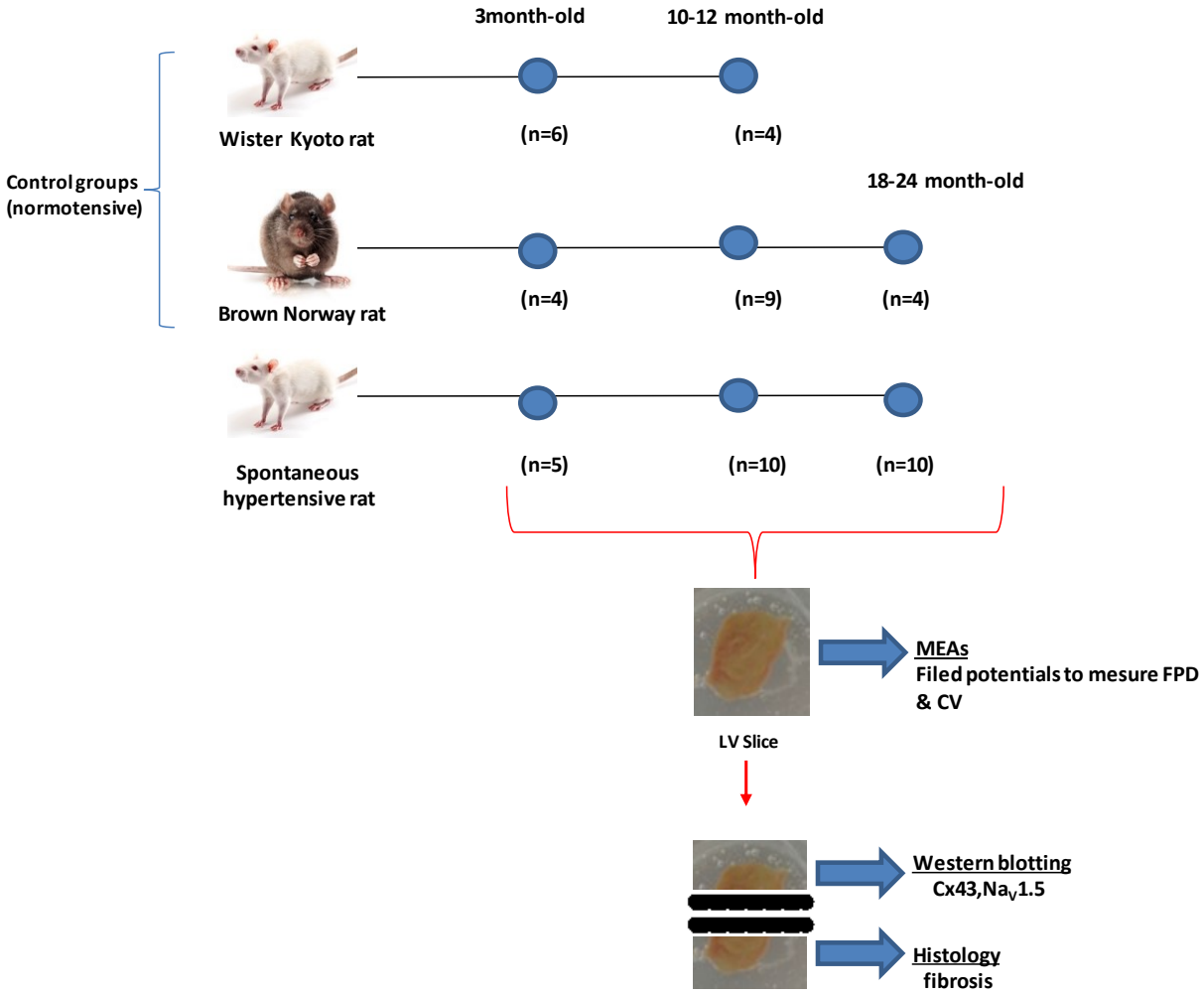


**Figure 5.1: Schematic representation of the experimental protocol used in the hypertension group.**

Wistar Kyoto and Brown Norway rats were used as normotensive controls for spontaneous hypertensive rats. Here, n refer to the numbers of animals used.

## 5.3. Results

### 5.3.1. *In vivo* cardiac function assessment and morphometric analysis in hypertension

Echocardiography and morphometric analysis was performed to evaluate cardiac function and confirm cardiac hypertrophy.

There was an increase in the left ventricular posterior wall thickness within the SHR group compared to the BN group. However, this effect was statistically significant only at 3 and 12-month time points (Figure 5.2 A). The ejection fraction increased in the SHR compared to the normotensive BN group at 3 and 12 months, and was unchanged at 20 months (Figure 5.2 B), respectively. In addition, to this, the SHR groups ejection fraction declined at 20 months compared with the 12-month group (18% decrease).

SHR showed a significant increase in the HW:BW ratio, compared to their corresponding normotensive groups, therefore, confirming the hypertrophic response (Figure 5.2 C).

Collectively, these results indicate compensated hypertrophy whereby the hearts have not begun to fail and explains the maintained or increased ejection fraction (Wei et al. 2010). However, the decrease in ejection fraction in SHR at 20 months compared with the 12-month group may indicate the beginning of a decompensating status.

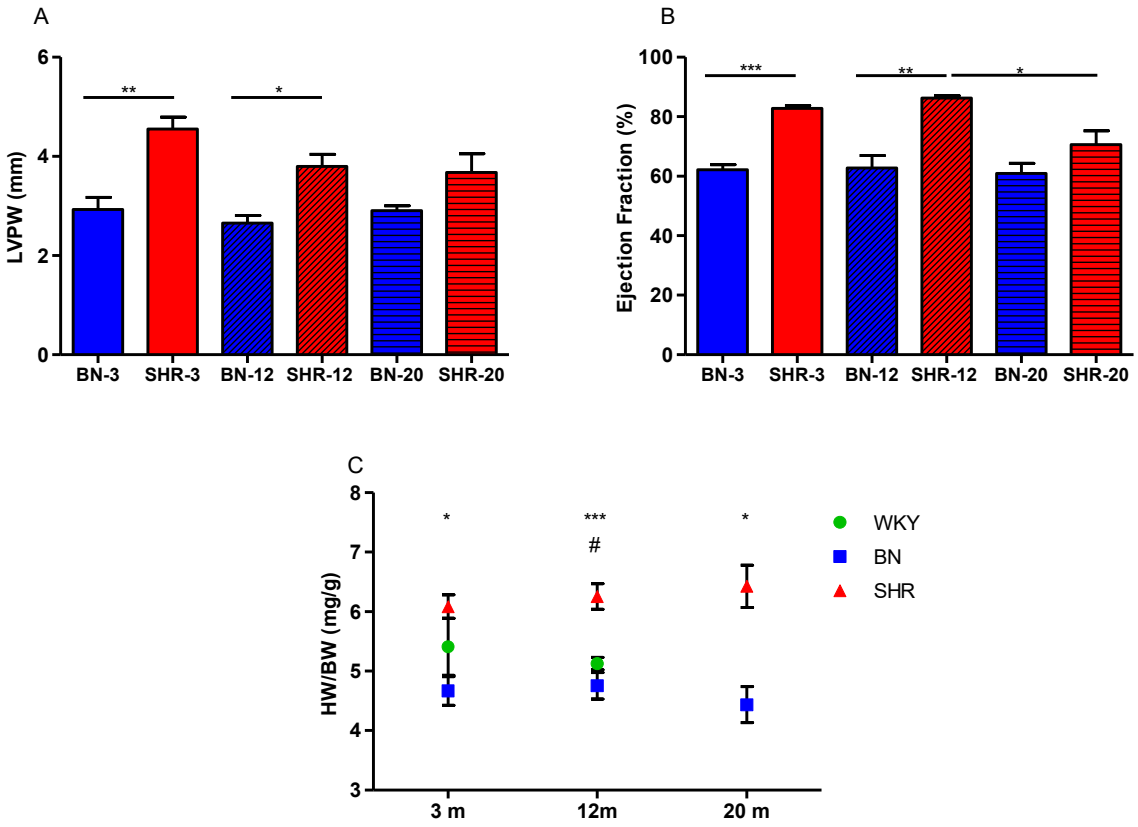


**Figure 5.2: *In vivo* heart function assessment and morphometric analysis in hypertension.**

A) Left ventricular posterior wall thickness was increased in SHR at 3 and 12 months (using unpaired t-test). B) In the SHR group, ejection fraction was increased at 3 and 12 months compared to BN but SHR at 20 months showed decrease in ejection fraction compared to the 12 months (using unpaired t-test); 3 months: BN n=3; SHR n=3, 12 months: BN n=3; SHR n=3, 20 months: BN n=3; SHR n=5. C) Heart weight to body weight ratio was increased in SHR group compared to the normotensive groups (using unpaired t-test); 3 months: WKY n=7; BN n=4; SHR n=5, 12 months: WKY n=4; BN n=9; SHR n=10, 20 months: BN n=4; SHR n=10. n=hearts ;* vs BN, # vs WKY.

Systolic blood pressure was only measured at the early time points and hypertension within these animals was confirmed at 3, 6 and 9 months, respectively (Table 5.1).

**Table 5.1: Systolic blood pressure in SHR group**

| Group | Blood Pressure(mmHg) | | |
|---|---|---|---|
| | 3months | 6 months | 9 months |
| WKY | 101±2.9<br>n=15 | 103±2.8<br>n=21 | 104±3<br>n=30 |
| BN | 123±6<br>n=63 | 115±24<br>n=51 | 115±18<br>n=36 |
| SHR | 182±82$^{\#\#\#}$<br>n=9 | 173±59$^{***,\#\#\#}$<br>n= 24 | 177±42$^{***,\#\#\#}$<br>n=21 |

Values are expressed as mean ±SEM, n=number of hearts. SHR displayed elevated blood pressure compared to the normotensive WKY and BN rats (using unpaired t-test).

$^{*}$ vs BN and $^{\#}$ vs WKY.

### 5.3.2. Electrophysiology: field potential duration changes

MEAs were used to evaluate the electrical properties within the myocardial slices. A significant difference in FPD was only present between the 12 month SHR group and WKY (Figure 5.3 A). The standard deviation of the FPD, which was used as an index of FPD heterogeneity, remained unchanged in the SHR group compared to the normotensive groups at all-time points (Figure 5.3 B).

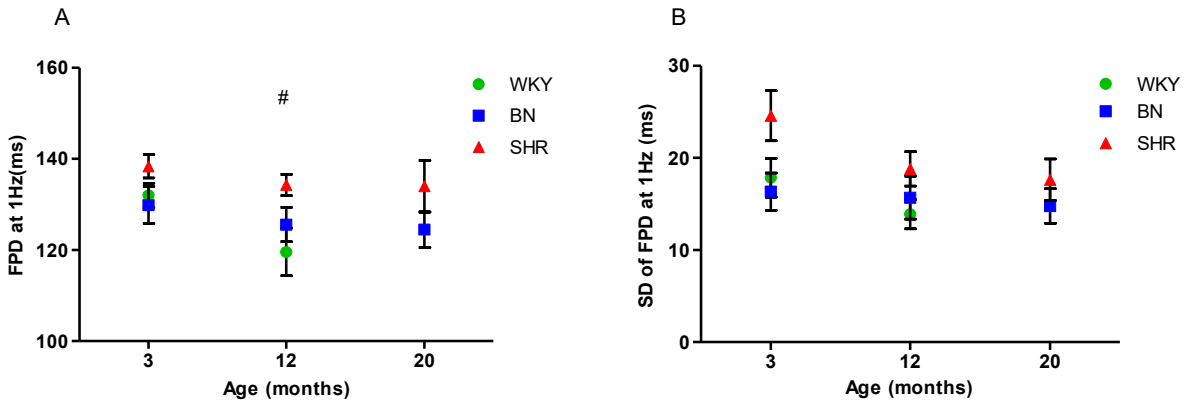


**Figure 5.3: Field potential duration and its heterogeneities in hypertension group.**

A) SHR showed significantly longer FPD only at the 12 month time-point compared with WKY (using unpaired t-test). B) SHR show an increase in the standard deviation of field potential compared to the normotensive groups at all-time points but this was not significant. (n=slices/hearts) 3 months: WKY n=16/3; BN n=10/3; SHR n=18/3, 12 months: WKY n=17/3; BN n=18/3; SHR n=18/3, 20 months: BN n=24/4; SHR n=16/6. # vs WKY.

### 5.3.3. Electrophysiology: frequency-dependent changes in field potential duration

To assess the effect of the stimulation frequency on FPD, slices were paced at 0.5, 1, 2 and 3 Hz. Within the experimental groups, neither SHR nor normotensive groups showed any significant response to a change in stimulation frequency (Figure 5.4 A-C).

Compared to WKY, SHR at 12 months also showed longer FPD when paced at other frequencies, as did BN at 3 Hz only (Figure 5.4 B).

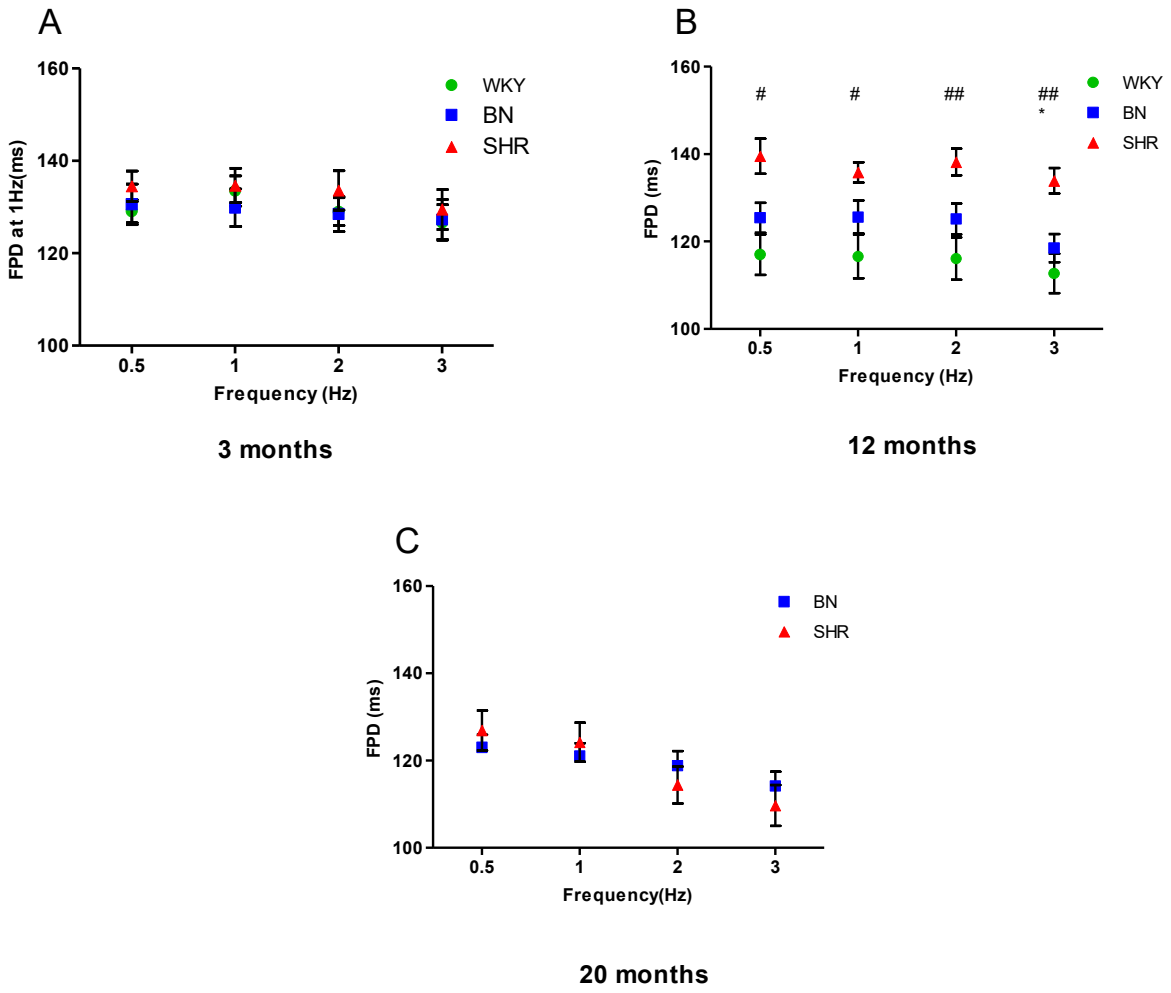


**Figure 5.4: Field potential duration at different pacing frequency in hypertension group.**

FPD at 3 months A) 12 months B) and 20 months C) slices pacing at different frequency. Longer FPD was observed in SHR groups compared to the normotensive groups at different frequencies but was only significant in the 12 months old group when compared with WKY normotensive group (using unpaired t-test). (n=slices/hearts) 3 months: WKY n=16/3; BN n=10/3; SHR n=18/3, 12 months: WKY n=17/3; BN n=18/3; SHR n=18/3, 20 months: BN n=24/4; SHR n=16/6. $^{\#}$ vs WKY.

### 5.3.4. Electrophysiology: changes in the transmural distribution of the field potential duration

FPD was measured from slices obtained from the epicardium, myocardium and endocardium to investigate the heterogeneity of FPD across the LV wall.

FPD in SHR was significantly increased within the endocardium at 3 months and in the midmyocardium at 12 months when compared to WKY (Figure 5.5 A, B). There were no significant changes in FPD transmural distributions between SHR and BN at 20 months (Figure 5.5 C). Thus, no change in FPD was observed transmurally within the individual groups at all-time points.

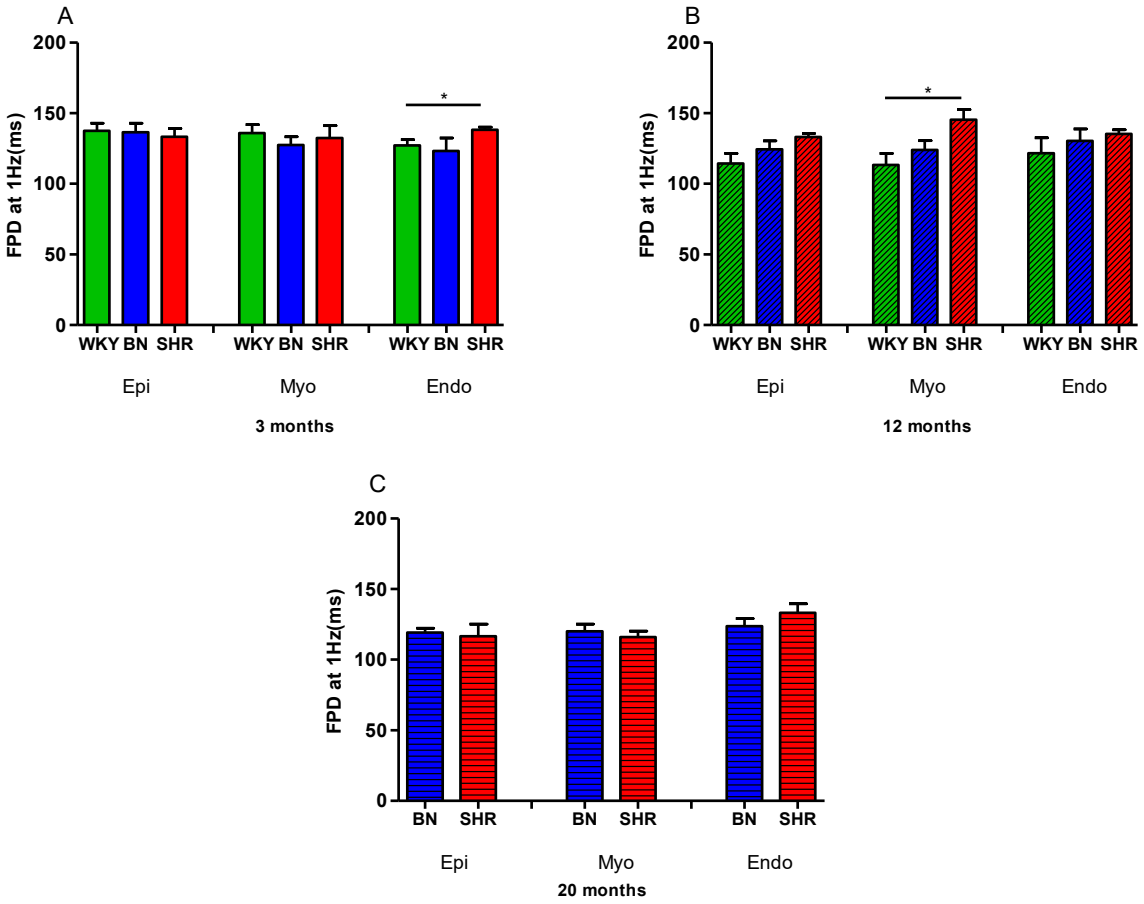


**Figure 5.5: Field potential duration in slices obtained from the Epi, Myo, and Endo regions of the left ventricular free wall of the hypertension group.**

A) SHR FPD was longer in Endo compared to WKY group but not to BN at 3months time-point (using unpaired t-test). B) SHR FPD was longer in Myo compared to WKY group but not to BN at 12months time-point (using unpaired t-test). C) No regional changes in FPD at 20 months. (n=Epi,Myo,Endo slices/hearts) 3 months: WKY n=6,4,5/3; BN n=4,3,3/3; SHR n=6,6,6/3, 12 months: WKY n=5,6,6/3; BN n=7,7,4/3; SHR 5,2,3/3, 20 months: BN n=5,10,7/4; SHR n=4,3,6/6.

### 5.3.5. Electrophysiology: conduction velocity

Stimulation from four different directions within a slice were recorded at 1 Hz and CV was determined by averaging the CV obtained from the four points of each slice.

CV was significantly slower in the 12 month SHR group compared to the corresponding WKY age group and at 20 months when compared to BN. CV was also significantly reduced within the SHR groups over time, therefore, suggesting a progression in both hypertension and cardiac remodelling (Figure5.6 A).

$CV_L$ was unchanged at 3 months but was slower at 12 and 24 months when compared to the normotensive groups. There was also a reduction in $CV_L$ between the 3 and 20 month SHR time points suggesting a progression in hypertension (Figure5.6 B).

The SHR group showed slower $CV_T$ at 3 months and no change at 12 and 20 months when compared to BN. On the other hand, the WKY group showed an unexpected slower $CV_T$ at 3 months that increased at 12 months. $CV_T$ in the BN group was significantly slower at 20 months compared to 3 and 12 months, thus suggesting an effect of aging within this animal strain (Figure 5.6 C).

The anisotropic ratio of CV was significantly lower in the SHR group at 20 months compared with BN. Table 5.2 summarises the data on conduction velocity anisotropy and anisotropic ratio obtained from slices of the experimental groups.

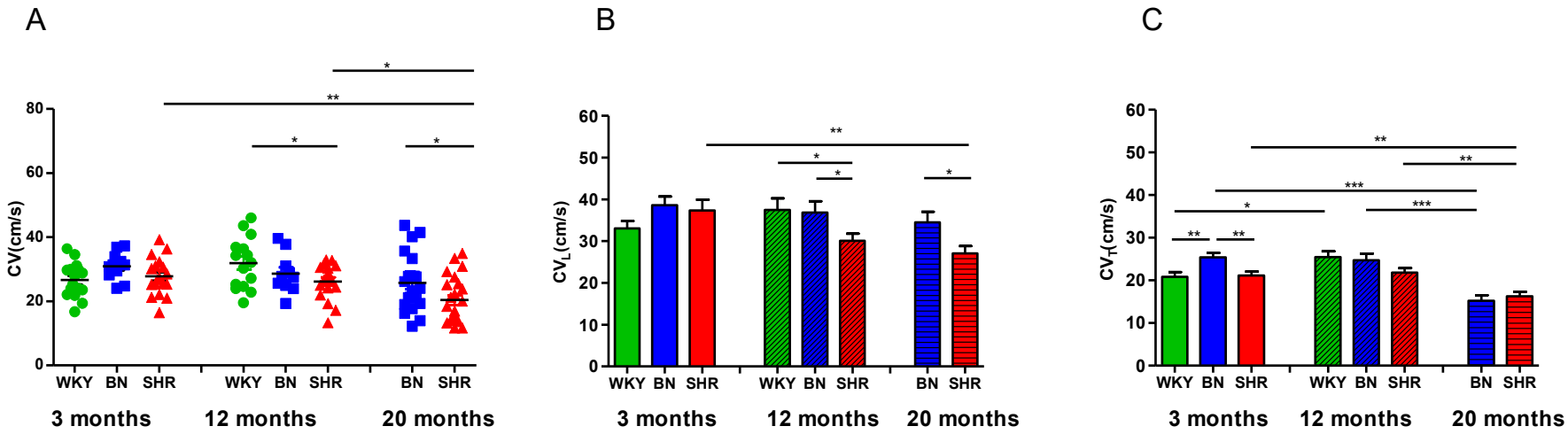


**Figure 5.6: Conduction velocity and Anisotropy in slices from hypertension group.**

A) Scatter plot of CV shows slower CV in the SHR group compared with normotensive animals but was only significant at 12 months compared with WKY and at 20 months compared to BN (using unpaired t-test). CV was reduced in SHR group with the progression of hypertension (using one-way ANOVA followed by the Tukey's post-hoc test). B) $CV_L$ was unchanged at 3 months but was slower in 12 and 20 months when compared to the normotensive groups (using unpaired t-test) also there was reduction in $CV_L$ in SHR with the progression of hypertension and only significant between 3 and 20 months( using one-way ANOVA followed by the Tukey's post-hoc test). C) SHR show slower $CV_T$ at 3 and 12 months but was only significant at 3month and not changed when compared with BN at 20 months using unpaired t-test). $CV_T$ in BN was significantly slower at 20 months compared with BN at 3 and 12 months also $CV_T$ was reduced within the SHR group with the progression of hypertension (using one-way ANOVA followed by the Tukey's post-hoc test). (n=slices/hearts) 3 months: WKY n=16/3; BN n=11/3; SHR n=18/3, 12 months: WKY n=15/3; BN n=10/3; SHR n=18/3, 20 months: BN n=21/4; SHR n=22/6. Each point represents the average CV for each slice.

**Table 5.2: Conduction velocity anisotropy and anisotropic ratio**

| Group | $CV_L$ (cm/sec) | $CV_T$ (cm/sec) | Anisotropic ratio ($CV_L/CV_T$) |
|---|---|---|---|
| WKY-3 | 33.09±2 | 20.83±1 | 1.6±0.1<br>n=16 |
| BN-3 | 38.62±2 | 25.38±1$^{++}$ | 1.5±0.1<br>n=11 |
| SHR-3 | 37.36±2 | 21.13±1$^{xx}$ | 1.8±0.1<br>n=18 |
| WKY-12 | 37.48±3 | 25.57±2$^{\dagger}$ | 1.5±0.1<br>n=15 |
| BN-12 | 36.52±3 | 24.66±1 | 1.6±0.1<br>n=10 |
| SHR-12 | 30.09±2$^{+,x}$ | 21.80±1$^{\sim\sim}$ | 1.4±0.05<br>n=18 |
| BN-20 | 34.52±2 | 15.17±1$^{\wedge\wedge\wedge}$ | 2.9±0.3<br>n=21 |
| SHR-20 | 27.06±2$^{x}$ | 16.22±1$^{\sim\sim}$ | 1.6±0.1$^{xx}$<br>n=22 |

Values are expressed as mean ±SEM using unpaired t-test. $^{+}$ Indicate significant differences from WKY within the same group, $^{x}$ from BN within the same group, $^{\sim}$from SHR-3, $^{\wedge}$fromBN-3, $^{\dagger}$ from WKY-3.
n=number of slices

### 5.3.6. Electrophysiology: conduction velocity transmural distribution

Conduction velocity was measured from slices taken in different transmural layers spanning from the epicardium to the endocardium. There was no change in transmural CV between the control and the diseased groups at 3 and 12 months, respectively (Figure 5.7 A, B). However, at 20 months, CV was significantly slower in SHR within the myocardium compared to BN. In addition, CV within the BN group was lower in the endocardium than the myocardium and epicardium (Figure 5.7 C). Hence, CV was significantly lower in the 20 weeks SHR compared to the 3 months SHR within the epicardium (Figure 5.7 D).

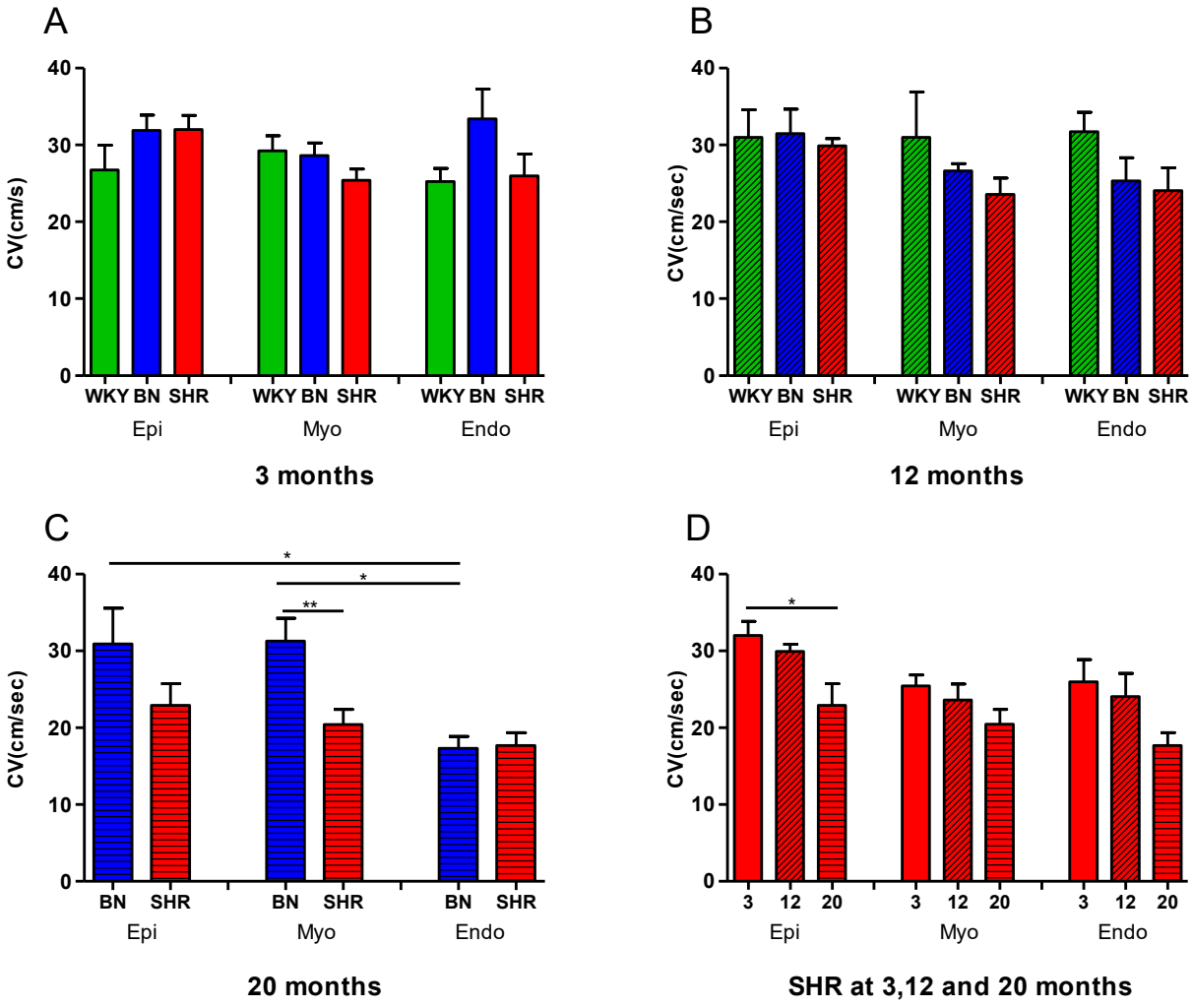


**Figure 5.7: Conduction velocity measured from slices at different transmural layers spanning from Epi to Endo in hypertension group.**

Conduction velocity transmural in SHR at A) 3 months B) 12 months and C) 20 months showed slower CV at Endo than Epi and Myo (using one-way ANOVA followed by the Tukey's post-hoc test) and slower CV in the Myo of SHR compared to BN (using unpaired t-test), and D) SHR group at 3, 12 and 24 months showed faster CV in the 3months group compared to the 20months in the Epi region (using one-way ANOVA followed by the Tukey's post-hoc). (n=Epi,Myo,Endo slices/hearts) 3 months: WKY n=6,6,5/3; BN n=5,4,2/3; SHR n=6,6,6/3, 12 months: WKY n=5,4,5/3; BN n=5,2,3/3; SHR 7,6,5/3, 20 months: BN n=8,8,6/4; SHR n=11,11,8/6.

### 5.3.7. Connexin 43 and $Na_v1.5$ protein expression

To determine whether changes in electrophysiological parameters were associated with Cx43 and Nav1.5 protein levels, the same slices used for the MEA experiments were tested accordingly. Cx43 was downregulated in SHR compared to the normotensive groups at all time points, however, $Na_v1.5$ was downregulated only in the SHR compared to BN at 20 months (Figure 5.8 A-C). Within the SHR groups both Cx43 and $Na_v1.5$ were downregulated at 20 months compared to the 3 months. The BN group also showed downregulation of Cx43 at 20 months compared to the younger groups. Despite this, there was no change in $Na_v1.5$ protein expression in BN with aging (Figure 5.8 D, E). We also compared the protein expression of Cx43 and $Na_v1.5$ in the BN and WKY groups at 3 and 12 months and there was no significant change in the expression of these proteins (Figure 5.8 F).

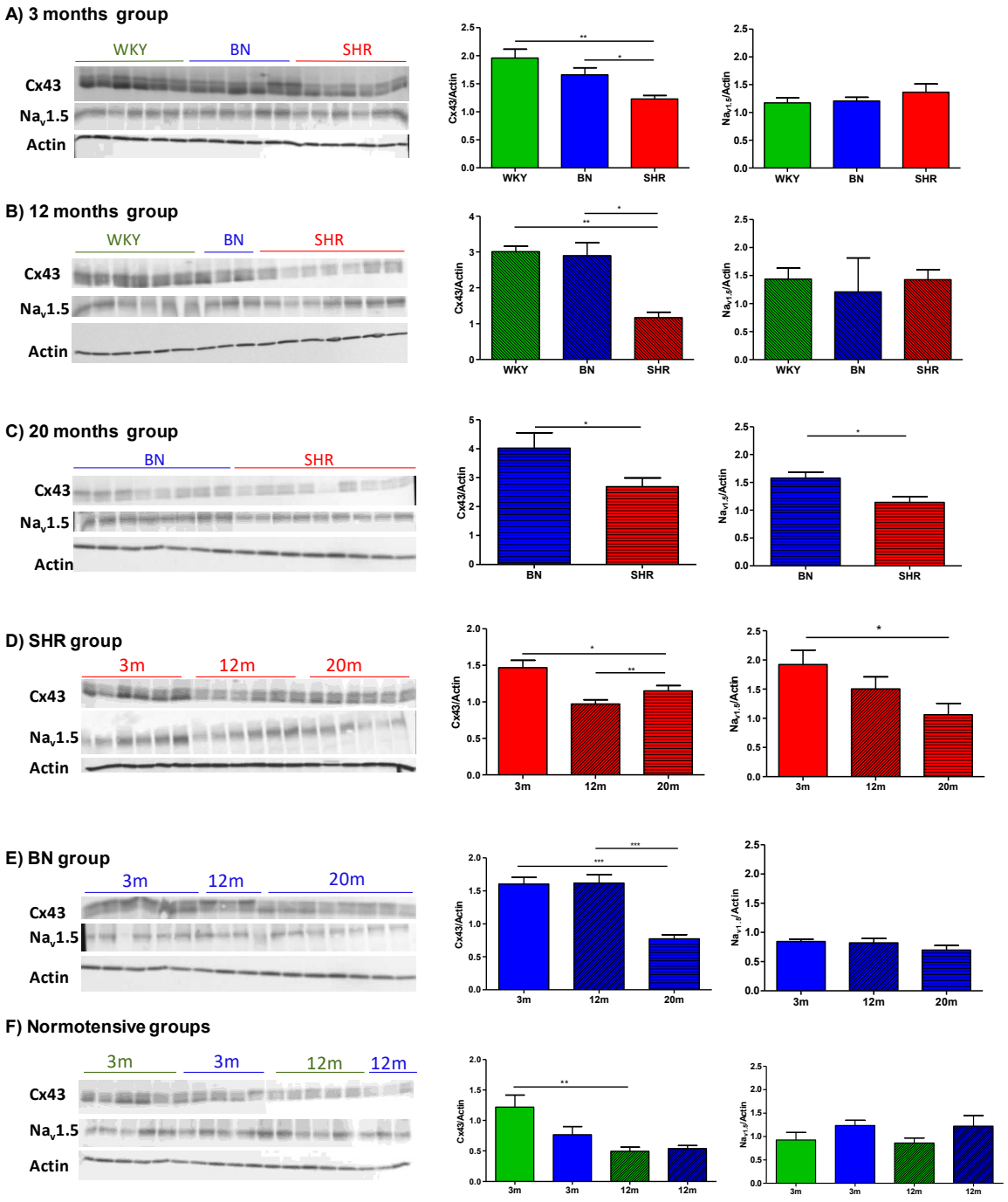


**Figure 5.8:The level of Cx43 and Nav1.5 proteins.**

Representative western blots probed for Cx43 and $Na_v1.5$ expressions and their corresponding quantification expression expressed as a ratio of actin in A) 3 months group (unpaired t-test) B) 12 months group (unpaired t-test) C) 20 months group (unpaired t-test) D) SHR group (one-way ANOVA followed by the Tukey's post-hoc) E) BN group (one-way ANOVA followed by the Tukey's post-hoc) F) WKY and BN group (unpaired t-test). (n=hearts) 3 months: WKY n=3; BN n=3; SHR n=3, 12 months: WKY n=3; BN n=3; SHR 3, 20 months: BN n=4; SHR n=6.

### 5.3.8. Myocardial fibrosis

Fibrosis was measured from slices obtained from SHR and normotensive rats and was found to be increased in SHR compared to the normotensive groups at all-time points. Furthermore, the level of fibrosis was also increased upon the progression of disease. There was also an effect of aging on fibrosis levels within the normotensive animal models (Figure 5.9).

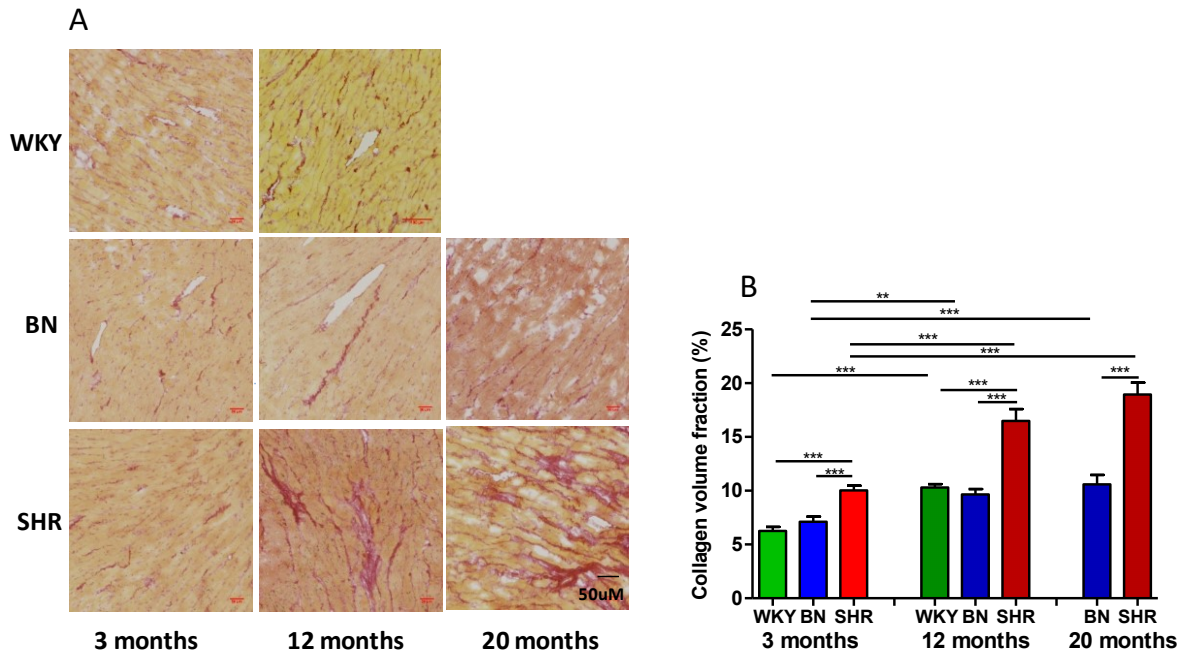


**Figure 5.9:Interstitial fibrosis level in hypertensive group.**

A) Representative images of picrosirius red stained sections showing increased interstitial fibrosis during disease development and aging. B) Quantitative analysis of collagen fraction area at 3, 12 and 20 months acquired from 10 sections per animal. unpaired t-test used to compare normotensive group with SHR within the same timepoint group while one-way ANOVA followed by the Tukey's post-hoc was used to compare fibrosis level in SHR and BN groups with age progression (n=section/hearts) 3 months: WKY n=11/3; BN n=26/3; SHR n=37/3, 12 months: WKY n=27/3; BN n=28/3; SHR 25/3, 20 months: BN n=20/4; SHR n=26/6.

## 5.4. Discussion

This chapter describes the electrophysiological and structural abnormalities recorded from the slice preparation in the hypertension rat model, SHR. The main findings of this chapter include: 1) SHR animals show cardiac hypertrophy at all-time points with signs of deterioration at 20 months; 2) FPD at different pacing rates were only prolonged in the 12 month old SHR group when compared to WKY; 3) SHR show no change in FPD heterogeneity at all-time points; 4) there was a longer FPD in the endocardium at 12 months and in the mid-myocardium at 20 months for the SHR group; 5) furthermore, SHR showed an overall change in $CV_L$, however, there was pronounced reduction in the oldest group; 6) this was accompanied by a reduction in Cx43 and $Na_v1.5$ protein levels; 7) BN and SHR groups also showed a reduction in $CV_T$ with age and disease progression, and this concurred with increased levels of fibrosis; 8) as well as this, no essential transmural changes in CV were found in SHR; and 8) finally, normotensive groups present structural and functional abnormalities, which are age-related.

### 5.4.1. SHR show LV hypertrophy

As in the TAC model (chapter 4), cardiac functional assessment by echocardiography was carried out prior to electrophysiological and structural evaluation.

SHR is a model of hypertrophy induced by hypertension that causes chronic homogeneous ventricular remodelling. However, the SHR model displays a slower progression to LV dysfunction compared with the TAC model; which may contribute to different responses in functional remodelling (Ward et al. 2011; Halapas et al. 2008; Cantor et al. 2005). To assess these changes during the development of pressure overload, we have chosen to measure electrophysiological parameters at different time points using myocardial slices.

The increased heart weight to body weight ratio, along with a higher LV posterior wall thickness in SHR, significantly indicates LV hypertrophy. Progression of LV hypertrophy to LV dysfunction has, therefore, been shown after 20 months in this model (Mirsky et al. 1983). We also show an increase in ejection fraction in SHR at 3, 9 and at 20 months compared to BN, suggesting a mechanism of compensatory hypertrophy. However, we observed that ejection fraction in SHR at 20 months was decreased by 18% compared to SHR at 12 months old animals, indicating a sign of cardiac deterioration in the oldest group.

Moreover, we measured systolic blood pressure at all-time points. The level of hypertension was greater in SHR compared to the normotensive strains and the level of hypertension was comparable to previous reports (Brooksby et al. 1993a; Brooksby et al. 1992; Shorofsky et al. 1999).

### 5.4.2. The normotensive rats exhibit structural and functional age related dysfunction

The SHR strain is produced from the inbreeding of hypertensive WKY rats and most studies have used WKY as the control group. However, previous reports show that inbred rat strains have a high incidence of pathology which occurs with advanced aging and makes it difficult to separate the effects of aging from those of disease (Walker et al. 2006). Susic et al., for example, showed progressive increases in myocardial collagen concentration, decreases in coronary flow reserve, and increases in minimal coronary vascular resistance in aged WKY and SHR rats (Susic et al. 1998). Another study showed that at the age of 6 months, WKY show LV hypertrophy which is not related to blood pressure or obstruction of the outflow tract. Both WKY and SHR exhibit an increase in papillary muscle stiffness and fibrosis levels compared with the normotensive Wistar rats, which, in turn, raises concerns about using this rat strain solely as a control for the SHR (Aiello et al. 2004). Furthermore, some reports showed that both breeds are genetically very different supporting the use of more than one

control strain besides WKY to be compared with SHR (Kurtz & Morris 1987; H'Doubler et al. 1991). For these reasons, we have used an additional normotensive group, the BN rats. We chose BN as this strain, along with the Fischer 344 (F344) and BN/F344 hybrid, has been used widely in gerontology studies due to their longer lifespan and lower rate of pathological development with aging (Wahr et al. 2000; Lipman et al. 1996; Capasso et al. 1990). In our study, this was not the case: BN displayed cardiac electrophysiological and structural changes as early as 12 months, and had age-dependent increases in fibrosis levels and conduction dysfunction. In addition, to this, Zaman et al., who used the same animals, observed that BN animals had a high incidence of atrial and ventricular arrhythmia at 3, 4, 6, and 12 months, and was similar to SHR animal models (Zaman et al. 2014). Finally, we found that the FPD values from the BN animals at all-time points were relatively higher when compared to the Lewis rats used as sham animals for the TAC group in chapter 4 (Figure4.3, A.). This suggests that a potential abnormal cardiac excitability exists at an early age in BN and that this progresses with aging in this rat strain. Further investigations are required to better validate these observations.

### 5.4.3. Field potential duration was relatively unchanged in SHR slices.

The prolongation of APD/FPD in hypertrophy and HF, and the different changes in ionic channels underlying this prolongation, were discussed in chapter 4. Prolongation of APD has been reported in tissue (Barbieri et al. 1994) and single isolated myocytes (Cerbai et al. 1994) in SHR and is mainly associated with a decrease in $I_{to}$ expression, the main current responsible for repolarisation in rats. Furthermore, it has also been shown that a decrease in $I_{to}$, not $Ik_1$, depends on the degree of hypertrophy which is more pronounced at 18 months than at 3 months after the development of hypertension. Surprisingly, SHR showed no change in FPD at all-time points, and paced at different rates compared to BN and WKY (three months). However, FPD was only prolonged in SHR at 12 months, when compared

with the WKY group. These findings could be explained by the occurrence of structural and functional abnormalities in the normotensive group, which by itself may have prolonged FPD. Regardless of the possible abnormality in the normotensive groups, SHR animals show a tendency to longer FPD compared to the normotensive group. As the duration of AP is heterogeneous across the LV, averaging the FPD from all slices might hide local differences. This explanation is supported by the observation that, when we measure FPD transmurally across the LV, we find that SHR FPD is significantly longer in the Endo region compared to WKY (in the 3 months' group). However, we cannot explain why there is a longer FPD at 3 months compared to 12 months in WKY. This is an anomaly that requires further investigation.

In addition, FPD changes in hypertrophy are complex and, therefore, more detailed investigations are needed to elucidate these variations, including $K^+$ and $Ca^{+2}$ currents and their expression in slices from both SHR and the normotensive groups.

FPD did not shorten with faster pacing within the same group of animals (BN, WKY and SHR), as we noticed in the TAC or UL groups (Figure 4.3, C and Figure 3.3, C). This discrepancy is also difficult to explain and might be due to differences in the strain or the age of the animals.

Heterogeneity of repolarisation is a potential source of arrhythmogenesis (C. S. Kuo et al. 1983). It may provide the basis for unidirectional block and, combined with a reduced conduction velocity, re-entrant arrhythmias (Mines 1914). However, APD heterogeneity was found to be more pronounced in isolated cardiomyocytes as electrical coupling reduces the heterogeneity in APD in multicellular preparation, such as slices (Zaniboni et al. 2000; Janse et al. 2005). In the intact heart, this phenomenon may become evident in pathological conditions because of the reduced intercellular electrical coupling following an increase in the level of fibrosis or a decrease in the level of Cx43 (Akar 2010). We have tested the FPD

heterogeneity in each slice from SHR and the normotensive groups at all-time points by measuring the standard deviation of FPD, as described in chapter 2 section 2.6.1.2. FPD heterogeneity was seen to increase in SHR compared to the normotensive controls mostly at the early stage (3months), however, this increase was not statistically significant. The TAC group (chapter 4), on the other hand, showed a different behaviour at an early time point with a clear increase in FPD heterogeneity. Nonetheless, at the late time point, this parameter was no longer different. Thus, indicating that cardiac overload in both groups (TAC and SHR) may increase FPD heterogeneity but could also be dependent on the cause and the stage of injury, and the type of strain used.

We tested the level of fibrosis and Cx43 in SHR rats. Changes in these parameters were found to contribute to left ventricular repolarisation heterogeneity as they cause a reduction in electrical coupling (Akar 2010). We found that the level of fibrosis in the SHR group was increased with decreased Cx43 levels at all-time points; nonetheless, these changes in fibrosis and Cx43 were not sufficient to cause noticeable changes in FPD heterogeneity. Similar findings were also obtained in the BN control group. Further investigations on FPD heterogeneity within slices and its underlying histological/molecular determinants are needed to understand the mechanisms responsible for the observed effects.

### 5.4.4. SHR show no changes in transmural dispersion of FPD

Many previous studies have demonstrated that LV myocardium is transmurally heterogeneous as it contains at least three electrophysiologically distinct cell types: Epicardial, M and endocardial cells (Antzelevitch et al. 1999; Antzelevitch Charles & Dumaine Robert 2011). Many studies have correlated M cells to the magnitude of dispersion in the repolarisation across the LV wall. M cells have, therefore, been described in canine (Weissenburger et al. 2000; el-Sherif et al. 1996; Sicouri & Antzelevitch 1991; Liu & Antzelevitch 1995b; Liu et al. 1993), guinea pig (Sicouri et al. 1996), rabbit (McIntosh 2000;

Idriss & Wolf 2004), pig (Stankovicova 2000) and human ventricles , respectively (G. R. Li et al. 1998; Glukhov et al. 2010; Drouin et al. 1995). In other studies, however, they failed to distinguish M cells in the ventricles of the pig and guinea pig (Rodríguez-Sinovas 1997; Bryant 1998). Moreover, other studies which identified M cells in the ventricles of canine hearts *in vitro* have also failed to identify them in an intact heart *in vivo* (Anyukhovsky et al. 1999; Anyukhovsky et al. 1996). Thus, this controversy is thought to be due to methodological differences in these studies (Antzelevitch et al. 1999; Antzelevitch Charles & Dumaine Robert 2011). Transmural studies from rat isolated cardiomyocytes have failed to identify cells with M cell characteristics and APD was found to be shortened monotonically in the direction of propagation (i.e., endocardium to epicardium) (Shipsey et al. 1997). This might be due to the less important role for $I_{Ks}$ in rats, while $I_{Ks}$ has an essential role on AP morphology and duration in other larger animals and humans (Jost et al. 2005; Varro et al. 2000). However, many studies have shown that modulation in the transmural heterogeneity of APD across the LV in rat models of hypertrophy and HF can predispose the heart to arrhythmias (Shipsey et al. 1997; Evans et al. 1995); conditions which SHR are vulnerable in developing (Zaugg et al. 1997).

We have tested the transmural changes of FPD in slices obtained from SHR and the normotensive groups, WKY and BN. Interestingly, slices from the normotensive groups show no transmural changes in FPD across the LV. In addition, FPD at 3 and 12 months showed significant prolongation for Endo and Myo, respectively, in SHR. In contrast, previous studies showed regional differences in APD between Endo and Epi myocytes in normotensive control animals but this physiological APD gradient was no longer observed in SHR (Roman-Campos et al. 2012; McCrossan et al. 2004). One explanation is that myocytes within slices are electrically coupled and, therefore, transmural APD differences are less pronounced in multicellular preparations (Boukens et al. 2009; Taggart et al. 1995).

### 5.4.5. SHR show changes in CV which are associated with alterations in Cx43, $Na_v1.5$ and fibrosis levels

Left ventricular hypertrophy is an early manifestation of cardiac remodelling in hypertension (Novo et al. 1991; Kohya et al. 1995). Therefore, abnormalities in CV and arrhythmias are well documented in animal models and humans with hypertension (Khwaounjoo et al. 2015; González-Fernández et al. 1992). As a result, defects in CV account for several structural and functional changes, including cell size, Cx43 density and distribution, fibrosis level, $I_{Na}$ channel density and excitability (Bacharova 2007). For this reason, we have measured CV in slices obtained from SHR and compared it with the normotensive groups. Following this, we also measured Cx43, $Na_v1.5$ and fibrosis levels from the same slices to correlate these parameters with CV abnormalities.

The total CV in the SHR group (averaged from CV measured in the four different directions) was slower in the 12 months group when compared to WKY. However, SHR showed only a decreasing trend for CV when compared with the 12 months BN group. SHR CV, however, was only significantly slower than BN at 20 months of age.

AR is an important parameter to measure as changes associated with this parameter factor can contribute to arrhythmogenesis (Valderrábano 2007). Using slice preparations can, therefore, have the advantage of maintaining the AR which allows longitudinal and transverse conduction velocity measurements.

In SHR, $CV_L$ was slower at 12 and 20 months when compared to the normotensive groups that were age-dependent. We furtherly tested the expression of Cx43 and $Na_v1.5$ as they are enriched at the longitudinal junctions and any changes in them can affect CV longitudinally. We found that Cx43 in SHR was significantly decreased at all-time points when compared to the normotensive groups. Thus, it was decreased within both BN and SHR as hypertension and aging were progressing.

On the other hand, $Na_v1.5$ in SHR was decreased only in the very aged group (20 months). Interestingly, Cx43 and $Na_v1.5$ protein levels were decreased within the SHR group while Cx43 protein levels decreased with age in the BN group; indicating that aging also affects Cx43. Despite this change in Cx43 levels, no change in $CV_L$ was observed. Despite this, Cx43 alterations in hypertension have been reported but continue to remain controversial. In agreement with our results, Radosinska et al. found that Cx43 levels declined significantly in the myocardium in both young (3-month-old) and old (12-month-old) SHRs and increased after supplements of omega-3 polyunsaturated fatty acids (Radosinska et al. 2011). In addition, Bacharova et al. revealed that the declined expression of Cx43 was responsible for the early stages of ventricular hypertrophy (Bacharova et al. 2008), whereas Zhang et al. discovered that the total membrane and mitochondrial Cx43 expression was decreased in SHR during end-stage hypertension, along with impaired localisation and distribution (Zhang et al. 2014). In contrast, in another study, Cx43 expression was reported to be increased in the LV of SHRs and could be reversed by Losartan administration (Fialová et al. 2008; Zhao et al. 2008). The reasons for these discrepancies are unknown but these studies were performed on SHR at different ages, and this could potentially explain the variability of the observed results.

$CV_T$ was slowed in SHR at 3 months only when compared to the BN group and increased when compared to WKY. However, WKY CV at 3 months was unexpectedly slower than the 12 month group which suggests a possible abnormality in the 3 month group. These results are difficult to explain and would require further investigation.

In contrast, there was no change in SHR $CV_T$ at 12 and 20 months when compared with BN. As well as this, both SHR and BN showed slower $CV_T$ with time. This suggests that aging and hypertension are, in fact, affecting this parameter. We have measured the level of fibrosis

as it has been known that excessive fibrosis accumulation is associated with abnormal conduction and arrhythmias (Almaas et al. 2013; Morita et al. 2014). Hence, we have found that the levels of fibrosis were increased with time in both SHR and BN, respectively.

### 5.4.6. SHR show no changes in transmural dispersion of CV

As mentioned previously, CV depends on the availability of $Na^+$ channels and intercellular electric coupling by gap junctions. Therefore, heterogeneity in the expression of $Na^+$ channels or/and connexins within the LV wall may lead to transmural differences in CV, which makes some parts of the heart more vulnerable to re-entrant arrhythmias (Allessie et al. 1977). For this reason, we have measured changes in transmural CV in this model. Although previous reports show changes in CV transmurally (Poelzing & Rosenbaum 2004; Poelzing et al. 2004; Glukhov et al. 2012) with a slower CV in the Epi region compared with the Endo region, this was not the case in our study and we were unable to detect vital transmural changes in CV.

## 5.5. Summary

Using the slice preparation, SHR animals showed no change in FPD at all time points when compared to normotensive groups and this could be due to abnormality in the control groups which need further investigations. On the other hand, CV, $CV_L$ and $CV_T$ were altered and were associated with alterations in Cx43, Nav1.5 protein levels and fibrosis. Finally, both hypertension and aging were seen to influence CV.

# CHAPTER 6.General discussion

## 6.1. Summary of findings

In this thesis, we have used the recently optimised technique of cardiac slices preparation to investigate electrical remodelling in various rat models of cardiac disease. Although other multicellular preparations are currently available to study heart failure, the MEA system we used with the slices offers a potential for multiple recordings within the same heart. Furthermore, using slices as quasi–2D tissue preparation not only enabled the simplified assessments of CV and FPD but also took into account the potential impact of other cell types such as fibroblasts and endothelial cells. At the same time, we were able to use the same slice used for MEA recordings to measure $Na_v1.5$, Cx43 and fibrosis in the SHR group, therefore, allowing us to investigate more precisely the structural and functional interactions. In the following sections, I will discuss the key results of this work highlighting their strengths and limitations.

## 6.2. Mechanical unloading model

As discussed previously, due to the limitations in obtaining human tissue, we have used a partial model of unloading to mimic the effects of LVAD implantation in humans to investigate heart function. In addition, LVAD insertions are associated with arrhythmias and there is currently little information about the mechanisms underlying this condition.

In this part of my thesis, the aim was to study the electrophysiological changes using slices from a rat model of mechanical unloading. We utilised the partial mechanical unloading model in normal rats as the partial mechanical unloading of the LV in this model is more close to the effect of LVADs in humans, seeing as the heart with this device is not fully unloaded.

Previous studies have demonstrated that prolonged mechanical unloading can cause deterioration of cardiac function. As a result, we have used an 8-week model to study these

effects. We observed a significant prolongation of FPD with preserved CV in the unloaded hearts compared with the control groups, therefore, indicating that prolonged mechanical unloading primarily affects cell excitability and not conduction. Due to technical difficulties in preserving the tissue, we were unable to elucidate the underlying mechanisms of FPD changes including $I_{to}$, $I_K$ and $I_{K1}$ protein expression. We only obtained slices to investigate FPD and CV at one-time point in normal hearts. Thus, more time points are required to investigate the effect of duration on the electrophysiological remodelling in slice preparations. Moreover, the data we obtained from this study provides a baseline for studying this model using slices from failed hearts.

### 6.3. TAC model

In this part of my thesis, we obtained slices from TAC in rats, a commonly used experimental model for pressure overload-induced cardiac hypertrophy and heart failure, to study electrophysiological alterations. We utilised two-time points, the early (10 weeks) and late (20weeks), as the response to chronic hemodynamic overload becomes maladaptive, resulting in cardiac dilatation and heart failure. Our animals showed compensated hypertrophy at both time points (increase HW:BW ratio, LVPW and EF) with no signs of functional deterioration at the late time point. As expected, slices from TAC showed prolonged FPD at both time points when stimulated at 1 Hz and in the 20 weeks' group when stimulated at different frequencies. Slices from TAC showed a significant increase in the FPD heterogeneity within the slice compared with control and also showed significant prolonged FPD in the Epi, which might indicate that slices from TAC are more prone to arrhythmia. Finally, $CV_L$ in TAC was significantly faster at the early time point and was slower at the late time point when compared to the control group, which was expected. However, $CV_T$ was unchanged at both time points when compared to the controls. Further investigation of the underlying mechanisms of FPD and CV changes, including changes in $I_{to}$, $I_K$, $I_{K1}$, Cx43 protein

expression and fibrosis, could not be achieved in this study due to technical difficulties in preserving the tissue.

Our data suggest that slices from TAC rats are suitable preparations to study electrical remodelling at the multicellular level and we were able to show distinct alterations, however, further investigation is needed to elucidate the mechanisms underlying the electrical changes in this model.

### 6.4. SHR model

Here, we utilised slices from SHR, another rat model of pressure overload-induced cardiac hypertrophy and heart failure, to study the electrophysiological remodelling in this preparation. In addition, we were able to preserve the slices after MEA measurements for further structural investigations, therefore, allowing us to measure the level of Nav1.5, Cx43 and fibrosis from the same slices.

Unexpectedly, FPD was not significantly changed in SHR compared to the normotensive group, although, there was an increased trend in FPD in the SHR group. Furthermore, FPD heterogeneity within slices was unchanged in SHR when compared to the normotensive group. This could be due to an anomaly in our controls or that this experiment produced a false negative result. Another possible explanation is that FPD is more sensitive to age than disease. However, further investigations are required to elucidate the mechanisms underlying these observations by measuring $I_{to}$, $I_K$, $I_{K1}$ protein expression in both SHR and controls. There was a significant increase in the FPD in the endocardium at 12 months and in the mid-myocardium at 20 months for the SHR group. However, according to the available data, we could not provide an explanation for these results and more experiments will be required in the future. An overall change in $CV_L$ was observed in SHR. Although, in the oldest group, there was a significant reduction in $CV_L$ which was accompanied by a reduction in Cx43 and

$Na_v1.5$ protein levels. Furthermore, a significant reduction in $CV_T$ with age and disease progression was found and was associated with increased levels of fibrosis.

In conclusion, measuring CV and FPD both locally and transmurally was achieved in slice preparations used, which, as a result, provides further support to the use of this model in heart failure studies. In addition, we were able to use the same slices used for MEA measurements to investigate the underlying mechanism of CV changes which is fundamental for studying structural and functional changes precisely.

Table 6.1 show summary of the main results in this thesis and their possible implications.

**Table 6.1: Summary of the main findings and their implications**

| Model | Duration | FPD and heterogeneity | FPD transmural | CV | CV transmural | Cx43 | $Na_v1.5$ | Fibrosis | Possible mechanisms | Excluded mechanisms |
|---|---|---|---|---|---|---|---|---|---|---|
| **MUL** | 8 weeks | ↑at different pacing rate with ↑ heterogeneity | ↑ at Myo | ↔ | ↔ | Not tested | Not tested | Not tested | ↓ of $I_{to}$ mainly at the Myo<br>↑ NCX | |
| **TAC** | 10 and 20 weeks | ↑ at different pacing rate with ↑ heterogeneity at 10 weeks | ↑ at Epi | CV and $CV_L$ ↑at 10 weeks, ↔ at 20 weeks | ↑at 10 weeks at the Myo | Not tested | Not tested | Not tested | ↓ of $I_{to}$ mainly at the Epi<br>↑ NCX<br>Increase in CV is may associated with hypertrophy and cell size | |
| **SHR** | 3,12 and 24 months | ↑at different pacing rate with ↔ heterogeneity at 12 months compare with WKY | ↑ at Endo at 3 months and Myo at 12 months compared with WKY | ↓CV, $CV_L$ and $CV_T$ with age & disease development | ↓at 20 months at the Myo | ↓at all time points compared with controls &↓ with age and disease development | ↓at late stage | ↑at all time points compared with controls &↑ with age and disease development | Abnormalities in FPD in the BN.<br>Aging & disease both contribute to the electrophysiological parameters alterations.<br>Changes in CV are associated with changes in Cx43, $Na_v1.5$ & fibrosis | $Na_v1.5$ level independent to CV changes at early stage of disease or in aging |

## 6.5. Study limitations

Despite the several novel findings in our work there were also several limitations that were identified. It would be advantageous to measure action potentials directly via optical mapping to compare the results, as the variability of t-wave morphology in MEA slightly diminished the accuracy and any subtle differences between the different disease models. However, several attempts were made to image the action potentials optically, including different dyes, incubation times and excitation contraction un-couplers (BDM and blebbistatin), however, these were unsuccessful.

Another limitation is that FPs showed fractionation in the depolarisation peak which makes slice analysis for FPD and CV both challenging and time consuming as an automated analysis could not be used. Although we succeeded in measuring transmural CV and FPD for the first time in rat LVs, the obtained information could not provide us with a scientific explanation due do incomplete transmural analysis measurements.

## 6.6. Future directions

Future work is needed to provide a more detailed mechanistic insight into the findings of this study. This includes adopting other ways to measure AP in addition to the MEAs such as microelectrode recording or optical mapping to obtain a more precise analysis of APs in rats. Furthermore, I would like to investigate $Na^+$ and $K^+$ currents and protein expression levels responsible for FPD alterations seen in this study. Challenging cardiac slices, for example and model of mechanical unloading (partial unloading), using the fast pacing method to induce arrhythmia would be interesting when identifying the underlying mechanisms. Moreover, measuring $Ca^{2+}$ transients and $Ca^{2+}$ cycling proteins would provide us with information regarding the role of $Ca^{2+}$ in both FPD and CV alterations.

## 6.7. Conclusion

We have successfully showed that slices are good multicellular preparations to study electrophysiological remodelling obtained from different rat models of cardiovascular disease. As well as this, we have studied transmural FPD and CV for the first time in LV rat slices. This study paves the way to the use of this multicellular preparation method in understanding the mechanisms of cardiac disease, and to test new treatments and therapeutic targets for future clinical advances.

# CHAPTER 7. References

Abbott, C.P. et al., 1964. A Technique for heart transplantation in the rat. *Archives of surgery (Chicago, Ill. : 1960)*, 89, pp.645–52.

Abbott, C.P., Dewitt, C.W. & Creech, O., 1965. The transplanted rat heart: histologic and electrocardiographic changes. *Transplantation*, 3, pp.432–45.

Abdel-Latif, A. et al., 2007. Adult bone marrow-derived cells for cardiac repair: a systematic review and meta-analysis. *Archives of internal medicine*, 167(10), pp.989–97.

Ahmmed, G.U. et al., 2000. Changes in Ca(2+) cycling proteins underlie cardiac action potential prolongation in a pressure-overloaded guinea pig model with cardiac hypertrophy and failure. *Circulation research*, 86(5), pp.558–570.

Aiello, E.A. et al., 2004. Myocardial hypertrophy of normotensive Wistar-Kyoto rats. *American journal of physiology. Heart and circulatory physiology*, 286(4), pp.H1229–35.

Akar, F.G., 2010. Left ventricular repolarization heterogeneity as an arrhythmic substrate in heart failure. *Minerva Cardioangiologica*, 58(2), pp.205–212.

Akar, F.G. et al., 2004. Mechanisms underlying conduction slowing and arrhythmogenesis in nonischemic dilated cardiomyopathy. *Circulation research*, 95(7), pp.717–25.

Akar, F.G. et al., 2005. Molecular mechanisms underlying K+ current downregulation in canine tachycardia-induced heart failure. *American journal of physiology. Heart and circulatory physiology*, 288(6), pp.H2887–96.

Akar, F.G. et al., 2002. Unique topographical distribution of M cells underlies reentrant mechanism of torsade de pointes in the long-QT syndrome. *Circulation*, 105(10), pp.1247–53.

Akar, F.G. & Rosenbaum, D.S., 2003. Transmural electrophysiological heterogeneities underlying arrhythmogenesis in heart failure. *Circulation Research*, 93(7), pp.638–645.

Allessie, M. a, Bonke, F.I. & Schopman, F.J., 1977. Circus movement in rabbit atrial muscle as a mechanism of tachycardia. III. The "leading circle" concept: a new model of circus movement in cardiac tissue without the involvement of an anatomical obstacle. *Circulation research*, 41(1), pp.9–18.

Almaas, V.M. et al., 2013. Increased amount of interstitial fibrosis predicts ventricular arrhythmias, and is associated with reduced myocardial septal function in patients with obstructive hypertrophic cardiomyopathy. *Europace : European pacing, arrhythmias, and cardiac electrophysiology : journal of the working groups on cardiac pacing, arrhythmias, and cardiac cellular electrophysiology of the European Society of Cardiology*, 15(9), pp.1319–27.

Ambardekar, A. V & Buttrick, P.M., 2011. Reverse remodelling with left ventricular assist devices: a review of clinical, cellular, and molecular effects. *Circulation. Heart failure*, 4(2), pp.224–33.

Amin, A.S., Tan, H.L. & Wilde, A.A.M., 2010. Cardiac ion channels in health and disease. *Heart rhythm : the official journal of the Heart Rhythm Society*, 7(1), pp.117–26.

An, W.F. et al., 2000. Modulation of A-type potassium channels by a family of calcium sensors. *Nature*, 403(6769), pp.553–6.

Anderson, K.P. et al., 1993. Myocardial electrical propagation in patients with idiopathic dilated cardiomyopathy. *Journal of Clinical Investigation*, 92(1), pp.122–140.

Antzelevitch Charles & Dumaine Robert, 2011. Electrical Heterogeneity in the Heart: Physiological, Pharmacological and Clinical Implications. In *Comprehensive Physiology*. Hoboken, NJ, USA: John Wiley & Sons, Inc.

Antzelevitch, C. et al., 1991. Heterogeneity Within the Ventricular Wall. *Circulation research*, 69(6), pp.1427–1449.

Antzelevitch, C., 2005. Role of transmural dispersion of repolarization in the genesis of drug-induced torsades de pointes. *Heart rhythm : the official journal of the Heart Rhythm Society*, 2(2 Suppl), pp.S9–15.

Antzelevitch, C. et al., 1999. The M cell: its contribution to the ECG and to normal and abnormal electrical function of the heart. *Journal of cardiovascular electrophysiology*, 10(8), pp.1124–52.

Antzelevitch, C. & Dumaine, R., 2011. Electrical Heterogeneity in the Heart: Physiological, Pharmacological and Clinical Implications. In *Comprehensive Physiology*. John wiley & Sons,Inc.., pp. 654–692.

Antzelevitch, C. & Fish, J., 2001. Electrical heterogeneity within the ventricular wall. *Basic Research in Cardiology*, 96(6), pp.517–527.

Anyukhovsky, E.P. et al., 1999. The controversial M cell. *Journal of cardiovascular electrophysiology*, 10(2), pp.244–60.

Anyukhovsky, E.P., Sosunov, E.A. & Rosen, M.R., 1996. Regional differences in electrophysiological properties of epicardium, midmyocardium, and endocardium. In vitro and in vivo correlations. *Circulation*, 94(8), pp.1981–8.

Apkon, M. & Nerbonne, J.M., 1991. Characterization of two distinct depolarization-activated K+ currents in isolated adult rat ventricular myocytes. *The Journal of general physiology*, 97(5), pp.973–1011.

Aquila, L.A. et al., 2004. Cytoskeletal structure and recovery in single human cardiac myocytes. *The Journal of heart and lung transplantation : the official publication of the International Society for Heart Transplantation*, 23(8), pp.954–63.

Aslanidi, O. V et al., 2010. Ionic mechanisms for electrical heterogeneity between rabbit Purkinje fiber and ventricular cells. *Biophysical journal*, 98(11), pp.2420–31.

Assayag, P. et al., 1997. Compensated cardiac hypertrophy: arrhythmogenicity and the new myocardial phenotype. I. Fibrosis. *Cardiovascular Research*, 34, pp.439–444.

Attwell, D., Cohen, I. & Eisner, D.A., 1981. The effects of heart rate on the action potential of guinea-pig and human ventricular muscle. *The Journal of physiology*, 313, pp.439–61.

Baartscheer, A., 2003. [Na+]i and the driving force of the Na+/Ca2+-exchanger in heart failure. *Cardiovascular Research*, 57(4), pp.986–995.

Babuty, D. et al., 1998. Severe and early alteration of action potential during acute cardiac rejection in rats. *Journal of cardiovascular electrophysiology*, 9(10), pp.1085–93.

Bacharova, L. et al., 2008. Discrepancy between increased left ventricular mass and “normal” QRS voltage is associated with decreased connexin 43 expression in early stage of left ventricular hypertrophy in spontaneously hypertensive rats. *Journal of electrocardiology*, 41(6), pp.730–4.

Bacharova, L., 2007. Electrical and Structural Remodelling in Left Ventricular Hypertrophy—A Substrate for a Decrease in QRS Voltage? *Annals of Noninvasive Electrocardiology*, 12(3), pp.260–273.

Barbieri, M. et al., 1994. Electrophysiological basis for the enhanced cardiac arrhythmogenic effect of isoprenaline in aged spontaneously hypertensive rats. *Journal of molecular and cellular cardiology*, 26(7), pp.849–60.

Barbuti, A., Baruscotti, M. & Difrancesco, D., 2007. The pacemaker current: From basics to the clinics. *Journal of Cardiovascular Electrophysiology*, 18(3), pp.342–347.

Barclay, C.J., 2005. Modelling diffusive O(2) supply to isolated preparations of mammalian skeletal and cardiac muscle. *Journal of muscle research and cell motility*, 26(4-5), pp.225–35.

Bavendiek, U. et al., 1998. Effect of inotropic interventions on the force-frequency relation in the human heart. *Basic research in cardiology*, 93 Suppl 1, pp.76–85.

Bedi, M. et al., 2007. Ventricular arrhythmias during left ventricular assist device support. *The American journal of cardiology*, 99(8), pp.1151–1153.

Beisvag, V. et al., 2009. Pathological and physiological hypertrophies are regulated by distinct gene programs. *European journal of cardiovascular prevention and rehabilitation : official journal of the European Society of Cardiology, Working Groups on Epidemiology & Prevention and Cardiac Rehabilitation and Exercise Physiology*, 16(6), pp.690–7.

Bernardo, B.C. et al., 2010. Molecular distinction between physiological and pathological cardiac hypertrophy: experimental findings and therapeutic strategies. *Pharmacology & therapeutics*, 128(1), pp.191–227.

Bers, D.M., 2002. Cardiac excitation-contraction coupling. *Nature*, 415(6868), pp.198–205.

Bers, D.M., Pogwizd, S.M. & Schlotthauer, K., 2002. Upregulated Na/Ca exchange is involved in both contractile dysfunction and arrhythmogenesis in heart failure. *Basic research in cardiology*, 97 Suppl 1, pp.I36–42.

Beuckelmann, D.J., Nabauer, M. & Erdmann, E., 1993. Alterations of K+ currents in isolated human ventricular myocytes from patients with terminal heart failure. *Circulation Research*, 73(2), pp.379–385.

Bing, O.H. et al., 1995. The spontaneously hypertensive rat as a model of the transition from compensated left ventricular hypertrophy to failure. *Journal of molecular and cellular cardiology*, 27(1), pp.383–96.

Birks, E.J. et al., 2006. Left ventricular assist device and drug therapy for the reversal of heart failure. *The New England journal of medicine*, 355(18), pp.1873–84.

Birks, E.J. et al., 2011. Reversal of severe heart failure with a continuous-flow left ventricular assist device and pharmacological therapy: a prospective study. *Circulation*, 123(4), pp.381–90.

de Boer, T.P. De et al., 2009. Myocardial tissue slices: organotypic pseudo-2D models for cardiac research & development. *Future cardiology*, 5, pp.425–430.

Borlak, J. & Thum, T., 2003. Hallmarks of ion channel gene expression in end-stage heart failure. *FASEB journal : official publication of the Federation of American Societies for Experimental Biology*, 17(12), pp.1592–608.

Boukens, B.J.D. et al., 2009. Developmental basis for electrophysiological heterogeneity in the ventricular and outflow tract myocardium as a substrate for life-threatening ventricular arrhythmias. *Circulation Research*, 104(1), pp.19–31.

Brandenburger, M. et al., 2012. Organotypic slice culture from human adult ventricular myocardium. *Cardiovascular Research*, 93(1), pp.50–59.

Brilla, C.G., Matsubara, L. & Weber, K.T., 1996. Advanced hypertensive heart disease in spontaneously hypertensive rats. Lisinopril-mediated regression of myocardial fibrosis. *Hypertension*, 28(2), pp.269–75.

Brinks, H. et al., 2009. Contractile function is preserved in unloaded hearts despite atrophic remodelling. *The Journal of thoracic and cardiovascular surgery*, 137(3), pp.742–6.

Bristow, M.R. et al., 2004. Cardiac-resynchronization therapy with or without an implantable defibrillator in advanced chronic heart failure. *The New England journal of medicine*, 350(21), pp.2140–50.

Brooksby, P., Levi, A.J. & Jones, J. V, 1992. Contractile properties of ventricular myocytes isolated from spontaneously hypertensive rat. *Journal of hypertension*, 10(6), pp.521–7.

Brooksby, P., Levi, A.J. & Jones, J. V, 1993a. Investigation of the mechanisms underlying the increased contraction of hypertrophied ventricular myocytes isolated from the spontaneously hypertensive rat. *Cardiovascular research*, 27(7), pp.1268–77.

Brooksby, P., Levi, A.J. & Jones, J. V, 1993b. The electrophysiological characteristics of hypertrophied ventricular myocytes from the spontaneously hypertensive rat. *Journal of hypertension*, 11(6), pp.611–22.

Bruckner, B. a. et al., 2001. Regression of fibrosis and hypertrophy in failing myocardium following mechanical circulatory support. *Journal of Heart and Lung Transplantation*, 20(00), pp.457–464.

Bruckner, B. a. et al., 2000. The implications for cardiac recovery of left ventricular assist device support on myocardial collagen content. *American Journal of Surgery*, 180(00), pp.498–502.

Bruckner, B.A. et al., 2001. Regression of fibrosis and hypertrophy in failing myocardium following mechanical circulatory support. *The Journal of heart and lung transplantation : the official publication of the International Society for Heart Transplantation*, 20(4), pp.457–64.

Bruckner, B.A. et al., 2000. The implications for cardiac recovery of left ventricular assist device support on myocardial collagen content. *American journal of surgery*, 180(6), pp.498–501; discussion 501–2.

Bryant, S., 1998. Regional differences in the delayed rectifier current (IKr and IKs) contribute to the differences in action potential duration in basal left ventricular myocytes in guinea-pig. *Cardiovascular Research*, 40(2), pp.322–331.

Bucchi, A. et al., 2006. Properties of ivabradine-induced block of HCN1 and HCN4 pacemaker channels. *The Journal of physiology*, 572(Pt 2), pp.335–46.

Burashnikov, A. et al., 2007. Atrium-Selective Sodium Channel Block as a Strategy for Suppression of Atrial Fibrillation: Differences in Sodium Channel Inactivation Between Atria and Ventricles and the Role of Ranolazine. *Circulation*, 116(13), pp.1449–1457.

Burchfield, J.S., Xie, M. & Hill, J.A., 2013. Pathological ventricular remodelling: mechanisms: part 1 of 2. *Circulation*, 128(4), pp.388–400.

Burgess, M.J., 1979. Relation of ventricular repolarization to electrocardiographic T wave-form and arrhythmia vulnerability. *The American journal of physiology*, 236(3), pp.H391–402.

Burnashev, N.A., Edwards, F.A. & Verkhratsky, A.N., 1990. Patch-clamp recordings on rat cardiac muscle slices. *Pflügers Archiv : European journal of physiologygers Archiv European Journal of Physiology*, 417(1), pp.123–125.

Bussek, A. et al., 2012a. Cardiac tissue slices with prolonged survival for in vitro drug safety screening. *Journal of Pharmacological and Toxicological Methods*, 66(2), pp.145–151.

Bussek, A. et al., 2009. Tissue slices from adult mammalian hearts as a model for pharmacological drug testing. *Cellular Physiology and Biochemistry*, 24(5-6), pp.527–536.

Calhoun, D.A. et al., 1994. Diurnal blood pressure variation and dietary salt in spontaneously hypertensive rats. *Hypertension*, 24(1), pp.1–7.

Camelliti, P. et al., 2011. Adult human heart slices are a multicellular system suitable for electrophysiological and pharmacological studies. *Journal of Molecular and Cellular Cardiology*, 51(3), pp.390–398.

Camelliti, P. et al., 2004. Fibroblast network in rabbit sinoatrial node: structural and functional identification of homogeneous and heterogeneous cell coupling. *Circulation research*, 94(6), pp.828–35.

Camelliti, P. et al., 2013. Mapping of repolarisation gradients in the canine left ventricular free wall using myocardial slices. *Proceedings of The Physiological Society*, Proc 37th.

Camelliti, P., Al-Ayoubi, S. & Terracciano, C., 2014. Mapping regional repolarisation gradients in the failing human ventricle using cardiac slices. *Heart*, 100(Suppl 4), pp.A20–A20.

Campbell, C., Tadros, N. & Heimbecker, R.O., 1986. Heterotopic heart-lung transplantation: a new experimental model. *The Journal of heart transplantation*, 5(6), pp.465–70.

Cantor, E.J.F. et al., 2005. A comparative serial echocardiographic analysis of cardiac structure and function in rats subjected to pressure or volume overload. *Journal of molecular and cellular cardiology*, 38(5), pp.777–86.

Capasso, J.M. et al., 1990. Severe myocardial dysfunction induced by ventricular remodelling in aging rat hearts. *The American journal of physiology*, 259(4 Pt 2), pp.H1086–96.

Carll, A.P. et al., 2011. Merits of non-invasive rat models of left ventricular heart failure. *Cardiovascular toxicology*, 11(2), pp.91–112.

Carmeliet, E., 2004. Intracellular Ca(2+) concentration and rate adaptation of the cardiac action potential. *Cell calcium*, 35(6), pp.557–73.

Carmeliet, E. & Vereecke, J., 2002. *Cardiac Cellular Electrophysiology*, Boston, MA: Springer US.

Casis, O. et al., 1998. Differences in regional distribution of K+ current densities in rat ventricle. *Life Sciences*, 63(5), pp.391–400.

Cerbai, E. et al., 1994. Ionic basis of action potential prolongation of hypertrophied cardiac myocytes isolated from hypertensive rats of different ages. *Cardiovascular Research*, 28(8), pp.1180–1187.

Cerbai, E., 2000. Long-term treatment of spontaneously hypertensive rats with losartan and electrophysiological remodelling of cardiac myocytes. *Cardiovascular Research*, 45(2), pp.388–396.

Chaudhary, K.W. et al., 2004. Altered myocardial Ca2+ cycling after left ventricular assist device support in the failing human heart. *Journal of the American College of Cardiology*, 44(4), pp.837–45.

Cheng, J. & Kodama, I., 2004. Two components of delayed rectifier K+ current in heart: molecular basis, functional diversity, and contribution to repolarization. *Acta pharmacologica Sinica*, 25(2), pp.137–45.

Cherry, E.M., Fenton, F.H. & Gilmour, R.F., 2012. Mechanisms of ventricular arrhythmias: a dynamical systems-based perspective. *AJP: Heart and Circulatory Physiology*, 302(12), pp.H2451–H2463.

Christiansen, S., Klocke, A. & Autschbach, R., 2008. Past, present, and future of long-term mechanical cardiac support in adults. *Journal of cardiac surgery*, 23(6), pp.664–76.

Clark, R.B. et al., 1993. Heterogeneity of action potential waveforms and potassium currents in rat ventricle. *Cardiovascular Research*, 27(10), pp.1795–9.

Claycomb, W.C., 1978. Biochemical aspects of cardiac muscle differentiation. *The Biochemical journal*, 171(2), pp.289–98.

Clerc, L., 1976. Directional differences of impulse spread in trabecular muscle from mammalian heart. *The Journal of physiology*, 255(2), pp.335–46.

Cooklin, M. et al., 1997. Changes in cell-to-cell electrical coupling associated with left ventricular hypertrophy. *Circulation research*, 80(6), pp.765–71.

Cooklin, M. et al., 1998. Conduction velocity and gap junction resistance in hypertrophied, hypoxic guinea-pig left ventricular myocardium. *Experimental Physiology*, 83(6), pp.763–770.

Coronel, R. et al., 2013. Electrophysiological changes in heart failure and their implications for arrhythmogenesis. *Biochimica et biophysica acta*, 1832(12), pp.2432–41.

Coronel, R., de Groot, J.R. & van Lieshout, J.J., 2001. Defining heart failure. *Cardiovascular research*, 50(3), pp.419–22.

Coumel, P., 1987. The management of clinical arrhythmias. An overview on invasive versus non-invasive electrophysiology. *European heart journal*, 8(2), pp.92–9.

Cutler, M.J., Jeyaraj, D. & Rosenbaum, D.S., 2011. Cardiac electrical remodelling in health and disease. *Trends in pharmacological sciences*, 32(3), pp.174–80.

Dandel, M., Knosalla, C. & Hetzer, R., 2014. Contribution of ventricular assist devices to the recovery of failing hearts: a review and the Berlin Heart Center Experience. *European journal of heart failure*, 16(3), pp.248–63.

Desplantez, T. et al., 2007. Gap junction channels and cardiac impulse propagation. *The Journal of membrane biology*, 218(1-3), pp.13–28.

Dickstein, K. et al., 2008. ESC Guidelines for the diagnosis and treatment of acute and chronic heart failure 2008: the Task Force for the Diagnosis and Treatment of Acute and Chronic Heart Failure 2008 of the European Society of Cardiology. Developed in collaboration with the Heart. *European heart journal*, 29(19), pp.2388–442.

Didié, M. et al., 2013. Preservation of left ventricular function and morphology in volume-loaded versus volume-unloaded heterotopic heart transplants. *American journal of physiology. Heart and circulatory physiology*, 305(4), pp.H533–41.

DiFrancesco, D., 2005. Cardiac pacemaker I(f) current and its inhibition by heart rate-reducing agents. *Current Medical Research and Opinion*, 21(7), pp.1115–22.

DiFrancesco, D. & Noble, D., 1985. A Model of Cardiac Electrical Activity Incorporating Ionic Pumps and Concentration Changes. *Philosophical Transactions of the Royal Society B: Biological Sciences*, 307(1133), pp.353–398.

Dipla, K. et al., 1998. Myocyte Recovery After Mechanical Circulatory Support in Humans With End-Stage Heart Failure. *Circulation*, 97(23), pp.2316–2322.

Dobrzynski, H., Boyett, M.R. & Anderson, R.H., 2007. New insights into pacemaker activity: Promoting understanding of sick sinus syndrome. *Circulation*, 115(14), pp.1921–1932.

Dorn, G.W. et al., 1999. Low- and high-level transgenic expression of beta2-adrenergic receptors differentially affect cardiac hypertrophy and function in Galphaq-overexpressing mice. *Proceedings of the National Academy of Sciences of the United States of America*, 96(11), pp.6400–5.

Dorn, G.W. & Force, T., 2005. Protein kinase cascades in the regulation of cardiac hypertrophy. *The Journal of clinical investigation*, 115(3), pp.527–37.

Dorn, G.W., Robbins, J. & Sugden, P.H., 2003. Phenotyping hypertrophy: eschew obfuscation. *Circulation research*, 92(11), pp.1171–5.

Drakos, S.G. et al., 2011. Reverse electrophysiologic remodelling after cardiac mechanical unloading for end-stage nonischemic cardiomyopathy. *The Annals of thoracic surgery*, 91(3), pp.764–9.

Draper, M.H. & Mya-tu, M., 1959. A comparison of the conduction velocity in cardiac tissues of various mammals. *Quarterly journal of experimental physiology and cognate medical sciences*, 44(1), pp.91–109.

Drouin, E. et al., 1995. Electrophysiologic characteristics of cells spanning the left ventricular wall of human heart: evidence for presence of M cells. *Journal of the American College of Cardiology*, 26(1), pp.185–92.

Edwards, F.A. et al., 1989. A thin slice preparation for patch clamp recordings from neurones of the mammalian central nervous system. *Pflügers Archiv European Journal of Physiology*, 414(5), pp.600–612.

Eghbali, M., 1992. Cardiac fibroblasts: function, regulation of gene expression, and phenotypic modulation. *Basic research in cardiology*, 87 Suppl 2, pp.183–9.

El-Mas, M.M. & Abdel-Rahman, A.A., 2005. Longitudinal studies on the effect of hypertension on circadian hemodynamic and autonomic rhythms in telemetered rats. *Life sciences*, 76(8), pp.901–15.

El-Sherif, N. et al., 1996. The electrophysiological mechanism of ventricular arrhythmias in the long QT syndrome. Tridimensional mapping of activation and recovery patterns. *Circulation research*, 79(3), pp.474–92.

Evans, S.J., Levi, A.J. & Jones, J. V, 1995. Wall stress induced arrhythmia is enhanced by low potassium and early left ventricular hypertrophy in the working rat heart. *Cardiovascular research*, 29(4), pp.555–62.

Fan, D. et al., 2012. Cardiac fibroblasts, fibrosis and extracellular matrix remodelling in heart disease. *Fibrogenesis & tissue repair*, 5(1), p.15.

Fauconnier, J., 2003. Ca2+ current-mediated regulation of action potential by pacing rate in rat ventricular myocytes. *Cardiovascular Research*, 57(3), pp.670–680.

Fedida, D. & Giles, W.R., 1991. Regional variations in action potentials and transient outward current in myocytes isolated from rabbit left ventricle. *The Journal of physiology*, 442, pp.191–209.

Fedorov, V. V et al., 2007. Application of blebbistatin as an excitation-contraction uncoupler for electrophysiologic study of rat and rabbit hearts. *Heart rhythm : the official journal of the Heart Rhythm Society*, 4(5), pp.619–26.

Fialová, M. et al., 2008. Adaptation of the heart to hypertension is associated with maladaptive gap junction connexin-43 remodelling. *Physiological research / Academia Scientiarum Bohemoslovaca*, 57(1), pp.7–11.

Fozzard, H.A. & Hanck, D.A., 1996. Structure and function of voltage-dependent sodium channels: comparison of brain II and cardiac isoforms. *Physiol Rev*, 76(3), pp.887–926.

Freeman, B.A. & O'Neil, J.J., 1984. Tissue slices in the study of lung metabolism and toxicology. *Environmental health perspectives*, 56, pp.51–60.

Frohlich, E.D. & Susic, D., 2012. Pressure overload. *Heart failure clinics*, 8(1), pp.21–32.

Gaztan, Larraitznaga, Francis E. Marchlinski, and B.P.B., 2012. Mechanisms of Cardiac Arrhythmias. *Update: Arrhythmias (II) Mechanisms*, 65(2), pp.174–185.

George, A.L., 2005. Inherited disorders of voltage-gated sodium channels. *The Journal of clinical investigation*, 115(8), pp.1990–9.

Glukhov, A. V. et al., 2012. Conduction remodelling in human end-stage nonischemic left ventricular cardiomyopathy. *Circulation*, 125(15), pp.1835–1847.

Glukhov, A. V. et al., 2010. Transmural dispersion of repolarization in failing and nonfailing human ventricle. *Circulation Research*, 106(5), pp.981–991.

Goldstein, S.A.N. et al., 2005. International Union of Pharmacology. LV. Nomenclature and Molecular Relationships of Two-P Potassium Channels. *Pharmacological Reviews*, 57(4), pp.527–540.

González-Fernández, R.A. et al., 1992. Reduction in cardiac conduction velocity delay by angiotensin converting enzyme inhibition in hypertensive patients with left ventricular hypertrophy. Detection by signal averaged electrocardiography. *American journal of hypertension*, 5(12 Pt 1), pp.896–9.

Gordon, C.R. et al., 2007. A new modified technique for heterotopic femoral heart transplantation in rats. *The Journal of surgical research*, 139(2), pp.157–63.

Le Grand, B.L. et al., 1994. Depressed transient outward and calcium currents in dilated human atria. *Cardiovascular research*, 28(4), pp.548–56.

Grant, A.O., 2009. Cardiac ion channels. *Circulation. Arrhythmia and electrophysiology*, 2(2), pp.185–94.

Grossman, W., Jones, D. & McLaurin, L.P., 1975. Wall stress and patterns of hypertrophy in the human left ventricle. *The Journal of clinical investigation*, 56(1), pp.56–64.

Gutman, G.A. et al., 2005. International Union of Pharmacology. LIII. Nomenclature and Molecular Relationships of Voltage-Gated Potassium Channels. *Pharmacological Reviews*, 57(4), pp.473–508.

H'Doubler, P.B. et al., 1991. Spontaneously hypertensive and Wistar Kyoto rats are genetically disparate. *Laboratory animal science*, 41(5), pp.471–3.

Habeler, W., Peschanski, M. & Monville, C., 2009. Organotypic heart slices for cell transplantation and physiological studies. *Organogenesis*, 5(2), pp.62–6.

Halapas, A. et al., 2008. In vivo models for heart failure research. *In Vivo*, 22(6), pp.767–780.

Halbach, M. et al., 2003. Estimation of action potential changes from field potential recordings in multicellular mouse cardiac myocyte cultures. *Cellular physiology and biochemistry : international journal of experimental cellular physiology, biochemistry, and pharmacology*, 13(5), pp.271–84.

Halbach, M. et al., 2006. Ventricular slices of adult mouse hearts--a new multicellular in vitro model for electrophysiological studies. *Cellular physiology and biochemistry : international journal of experimental cellular physiology, biochemistry, and pharmacology*, 18(1-3), pp.1–8.

Han, J. et al., 2002. Ketamine abolishes ischemic preconditioning through inhibition of K(ATP) channels in rabbit hearts. *American journal of physiology. Heart and circulatory physiology*, 283(1), pp.H13–21.

Harding, J.D. et al., 2001. Electrophysiological alterations after mechanical circulatory support in patients with advanced cardiac failure. *Circulation*, 104(11), pp.1241–1247.

Hart, G., 1994. Cellular electrophysiology in cardiac hypertrophy and failure. *Cardiovascular Research*, 28(7), pp.933–946.

Hasenfuss, G., 1998. Animal models of human cardiovascular disease, heart failure and hypertrophy. *Cardiovascular Research*, 39(1), pp.60–76.

Hasenfuss, G. & Pieske, B., 2002. Calcium cycling in congestive heart failure. *Journal of molecular and cellular cardiology*, 34(8), pp.951–69.

Heerdt, P.M. et al., 2000. Chronic unloading by left ventricular assist device reverses contractile dysfunction and alters gene expression in end-stage heart failure. *Circulation*, 102(22), pp.2713–9.

Heerdt, P.M. et al., 2002. Disease-specific remodelling of cardiac mitochondria after a left ventricular assist device. *The Annals of thoracic surgery*, 73(4), pp.1216–21.

Henein, M. et al., 2002. Images in cardiovascular medicine. Temporal and spatial changes in left ventricular pattern of flow during continuous assist device “HeartMate II”. *Circulation*, 105(19), pp.2324–5.

Henriques, J.P.S. & de Mol, B.A.J.M., 2008. New percutaneous mechanical left ventricular support for acute MI: the AMC MACH program. *Nature clinical practice. Cardiovascular medicine*, 5(2), pp.62–3.

Heron, I., 1971. A technique for accessory cervical heart transplantation in rabbits and rats. *Acta pathologica et microbiologica Scandinavica. Section A, Pathology*, 79(4), pp.366–72.

Herrmann, H.J., Fiedler, U. & Blodner, R., 1995. Pathogenesis of myocardial fibrosis in spontaneously hypertensive rats (SHR). *Eur. Heart J.*, 16(2), pp.243–252.

Herrmann, S. et al., 2007. HCN4 provides a "depolarization reserve" and is not required for heart rate acceleration in mice. *The EMBO journal*, 26(October), pp.4423–4432.

Himmel, H.M. et al., 2012. Field and action potential recordings in heart slices: Correlation with established in vitro and in vivo models. *British Journal of Pharmacology*, 166(1), pp.276–296.

Hodgkin, A.L. & Huxley, A.F., 1952. Propagation of electrical signals along giant nerve fibers. *Proceedings of the Royal Society of London. Series B, Biological sciences*, 140(899), pp.177–83.

Hodgkin, A.L. & Katz, B., 1949. The effect of sodium ions on the electrical activity of giant axon of the squid. *The Journal of physiology*, 108(1), pp.37–77.

Houser, S.R. et al., 2012. Animal models of heart failure: a scientific statement from the American Heart Association. *Circulation research*, 111(1), pp.131–50.

Houser, S.R., Piacentino, V. & Weisser, J., 2000. Abnormalities of calcium cycling in the hypertrophied and failing heart. *Journal of molecular and cellular cardiology*, 32(9), pp.1595–607.

Hunt, S.A. et al., 2009. 2009 focused update incorporated into the ACC/AHA 2005 Guidelines for the Diagnosis and Management of Heart Failure in Adults: a report of the American College of Cardiology Foundation/American Heart Association Task Force on Practice Guidelines: develope. *Circulation*, 119(14), pp.e391–479.

Ibrahim, M., Kukadia, P., et al., 2012. Cardiomyocyte Ca2+ handling and structure is regulated by degree and duration of mechanical load variation. *Journal of cellular and molecular medicine*, 16(12), pp.2910–8.

Ibrahim, M. et al., 2013. Heterotopic abdominal heart transplantation in rats for functional studies of ventricular unloading. *The Journal of surgical research*, 179(1), pp.e31–9.

Ibrahim, M., Rao, C., et al., 2012. Mechanical unloading and cell therapy have a synergistic role in the recovery and regeneration of the failing heart. *European journal of cardio-thoracic surgery : official journal of the European Association for Cardio-thoracic Surgery*, 42(2), pp.312–8.

Ibrahim, M., Navaratnarajah, M., et al., 2012. Mechanical unloading reverses transverse tubule remodelling and normalizes local Ca 2+ -induced Ca 2+ release in a rodent model of heart failure. *European Journal of Heart Failure*, 14(6), pp.571–580.

Ibrahim, M. et al., 2010. Prolonged mechanical unloading affects cardiomyocyte excitation-contraction coupling, transverse-tubule structure, and the cell surface. *FASEB journal : official publication of the Federation of American Societies for Experimental Biology*, 24(9), pp.3321–9.

Ibrahim, M. & Yacoub, M.H., 2014. Bridge to recovery and weaning protocols. *Heart failure clinics*, 10(1 Suppl), pp.S47–55.

Idriss, S.F. & Wolf, P.D., 2004. Transmural action potential repolarization heterogeneity develops postnatally in the rabbit. *Journal of cardiovascular electrophysiology*, 15(7), pp.795–801.

Iemitsu, M. et al., 2001. Physiological and pathological cardiac hypertrophy induce different molecular phenotypes in the rat. *American journal of physiology. Regulatory, integrative and comparative physiology*, 281(6), pp.R2029–36.

Ito, K. et al., 2003. Contractile reserve and calcium regulation are depressed in myocytes from chronically unloaded hearts. *Circulation*, 107(8), pp.1176–1182.

Janicki, J.S. & Brower, G.L., 2002. The role of myocardial fibrillar collagen in ventricular remodelling and function. *Journal of cardiac failure*, 8(6 Suppl), pp.S319–25.

Janse, M.J. et al., 2005. Repolarization gradients in the canine left ventricle before and after induction of short-term cardiac memory. *Circulation*, 112(12), pp.1711–8.

Jessup, M. & Brozena, S., 2003. Heart failure. *The New England journal of medicine*, 348(20), pp.2007–18.

Joffres, M. et al., 2013. Hypertension prevalence, awareness, treatment and control in national surveys from England, the USA and Canada, and correlation with stroke and ischaemic heart disease mortality: a cross-sectional study. *BMJ open*, 3(8), p.e003423.

De Jonge, N. et al., 2001. Does unloading the heart by a left ventricular assist device result in sustained reversal of myocyte dysfunction in end-stage heart failure? *The Journal of Heart and Lung Transplantation*, 20(2), p.202.

De Jonge, N. et al., 2005. Similar left and right ventricular sarcomere structure after support with a left ventricular assist device suggests the utility of right ventricular biopsies to monitor left ventricular reverse remodelling. *International journal of cardiology*, 98(3), pp.465–70.

Josephson, I.R., Sanchez-Chapula, J. & Brown, A.M., 1984. Early outward current in rat single ventricular cells. *Circulation research*, 54(2), pp.157–62.

Jost, N. et al., 2005. Restricting excessive cardiac action potential and QT prolongation: a vital role for IKs in human ventricular muscle. *Circulation*, 112(10), pp.1392–9.

Jugdutt, B.I., 2003. Remodelling of the myocardium and potential targets in the collagen degradation and synthesis pathways. *Current drug targets. Cardiovascular & haematological disorders*, 3(1), pp.1–30.

Kaab, S. et al., 1996. Ionic Mechanism of Action Potential Prolongation in Ventricular Myocytes From Dogs With Pacing-Induced Heart Failure. *Circulation Research*, 78(2), pp.262–273.

Kaab, S. et al., 1998. Molecular basis of transient outward potassium current downregulation in human heart failure: a decrease in Kv4.3 mRNA correlates with a reduction in current density. *Circulation*, 98(14), pp.1383–93.

Kamkin, A. et al., 1999. Mechanically induced potentials in fibroblasts from human right atrium. *Experimental physiology*, 84(2), pp.347–56.

Kamp, T.J. & Hell, J.W., 2000. Regulation of cardiac L-type calcium channels by protein kinase A and protein kinase C. *Circulation research*, 87(12), pp.1095–102.

Kang, C. et al., 2016. Human Organotypic Cultured Cardiac Slices: New Platform For High Throughput Preclinical Human Trials. *Scientific reports*, 6, p.28798.

De Kanter, R. et al., 2005. A new technique for preparing precision-cut slices from small intestine and colon for drug biotransformation studies. *Journal of pharmacological and toxicological methods*, 51(1), pp.65–72.

De Kanter, R. et al., 2002. Drug-metabolizing activity of human and rat liver, lung, kidney and intestine slices. *Xenobiotica; the fate of foreign compounds in biological systems*, 32(5), pp.349–62.

Kaprielian, R.R. et al., 1998. Downregulation of immunodetectable connexin43 and decreased gap junction size in the pathogenesis of chronic hibernation in the human left ventricle. *Circulation*, 97(7), pp.651–60.

Kehat, I. & Molkentin, J.D., 2010. Molecular pathways underlying cardiac remodelling during pathophysiological stimulation. *Circulation*, 122(25), pp.2727–35.

De Keulenaer, G.W. & Brutsaert, D.L., 2011. Systolic and diastolic heart failure are overlapping phenotypes within the heart failure spectrum. *Circulation*, 123(18), pp.1996–2004; discussion 2005.

Khwaounjoo, P. et al., 2015. Functional Imaging and Modeling of the Heart: 8th International Conference, FIMH 2015, Maastricht, The Netherlands, June 25-27, 2015. Proceedings. In H. van Assen, P. Bovendeerd, & T. Delhaas, eds. Cham: Springer International Publishing, pp. 48–56.

King, J.H., Huang, C.L.-H. & Fraser, J.A., 2013. Determinants of myocardial conduction velocity: implications for arrhythmogenesis. *Frontiers in physiology*, 4, p.154.

Kitzman, D.W., 2008. Diastolic dysfunction: one piece of the heart failure with normal ejection fraction puzzle. *Circulation*, 117(16), pp.2044–6.

Kléber, A.G. & Rudy, Y., 2004. Basic mechanisms of cardiac impulse propagation and associated arrhythmias. *Physiological reviews*, 84(2), pp.431–88.

Kleiman, R.B. & Houser, S.R., 1989. Outward currents in normal and hypertrophied feline ventricular myocytes. *The American journal of physiology*, 256(5 Pt 2), pp.H1450–61.

Klotz, S. et al., 2005. Left ventricular assist device support normalizes left and right ventricular beta-adrenergic pathway properties. *Journal of the American College of Cardiology*, 45(5), pp.668–76.

Klotz, S., Jan Danser, A.H. & Burkhoff, D., 2008. Impact of left ventricular assist device (LVAD) support on the cardiac reverse remodelling process. *Progress in biophysics and molecular biology*, 97(2-3), pp.479–96.

Kohya, T. et al., 1995. Regression of Left Ventricular Hypertrophy Prevents Ischemia-Induced Lethal Arrhythmias : Beneficial Effect of Angiotensin II Blockade. *Circulation Research*, 76(5), pp.892–899.

Komukai, K. et al., 2002. K(+) current distribution in rat sub-epicardial ventricular myocytes. *Pflügers Archiv : European journal of physiology*, 444(4), pp.532–8.

Kong, S.W. et al., 2005. Genetic expression profiles during physiological and pathological cardiac hypertrophy and heart failure in rats. *Physiological genomics*, 21(1), pp.34–42.

Korecky, B. & Masika, M., 1991. Use of heterotopically isotransplanted rat heart to study the effect of load on cardiac mass. *Journal of cardiovascular pharmacology*, 17 Suppl 2, p.S105.

Kowey, P.R. et al., 1992. Effect of gallopamil on electrophysiologic abnormalities and ventricular arrhythmias associated with left ventricular hypertrophy in the feline heart. *American heart journal*, 124(4), pp.898–905.

Kowey, P.R. et al., 1991. Electrophysiological Effects of Left Ventricular Hypertrophy Effect of Calcium and Potassium Channel Blockade. *Circulation*, 83, pp.2067–75.

Krebs, H.A., 1950. Body size and tissue respiration. *Biochimica et Biophysica Acta*, 4, pp.249–269.

Krenning, G., Zeisberg, E.M. & Kalluri, R., 2010. The origin of fibroblasts and mechanism of cardiac fibrosis. *Journal of cellular physiology*, 225(3), pp.631–7.

Krumdieck, C.L., dos Santos, J. & Ho, K.-J., 1980. A new instrument for the rapid preparation of tissue slices. *Analytical Biochemistry*, 104(1), pp.118–123.

Kubo, Y. et al., 2005. International Union of Pharmacology. LIV. Nomenclature and Molecular Relationships of Inwardly Rectifying Potassium Channels. *Pharmacological Reviews*, 57(4), pp.509–526.

Kukushkin, N.I., Gainullin, R.Z. & Sosunov, E.A., 1983. Transient outward current and rate dependence of action potential duration in rabbit cardiac ventricular muscle. *Pflügers Archiv European Journal of Physiology*, 399(2), pp.87–92.

Kumar, N.M. & Gilula, N.B., 1996. The gap junction communication channel. *Cell*, 84(3), pp.381–8.

Kuo, C.S. et al., 1983. Characteristics and possible mechanism of ventricular arrhythmia dependent on the dispersion of action potential durations. *Circulation*, 67(6), pp.1356–67.

Kuo, H.C. et al., 2001. A defect in the Kv channel-interacting protein 2 (KChIP2) gene leads to a complete loss of I(to) and confers susceptibility to ventricular tachycardia. *Cell*, 107(6), pp.801–13.

Kurtz, T.W. & Morris, R.C., 1987. Biological variability in Wistar-Kyoto rats. Implications for research with the spontaneously hypertensive rat. *Hypertension*, 10(1), pp.127–31.

Lebeche, D. et al., 2004. In vivo cardiac gene transfer of Kv4.3 abrogates the hypertrophic response in rats after aortic stenosis. *Circulation*, 110(22), pp.3435–43.

Lebeche, D., Kaprielian, R. & Hajjar, R., 2006. Modulation of action potential duration on myocyte hypertrophic pathways. *Journal of molecular and cellular cardiology*, 40(5), pp.725–35.

Levin, H.R. et al., 1995. Reversal of chronic ventricular dilation in patients with end-stage cardiomyopathy by prolonged mechanical unloading. *Circulation*, 91(11), pp.2717–20.

Levy, D. et al., 1996. The progression from hypertension to congestive heart failure. *JAMA*, 275(20), pp.1557–62.

Li, G.R. et al., 1999. Transmembrane ICa contributes to rate-dependent changes of action potentials in human ventricular myocytes. *The American journal of physiology*, 276(1 Pt 2), pp.H98–H106.

Li, G.R. et al., 1998. Transmural heterogeneity of action potentials and Ito1 in myocytes isolated from the human right ventricle. *The American journal of physiology*, 275(2 Pt 2), pp.H369–77.

Li, G.-R., Lau, C.-P., Ducharme, A., et al., 2002. Transmural action potential and ionic current remodelling in ventricles of failing canine hearts. *American journal of physiology. Heart and circulatory physiology*, 283(3), pp.H1031–41.

Li, G.-R., Lau, C.-P. & Shrier, A., 2002. Heterogeneity of sodium current in atrial vs epicardial ventricular myocytes of adult guinea pig hearts. *Journal of molecular and cellular cardiology*, 34(9), pp.1185–94.

Li, L. et al., 1998. Cardiac myocyte calcium transport in phospholamban knockout mouse: relaxation and endogenous CaMKII effects. *The American journal of physiology*, 274(4 Pt 2), pp.H1335–47.

Li, Y.Y., Feng, Y., McTiernan, C.F., Pei, W., Moravec, C.S., Wang, P., Rosenblum, W., Kormos, R.L. & Feldman, A.M., 2001. Downregulation of matrix metalloproteinases and reduction in collagen damage in the failing human heart after support with left ventricular assist devices. *Circulation*, 104(10), pp.1147–52.

Lipman, R.D. et al., 1996. Pathologic characterization of brown Norway, brown Norway x Fischer 344, and Fischer 344 x brown Norway rats with relation to age. *The journals of gerontology. Series A, Biological sciences and medical sciences*, 51(1), pp.B54–9.

Litovsky, S.H. & Antzelevitch, C., 1989. Rate dependence of action potential duration and refractoriness in canine ventricular endocardium differs from that of epicardium: role of the transient outward current. *Journal of the American College of Cardiology*, 14(4), pp.1053–66.

Liu, D.-W. & Antzelevitch, C., 1995a. Characteristics of the Delayed Rectifier Current (IKr and IKs) in Canine Ventricular Epicardial, Midmyocardial, and Endocardial Myocytes : A Weaker IKs Contributes to the Longer Action Potential of the M Cell. *Circulation Research*, 76(3), pp.351–365.

Liu, D.W., Gintant, G.A. & Antzelevitch, C., 1993. Ionic bases for electrophysiological distinctions among epicardial, midmyocardial, and endocardial myocytes from the free wall of the canine left ventricle. *Circulation research*, 72(3), pp.671–87.

Liu, Y. et al., 2015. Effect of chronic left ventricular unloading on myocardial remodelling: Multimodal assessment of two heterotopic heart transplantation techniques. *The Journal of heart and lung transplantation : the official publication of the International Society for Heart Transplantation*, 34(4), pp.594–603.

Lohse, M.J., Engelhardt, S. & Eschenhagen, T., 2003. What Is the Role of beta-Adrenergic Signaling in Heart Failure? *Circulation Research*, 93(10), pp.896–906.

Lue, W.M. & Boyden, P.A., 1992. Abnormal electrical properties of myocytes from chronically infarcted canine heart. Alterations in Vmax and the transient outward current. *Circulation*, 85(3), pp.1175–1188.

Lujan, H.L. et al., 2012. Ventricular function during exercise in mice and rats. *American journal of physiology. Regulatory, integrative and comparative physiology*, 302(1), pp.R68–74.

Di Lullo, G.A. et al., 2002. Mapping the ligand-binding sites and disease-associated mutations on the most abundant protein in the human, type I collagen. *The Journal of biological chemistry*, 277(6), pp.4223–31.

MacLeod, K., Ali, I. & Rauf, A., 2013. *An Essential Introduction to Cardiac Electrophysiology*, Imperial College Press.

Madigan, J.D. et al., 2001. Time course of reverse remodelling of the left ventricle during support with a left ventricular assist device. *The Journal of thoracic and cardiovascular surgery*, 121(5), pp.902–8.

Maillet, M., van Berlo, J.H. & Molkentin, J.D., 2012. Molecular basis of physiological heart growth: fundamental concepts and new players. *Nature Reviews Molecular Cell Biology*, 14(1), pp.38–48.

Maleckar, M.M. et al., 2009. Electrotonic coupling between human atrial myocytes and fibroblasts alters myocyte excitability and repolarization. *Biophysical journal*, 97(8), pp.2179–90.

Manabe, I., Shindo, T. & Nagai, R., 2002. Gene expression in fibroblasts and fibrosis: involvement in cardiac hypertrophy. *Circulation research*, 91(12), pp.1103–13.

Mancini, D.M., Beniaminovitz, A., et al., 1998. Low incidence of myocardial recovery after left ventricular assist device implantation in patients with chronic heart failure. *Circulation*, 98(22), pp.2383–9.

Mangoni, M.E. et al., 2006. Voltage-dependent calcium channels and cardiac pacemaker activity: From ionic currents to genes. *Progress in Biophysics and Molecular Biology*, 90(1-3), pp.38–63.

Marban, E., 1999. Heart Failure:The Electrophysiologic Connection. *Journal of Cardiovascular Electrophysiology*, 10(10), pp.1425–1428.

Marionneau, C. et al., 2008. Distinct cellular and molecular mechanisms underlie functional remodelling of repolarizing K+ currents with left ventricular hypertrophy. *Circulation research*, 102(11), pp.1406–15.

Massare, J. et al., 2010. Diminished cardiac fibrosis in heart failure is associated with altered ventricular arrhythmia phenotype. *Journal of cardiovascular electrophysiology*, 21(9), pp.1031–7.

Maybaum, S., Mancini, D., Xydas, S., Starling, R.C., et al., 2007. Cardiac improvement during mechanical circulatory support: a prospective multicenter study of the LVAD Working Group. *Circulation*, 115(19), pp.2497–505.

McCarthy, P.M. et al., 1995a. Hemodynamic and physiologic changes during support with an implantable left ventricular assist device. *Journal of Thoracic & Cardiovascular Surgery*, 109(3), pp.408–409.

McCrossan, Z.A., Billeter, R. & White, E., 2004. Transmural changes in size, contractile and electrical properties of SHR left ventricular myocytes during compensated hypertrophy. *Cardiovascular research*, 63(2), pp.283–92.

McDougall, S.J. et al., 2000. Restraint stress : differential cardiovascular responses in Wistar-Kyoto and spontaneously hypertensive rats. *Hypertension (Dallas, Tex. : 1979)*, 35(1 Pt 1), pp.126–9.

McIntosh, M., 2000. Heterogeneous changes in action potential and intracellular Ca2+ in left ventricular myocyte sub-types from rabbits with heart failure. *Cardiovascular Research*, 45(2), pp.397–409.

McIntosh, M.A. et al., 1998. Action potential prolongation and potassium currents in left-ventricular myocytes isolated from hypertrophied rabbit hearts. *Journal of molecular and cellular cardiology*, 30(1), pp.43–53.

McMullen, J.R. & Jennings, G.L., 2007. Differences between pathological and physiological cardiac hypertrophy: novel therapeutic strategies to treat heart failure. *Clinical and experimental pharmacology & physiology*, 34(4), pp.255–62.

Medina-Ravell, V.A. et al., 2003. Effect of epicardial or biventricular pacing to prolong QT interval and increase transmural dispersion of repolarization: does resynchronization therapy pose a risk for patients predisposed to long QT or torsade de pointes. *Circulation*, 107(5), pp.740–6.

Meiry, G. et al., 2001. Evolution of action potential propagation and repolarization in cultured neonatal rat ventricular myocytes. *Journal of cardiovascular electrophysiology*, 12(11), pp.1269–1277.

Mendez, C., Mueller, W.J. & Urguiaga, X., 1970. Propagation of impulses across the Prukinje fiber-muscle junctions in the dog heart. *Circulation research*, 26(2), pp.135–50.

Menon, S.G. et al., 1998. Relative importance of cytotoxic T lymphocytes and nitric oxide-dependent cytotoxicity in contractile dysfunction of rejecting murine cardiac allografts. *Transplantation*, 66(4), pp.413–419.

Meregalli, P.G., Wilde, A.A.M. & Tan, H.L., 2005. Pathophysiological mechanisms of Brugada syndrome: depolarization disorder, repolarization disorder, or more? *Cardiovascular research*, 67(3), pp.367–78.

Meyer, T. et al., 2010. Cardiac slices as a predictive tool for arrhythmogenic potential of drugs and chemicals. *Expert opinion on drug metabolism & toxicology*, 6(12), pp.1461–75.

Mihl, C., Dassen, W.R.M. & Kuipers, H., 2008. Cardiac remodelling: concentric versus eccentric hypertrophy in strength and endurance athletes. *Netherlands heart journal : monthly journal of the Netherlands Society of Cardiology and the Netherlands Heart Foundation*, 16(4), pp.129–33.

Milani-Nejad, N. & Janssen, P.M.L., 2014. Small and large animal models in cardiac contraction research: advantages and disadvantages. *Pharmacology & therapeutics*, 141(3), pp.235–49.

Mines, G.R., 1914. On circulating excitations in heart muscles and their possible relation to tachycardia and fibrillation. *Transactions of the Royal Society of Canada*, pp.43–52.

Miragoli, M., Gaudesius, G. & Rohr, S., 2006. Electrotonic modulation of cardiac impulse conduction by myofibroblasts. *Circulation research*, 98(6), pp.801–10.

Mirsky, I. et al., 1983. The contractile state as the major determinant in the evolution of left ventricular dysfunction in the spontaneously hypertensive rat. *Circulation research*, 53(6), pp.767–78.

Mitchell, M.R. et al., 1984. Strontium, nifedipine and 4-aminopyridine modify the time course of the action potential in cells from rat ventricular muscle. *British journal of pharmacology*, 81(3), pp.551–6.

Mitsuyama, H. et al., 2014. Ca2+/calmodulin-dependent protein kinase II increases the susceptibility to the arrhythmogenic action potential alternans in spontaneously hypertensive rats. *American journal of physiology. Heart and circulatory physiology*, 307(2), pp.H199–206.

Molina, E.J. et al., 2009. Novel experimental model of pressure overload hypertrophy in rats. *The Journal of surgical research*, 153(2), pp.287–94.

Del Monte, F. et al., 2002. Novel technique of aortic banding followed by gene transfer during hypertrophy and heart failure. *Physiological Genomics*, 9(1), pp.49–56.

Morita, H., Wu, J. & Zipes, D.P., 2008. The QT syndromes: long and short. *The Lancet*, 372(9640), pp.750–763.

Morita, N. et al., 2014. Cardiac fibrosis as a determinant of ventricular tachyarrhythmias. *Journal of arrhythmia*, 30(6), pp.389–394.

Müller, J. et al., 1997. Weaning from mechanical cardiac support in patients with idiopathic dilated cardiomyopathy. *Circulation*, 96(2), pp.542–9.

Muranaka, H. et al., 2010. Prolonged mechanical unloading preserves myocardial contractility but impairs relaxation in rat heart of dilated cardiomyopathy accompanied by myocardial stiffness and apoptosis. *The Journal of thoracic and cardiovascular surgery*, 140(4), pp.916–22.

Mustroph, J., Maier, L.S. & Wagner, S., 2014. CaMKII regulation of cardiac K channels. *Frontiers in pharmacology*, 5, p.20.

Nadruz, W., 2015. Myocardial remodelling in hypertension. *Journal of human hypertension*, 29(1), pp.1–6.

Nakatani, S. et al., 1996a. Left ventricular echocardiographic and histologic changes: Impact of chronic unloading by an implantable ventricular assist device. *Journal of the American College of Cardiology*, 27(4), pp.894–901.

Namadurai, S. et al., 2015. A new look at sodium channel β subunits. *Open biology*, 5(1), p.140192.

Nanthakumar, K. et al., 2007. Optical mapping of Langendorff-perfused human hearts: establishing a model for the study of ventricular fibrillation in humans. *American journal of physiology. Heart and circulatory physiology*, 293(1), pp.H875–80.

Navaratnarajah, M. et al., 2013. Influence of ivabradine on reverse remodelling during mechanical unloading. *Cardiovascular Research*, 97(2), pp.230–239.

Nerbonne, J.M., 2000. Molecular basis of functional voltage-gated K+ channel diversity in the mammalian myocardium. *The Journal of physiology*, 525 Pt 2, pp.285–98.

Nerbonne, J.M., 2004. Studying cardiac arrhythmias in the mouse--a reasonable model for probing mechanisms? *Trends in cardiovascular medicine*, 14(3), pp.83–93.

Nerbonne, J.M. & Kass, R.S., 2005. Molecular physiology of cardiac repolarization. *Physiological reviews*, 85(4), pp.1205–53.

Ng, F.S. et al., 2014. Adverse remodelling of the electrophysiological response to ischemia-reperfusion in human heart failure is associated with remodelling of metabolic gene expression. *Circulation. Arrhythmia and electrophysiology*, 7(5), pp.875–82.

Niwa, N. & Nerbonne, J.M., 2010. Molecular determinants of cardiac transient outward potassium current (I(to)) expression and regulation. *Journal of molecular and cellular cardiology*, 48(1), pp.12–25.

Novo, S. et al., 1991. Cardiovascular structural changes in hypertension: possible regression during long-term antihypertensive treatment. *European heart journal*, 12 Suppl G, pp.47–52.

Nuss, H.B. et al., 1999. Cellular basis of ventricular arrhythmias and abnormal automaticity in heart failure. *The American journal of physiology*, 277(1 Pt 2), pp.H80–91.

O'Rourke, B. et al., 1999. Mechanisms of altered excitation-contraction coupling in canine tachycardia-induced heart failure, I: experimental studies. *Circulation research*, 84(5), pp.562–70.

Ogletree, M.L. et al., 2010. Duration of left ventricular assist device support: Effects on abnormal calcium cycling and functional recovery in the failing human heart. *The Journal of heart and lung transplantation : the official publication of the International Society for Heart Transplantation*, 29(5), pp.554–61.

Oka, T. et al., 2014. Angiogenesis and cardiac hypertrophy: Maintenance of cardiac function and causative roles in heart failure. *Circulation Research*, 114(3), pp.565–571.

Okamoto, K. & Aoki, K., 1963. Development of a strain of spontaneously hypertensive rats. *Japanese circulation journal*, 27, pp.282–93.

Olivetti, G. et al., 2000. Recent advances in cardiac hypertrophy. *Cardiovascular Research*, 45(1), pp.68–75.

Ono, K. & Lindsey, E.S., 1969. Improved technique of heart transplantation in rats. *The Journal of thoracic and cardiovascular surgery*, 57(2), pp.225–9.

Ono, K., Lindsey, E.S. & Creech, O., 1969. Transplanted rat heart: local graft irradiation. *Transplantation*, 7(3), pp.176–82.

Oriyanhan, W. et al., 2007. Determination of optimal duration of mechanical unloading for failing hearts to achieve bridge to recovery in a rat heterotopic heart transplantation model. *The Journal of heart and lung transplantation : the official publication of the International Society for Heart Transplantation*, 26(1), pp.16–23.

Parikh, A. et al., 2013. Relaxin suppresses atrial fibrillation by reversing fibrosis and myocyte hypertrophy and increasing conduction velocity and sodium current in spontaneously hypertensive rat hearts. *Circulation Research*, 113(3), pp.313–321.

Patel, S.P. et al., 2004. Regulation of Kv4.3 voltage-dependent gating kinetics by KChIP2 isoforms. *The Journal of physiology*, 557(Pt 1), pp.19–41.

Patel, S.P., Campbell, D.L. & Strauss, H.C., 2002. Elucidating KChIP effects on Kv4.3 inactivation and recovery kinetics with a minimal KChIP2 isoform. *The Journal of*

*physiology*, 545(Pt 1), pp.5–11.

Patten, R.D. & Hall-Porter, M.R., 2009. Small animal models of heart failure: development of novel therapies, past and present. *Circulation. Heart failure*, 2(2), pp.138–44.

Payet, M., 1981. Frequency dependence of the ionic currents determining the action potential repolarization in rat ventricular muscle. *Journal of Molecular and Cellular Cardiology*, 13(2), pp.207–215.

Perrino, C. et al., 2006. Intermittent pressure overload triggers hypertrophy-independent cardiac dysfunction and vascular rarefaction. *The Journal of clinical investigation*, 116(6), pp.1547–60.

Piacentino, V. et al., 2003. Cellular basis of abnormal calcium transients of failing human ventricular myocytes. *Circulation research*, 92(6), pp.651–8.

Pillekamp, F. et al., 2005. Establishment and characterization of a mouse embryonic heart slice preparation. *Cellular physiology and biochemistry : international journal of experimental cellular physiology, biochemistry, and pharmacology*, 16(1-3), pp.127–32.

Pincus, M.H., 1933. Effect of Pitressin and Pitocin on Oxygen Consumption of Excised Tissue. *Experimental Biology and Medicine*, 30(8), pp.1171–1174.

Pinto, Y.M., Paul, M. & Ganten, D., 1998. Lessons from rat models of hypertension: from Goldblatt to genetic engineering. *Cardiovascular research*, 39(1), pp.77–88.

Pitt, G.S., Dun, W. & Boyden, P.A., 2006. Remodeled cardiac calcium channels. *Journal of molecular and cellular cardiology*, 41(3), pp.373–88.

Poelzing, S. et al., 2004. Heterogeneous connexin43 expression produces electrophysiological heterogeneities across ventricular wall. *American journal of physiology. Heart and circulatory physiology*, 286(5), pp.H2001–H2009.

Poelzing, S. & Rosenbaum, D.S., 2004. Altered connexin43 expression produces arrhythmia substrate in heart failure. *American journal of physiology. Heart and circulatory physiology*, 287(4), pp.H1762–H1770.

Pogwizd, S.M. et al., 2001. Arrhythmogenesis and contractile dysfunction in heart failure: Roles of sodium-calcium exchange, inward rectifier potassium current, and residual beta-adrenergic responsiveness. *Circulation research*, 88(11), pp.1159–67.

Potreau, D., Gomez, J.P. & Fares, N., 1995. Depressed transient outward current in single hypertrophied cardiomyocytes isolated from the right ventricle of ferret heart. *Cardiovascular Research*, 30(3), pp.440–448.

Pruijsten, R. V et al., 2008. Left ventricular assist device: a functional comparison with heart transplantation. *Netherlands heart journal : monthly journal of the Netherlands Society of Cardiology and the Netherlands Heart Foundation*, 16(2), pp.41–6.

Pye, M.P. & Cobbe, S.M., 1992. Mechanisms of ventricular arrhythmias in cardiac failure and hypertrophy. *Cardiovascular Research*, 26(8), pp.740–750.

Radosinska, J. et al., 2011. Myocardial NOS activity and connexin-43 expression in untreated and omega-3 fatty acids-treated spontaneously hypertensive and hereditary hypertriglyceridemic rats. *Molecular and cellular biochemistry*, 347(1-2), pp.163–73.

Rao, V.K. & Lisitza, M., 1985. Accessory heart transplantation to groin in the rat. A new model for retransplantation experiments. *Transplantation*, 40(5), pp.567–9.

Ravens, U. & Wettwer, E., 1998. Electrophysiological aspects of changes in heart rate. *Basic research in cardiology*, 93 Suppl 1, pp.60–5.

Razeghi, P. et al., 2002. Reverse remodelling of the failing human heart with mechanical unloading. Emerging concepts and unanswered questions. *Cardiology*, 98(4), pp.167–74.

Refaat, M. et al., 2008. Ventricular arrhythmias after left ventricular assist device implantation. *Pacing and clinical electrophysiology : PACE*, 31(10), pp.1246–52.

Remme, C.A. & Bezzina, C.R., 2010. Sodium channel (dys)function and cardiac arrhythmias. *Cardiovascular therapeutics*, 28(5), pp.287–94.

Rials, S.J. et al., 1995. Effect of left ventricular hypertrophy and its regression on ventricular electrophysiology and vulnerability to inducible arrhythmia in the feline heart. *Circulation*, 91(2), pp.426–30.

Rivello, H.G. et al., 2001. Cardiac myocyte nuclear size and ploidy status decrease after mechanical support. *Cardiovascular pathology : the official journal of the Society for Cardiovascular Pathology*, 10(2), pp.53–7.

Rockman, H.A. et al., 1991. Segregation of atrial-specific and inducible expression of an atrial natriuretic factor transgene in an in vivo murine model of cardiac hypertrophy. *Proceedings of the National Academy of Sciences of the United States of America*, 88(18), pp.8277–81.

Rodríguez-Sinovas, A., 1997. Lack of evidence of M-cells in porcine left ventricular myocardium. *Cardiovascular Research*, 33(2), pp.307–313.

Roman-Campos, D. et al., 2012. Chronic exercise partially restores the transmural heterogeneity of action potential duration in left ventricular myocytes of spontaneous hypertensive rats. *Clinical and experimental pharmacology & physiology*, 39(2), pp.155–7.

Rose, J. et al., 2005. Molecular correlates of altered expression of potassium currents in failing rabbit myocardium. *American journal of physiology. Heart and circulatory physiology*, 288(5), pp.H2077–87.

Rubart, M. & Zipes, D.P., 2005. Mechanisms of sudden cardiac death. *The Journal of Cllinical Investigation*, 115(9), pp.2305–2315.

Ryder, K.O., Bryant, S.M. & Hart, G., 1993. Membrane current changes in left ventricular myocytes isolated from guinea pigs after abdominal aortic coarctation. *Cardiovascular Research*, 27(7), pp.1278–1287.

Sáez, J.C. et al., 1997. Phosphorylation of connexin43 and the regulation of neonatal rat cardiac myocyte gap junctions. *Journal of molecular and cellular cardiology*, 29(8), pp.2131–45.

Sanguinetti, M.C. & Jurkiewicz, N.K., 1990. Two components of cardiac delayed rectifier K+ current. Differential sensitivity to block by class III antiarrhythmic agents. *The Journal of general physiology*, 96(1), pp.195–215.

Sano, T., Takayama, N. & Shimamoto, T., 1959. Directional difference of conduction velocity in the cardiac ventricular syncytium studied by microelectrodes. *Circulation research*, 7(2), pp.262–7.

Schaefer, A. et al., 2016. A New Animal Model for Investigation of Mechanical Unloading in Hypertrophic and Failing Hearts: Combination of Transverse Aortic Constriction and Heterotopic Heart Transplantation. *PloS one*, 11(2), p.e0148259.

Scheinin, S.A. et al., 1992. The effect of prolonged left ventricular support on myocardial histopathology in patients with end-stage cardiomyopathy. *ASAIO journal (American Society for Artificial Internal Organs : 1992)*, 38(3), pp.M271–4.

Schmitt, N., Grunnet, M. & Olesen, S.-P., 2014. Cardiac Potassium Channel Subtypes: New Roles in Repolarization and Arrhythmia. *Physiological Reviews*, 94(2), pp.609–653.

Schouten, V.J., 1986. The negative correlation between action potential duration and force of contraction during restitution in rat myocardium. *Journal of molecular and cellular cardiology*, 18(10), pp.1033–45.

Schouten, V.J. & ter Keurs, H.E., 1991. Role of Ica and Na+/Ca2+ exchange in the force-frequency relationship of rat heart muscle. *Journal of molecular and cellular cardiology*, 23(9), pp.1039–50.

Severs, N.J., 1990. The cardiac gap junction and intercalated disc. *International Journal of Cardiology*, 26(2), pp.137–173.

Shah, A.M. & Mann, D.L., 2011. In search of new therapeutic targets and strategies for heart failure: recent advances in basic science. *Lancet (London, England)*, 378(9792), pp.704–12.

Shen, W.K., Terzic, A. & Stanton, M.S., 1997. Triggered activity and arrhythmogenesis: A clinical update. *ACC Current Journal Review*, 6(4), pp.16–19.

Shigematsu, S. et al., 1997. Rate-dependent prolongation of action potential duration in isolated rat ventricular myocytes. *Basic Research in Cardiology*, 92(3), pp.123–128.

Shimoni, Y. et al., 1994. Short-term diabetes alters K+ currents in rat ventricular myocytes. *Circulation Research*, 74(4), pp.620–628.

Shipsey, S.J., Bryant, S.M. & Hart, G., 1997. Effects of hypertrophy on regional action potential characteristics in the rat left ventricle: a cellular basis for T-wave inversion? *Circulation*, 96(6), pp.2061–8.

Shorofsky, S.R. et al., 1999. Cellular mechanisms of altered contractility in the hypertrophied heart: big hearts, big sparks. *Circulation research*, 84(4), pp.424–34.

Sicouri, S. et al., 2010. Transseptal dispersion of repolarization and its role in the development of Torsade de Pointes arrhythmias. *Journal of cardiovascular electrophysiology*, 21(4), pp.441–7.

Sicouri, S. & Antzelevitch, C., 1991. A subpopulation of cells with unique electrophysiological properties in the deep subepicardium of the canine ventricle. The M cell. *Circulation Research*, 68(6), pp.1729–1741.

Sicouri, S., Quist, M. & Antzelevitch, C., 1996. Evidence for the presence of M cells in the guinea pig ventricle. *Journal of cardiovascular electrophysiology*, 7(6), pp.503–11.

Sipido, K., 1998. Frequency dependence of Ca2+ release from the sarcoplasmic reticulum in human ventricular myocytes from end-stage heart failure. *Cardiovascular Research*, 37(2), pp.478–488.

Sipido, K.R. et al., 2007. Na/Ca exchange and cardiac ventricular arrhythmias. *Annals of the New York Academy of Sciences*, 1099, pp.339–48.

Soppa, G.K.R., Barton, P.J.R., et al., 2008. Left ventricular assist device-induced molecular changes in the failing myocardium. *Current opinion in cardiology*, 23(3), pp.206–18.

Soppa, G.K.R., Lee, J., Stagg, M.A., Siedlecka, U., et al., 2008. Prolonged mechanical unloading reduces myofilament sensitivity to calcium and sarcoplasmic reticulum calcium uptake leading to contractile dysfunction. *The Journal of heart and lung transplantation : the official publication of the International Society for Heart Transplantation*, 27(8), pp.882–9.

Soppa, G.K.R., Lee, J., Stagg, M.A., Felkin, L.E., et al., 2008. Role and possible mechanisms of clenbuterol in enhancing reverse remodelling during mechanical unloading in murine heart failure. *Cardiovascular Research*, 77(4), pp.695–706.

Soucy, K.G. et al., 2015. Feasibility study of particulate extracellular matrix (P-ECM) and left ventricular assist device (HVAD) therapy in chronic ischemic heart failure bovine model. *ASAIO journal (American Society for Artificial Internal Organs : 1992)*, 61(2), pp.161–9.

Spach, M.S. et al., 1982. The functional role of structural complexities in the propagation of depolarization in the atrium of the dog. Cardiac conduction disturbances due to discontinuities of effective axial resistivity. *Circulation research*, 50(2), pp.175–91.

Spinale, F.G. et al., 2000. A matrix metalloproteinase induction/activation system exists in the human left ventricular myocardium and is upregulated in heart failure. *Circulation*, 102(16), pp.1944–9.

St Lezin, E. et al., 1992. Hypertensive strains and normotensive “control” strains. How closely are they related? *Hypertension*, 19(5), pp.419–24.

Stankovicova, T., 2000. M cells and transmural heterogeneity of action potential configuration in myocytes from the left ventricular wall of the pig heart. *Cardiovascular Research*, 45(4), pp.952–960.

Suckau, L. et al., 2009. Long-term cardiac-targeted RNA interference for the treatment of heart failure restores cardiac function and reduces pathological hypertrophy. *Circulation*, 119(9), pp.1241–52.

Sun, X. & Wang, H.-S., 2005. Role of the transient outward current (Ito) in shaping canine ventricular action potential--a dynamic clamp study. *The Journal of physiology*, 564(Pt 2), pp.411–9.

Surawicz, B., 1997. Ventricular Fibrillation and Dispersion of Repolarization. *Journal of Cardiovascular Electrophysiology*, 8(9), pp.1009–1012.

Susic, D. et al., 1998. Coronary hemodynamics in aging spontaneously hypertensive and normotensive Wistar-Kyoto rats. *Journal of hypertension*, 16(2), pp.231–7.

Taggart, P. et al., 1995. Repolarization gradients derived by subtraction of monophasic action potential recordings in the human heart. Studies incorporating altered mechanical loading and ischemia. *Journal of electrocardiology*, 28, pp.156–61.

Tamargo, J. et al., 2004. Pharmacology of cardiac potassium channels. *Cardiovascular research*, 62(1), pp.9–33.

Tang-Quan, K.R. et al., 2010. Non-volume-loaded heart provides a more relevant heterotopic transplantation model. *Transplant immunology*, 23(1-2), pp.65–70.

Terracciano, C. et al., 2009. Chronic mechanical unloading of rat hearts disrupts local calcium-induced calcium release in isolated cardiomyocytes. *European heart journal*, 30, p.176.

Terracciano, C.M. et al., 2011. Mechano-electric coupling in patients treated with ventricular assist devices: insights from individual cases and clinical trials. In P. Kohl, M. Franz, & F. Sachs, eds. *Cardiac Mechano-Electric Coupling and Arrhythmias*. OUP Oxford, p. 512.

Terracciano, C.M., Miller, L.W. & Yacoub, M.H., 2010. Contemporary use of ventricular assist devices. *Annual review of medicine*, 61, pp.255–70.

Terracciano, C.M.N. et al., 2003. Changes in sarcolemmal Ca entry and sarcoplasmic reticulum Ca content in ventricular myocytes from patients with end-stage heart failure following myocardial recovery after combined pharmacological and ventricular assist device therapy. *European heart journal*, 24(14), pp.1329–39.

Terracciano, C.M.N. et al., 2004. Clinical recovery from end-stage heart failure using left-ventricular assist device and pharmacological therapy correlates with increased sarcoplasmic reticulum calcium content but not with regression of cellular hypertrophy. *Circulation*, 109(19), pp.2263–5.

Terracciano, C.M.N. et al., 2007. The role of the cardiac Na+/Ca2+ exchanger in reverse remodelling: relevance for LVAD-recovery. *Annals of the New York Academy of Sciences*, 1099, pp.349–60.

Thom, T. et al., 2006. Heart disease and stroke statistics--2006 update: a report from the American Heart Association Statistics Committee and Stroke Statistics Subcommittee. *Circulation*, 113(6), pp.e85–151.

Thuringer, D. et al., 1996. Ionic basis of the action potential prolongation in ventricular myocytes from Syrian hamsters with dilated cardiomyopathy. *Cardiovascular Research*, 31(5), pp.747–757.

Tinker, A. & Harmer, S.C., 2010. K+ channels in the heart: new insights and therapeutic implications. *Expert review of clinical pharmacology*, 3(3), pp.305–19.

Tomaselli, G., 1999. Electrophysiological remodelling in hypertrophy and heart failure. *Cardiovascular Research*, 42(2), pp.270–283.

Toyama, J. et al., 1997. Vesnarinone Prolongs Action Potential Duration Without Reverse Frequency Dependence in Rabbit Ventricular Muscle by Blocking the Delayed Rectifier K+ Current. *Circulation*, 96(10), pp.3696–3703.

Toyoshima, H., Park, Y.D., Ishikawa, Y., Nagata, S., Hirata, Y., Sakakibara, H., Shimomura, K., & Nakayama, R., 1982. Effect of ventricular hypertrophy on conduction velocity of activation front in the ventricular myocardium. *The american Journal of cardiology*, 49(8), pp.1938–1945.

Tse, G., 2016. Mechanisms of cardiac arrhythmias. *Journal of Arrhythmia*, 32(2), pp.75–81.

Tsutsui, H. et al., 1999. Chronic colchicine administration attenuates cardiac hypertrophy in spontaneously hypertensive rats. *Journal of molecular and cellular cardiology*, 31(6), pp.1203–13.

Ueda, K. et al., 2008. Syntrophin mutation associated with long QT syndrome through activation of the nNOS-SCN5A macromolecular complex. *Proceedings of the National Academy of Sciences*, 105(27), pp.9355–9360.

Ueda, N., Zipes, D.P. & Wu, J., 2004. Functional and transmural modulation of M cell behavior in canine ventricular wall. *American journal of physiology. Heart and circulatory physiology*, 287(6), pp.H2569–75.

Undrovinas, A.I., Maltsev, V.A. & Sabbah, H.N., 1999. Repolarization abnormalities in cardiomyocytes of dogs with chronic heart failure: role of sustained inward current. *Cellular and molecular life sciences : CMLS*, 55(3), pp.494–505.

Valderrábano, M., 2007. Influence of anisotropic conduction properties in the propagation of the cardiac action potential. *Progress in biophysics and molecular biology*, 94(1-2), pp.144–68.

Valdivia, C.R. et al., 2005. Increased late sodium current in myocytes from a canine heart failure model and from failing human heart. *Journal of molecular and cellular cardiology*, 38(3), pp.475–83.

Varro, A. et al., 2000. The role of the delayed rectifier component IKs in dog ventricular muscle and Purkinje fibre repolarization. *The Journal of physiology*, 523 Pt 1, pp.67–81.

Verkerk, A.O. et al., 2007. Pacemaker current (If) in the human sinoatrial node. *European Heart Journal*, 28(20), pp.2472–2478.

Wahr, P.A., Michele, D.E. & Metzger, J.M., 2000. Effects of aging on single cardiac myocyte function in Fischer 344 x Brown Norway rats. *American journal of physiology. Heart and circulatory physiology*, 279(2), pp.H559–65.

Walker, E.M. et al., 2006. Age-associated changes in hearts of male Fischer 344/Brown Norway F1 rats. *Annals of clinical and laboratory science*, 36(4), pp.427–38.

Wang, H.S., Dixon, J.E. & McKinnon, D., 1997. Unexpected and differential effects of Cl- channel blockers on the Kv4.3 and Kv4.2 K+ channels. Implications for the study of the I(to2) current. *Circulation research*, 81(5), pp.711–8.

Wang, J. et al., 2009. Chronic partial unloading restores beta-adrenergic responsiveness and reverses receptor downregulation in failing rat hearts. *The Journal of thoracic and cardiovascular surgery*, 137(2), pp.465–70.

Wang, K., Lee, P., Mirams, G.R., et al., 2015. Cardiac tissue slices: preparation, handling, and successful optical mapping. *American Journal of Physiology - Heart and Circulatory Physiology*, 308(9), pp.H1112–H1125.

Wang, K. et al., 2014. Living cardiac tissue slices: An organotypic pseudo two-dimensional model for cardiac biophysics research. *Progress in Biophysics and Molecular Biology*, 115(2-3), pp.314–327.

Wang, Y. et al., 2008. Ca2+/calmodulin-dependent protein kinase II-dependent remodelling of Ca2+ current in pressure overload heart failure. *The Journal of biological chemistry*, 283(37), pp.25524–32.

Wang, Y. & Hill, J.A., 2010. Electrophysiological remodelling in heart failure. *Journal of Molecular and Cellular Cardiology*, 48(4), pp.619–632.

Wang, Y.G. et al., 2000. Fast pacing facilitates discontinuous action potential propagation between rabbit atrial cells. *American journal of physiology. Heart and circulatory physiology*, 279(5), pp.H2095–103.

Ward, M.L., Crossman, D.J. & Cannell, M.B., 2011. Mechanisms of reduced contractility in an animal model of hypertensive heart failure. *Clinical and Experimental Pharmacology and Physiology*, 38(10), pp.711–716.

Webb, J.L., Saunders, P.R. & Thienes, C.H., 1949. The metabolism of the heart in relation to drug action; the endogenous aerobic metabolism of rat heart slices. *Archives of biochemistry*, 22(3), pp.444–50.

Wei, S. et al., 2010. T-tubule remodelling during transition from hypertrophy to heart failure. *Circulation Research*, 107(4), pp.520–531.

Wei, A.D. et al., 2005. International Union of Pharmacology. LII. Nomenclature and Molecular Relationships of Calcium-Activated Potassium Channels. *Pharmacological Reviews*, 57(4), pp.463–472.

Weissenburger, J., Nesterenko, V. V & Antzelevitch, C., 2000. Transmural heterogeneity of ventricular repolarization under baseline and long QT conditions in the canine heart in vivo: torsades de pointes develops with halothane but not pentobarbital anesthesia. *Journal of cardiovascular electrophysiology*, 11(3), pp.290–304.

Welsh, D.C. et al., 2001. Preserved contractile function despite atrophic remodelling in unloaded rat hearts. *American journal of physiology. Heart and circulatory physiology*, 281(3), pp.H1131–6.

Wettschureck, N. et al., 2001. Absence of pressure overload induced myocardial hypertrophy after conditional inactivation of Galphaq/Galpha11 in cardiomyocytes. *Nature medicine*, 7(11), pp.1236–40.

Wettwer, E. et al., 1993. Transient outward current in human and rat ventricular myocytes. *Cardiovascular Research*, 27(9), pp.1662–1669.

Wichers, L.B. et al., 2004. Effects of instilled combustion-derived particles in spontaneously hypertensive rats. Part I: Cardiovascular responses. *Inhalation toxicology*, 16(6-7), pp.391–405.

Wickenden, A., 1998. The role of action potential prolongation and altered intracellular calcium handling in the pathogenesis of heart failure. *Cardiovascular Research*, 37(2), pp.312–323.

Wiegerinck, R.F. et al., 2006. Larger cell size in rabbits with heart failure increases myocardial conduction velocity and QRS duration. *Circulation*, 113(6), pp.806–13.

Wilson, E.M. & Spinale, F.G., 2001. Myocardial remodelling and matrix metalloproteinases in heart failure: turmoil within the interstitium. *Annals of medicine*, 33(9), pp.623–34.

Wohlschlaeger, J. et al., 2005. Reverse remodelling following insertion of left ventricular assist devices (LVAD): a review of the morphological and molecular changes. *Cardiovascular research*, 68(3), pp.376–86.

Xiao, R.-P. et al., 2006. Subtype-specific α1- and β-adrenoceptor signaling in the heart. *Trends in Pharmacological Sciences*, 27(6), pp.330–337.

Xie, Y. et al., 2009. Effects of fibroblast-myocyte coupling on cardiac conduction and vulnerability to reentry: A computational study. *Heart rhythm : the official journal of the Heart Rhythm Society*, 6(11), pp.1641–9.

Xu, H., Guo, W. & Nerbonne, J.M., 1999. Four kinetically distinct depolarization-activated K+ currents in adult mouse ventricular myocytes. *The Journal of general physiology*, 113(5), pp.661–678.

Yacoub, M.. et al., 2001. A novel combination therapy to reverse end-stage heart failure. *Transplantation Proceedings*, 33(5), pp.2762–2764.

Yacoub, M.H. & Miller, L.W., 2008. Long-term left-ventricular-assist-device therapy is here to stay. *Nature clinical practice. Cardiovascular medicine*, 5(2), pp.60–1.

Yan, G.X. & Antzelevitch, C., 1996. Cellular basis for the electrocardiographic J wave. *Circulation*, 93(2), pp.372–9.

Yan, G.X. & Antzelevitch, C., 1998. Cellular basis for the normal T wave and the electrocardiographic manifestations of the long-QT syndrome. *Circulation*, 98(18), pp.1928–1936.

Yasuhara, S. et al., 1996. Myocardial VO2 of mechanically unloaded contraction of rat ventricular slices measured by a new approach. *The American journal of physiology*, 270(3 Pt 2), pp.H1063–70.

Yu, F.H. & Catterall, W.A., 2003. Overview of the voltage-gated sodium channel family. *Genome biology*, 4(3), p.207.

Yue, L. et al., 1997. Ionic remodelling underlying action potential changes in a canine model of atrial fibrillation. *Circulation research*, 81(4), pp.512–25.

Zaman, J., Patel, P. & Peters, N., 2014. Arrhythmia Inducibility in a Novel Normotensive Rodent Model of Arrhythmia is not Related to Connexin 43 Quantity and Phosphorylation States - Determining the Contribution of Hypertension and ageing on the Myocardial Substrate. *Heart*, 100(Suppl 3), pp.A113–A114.

Zaniboni, M. et al., 2000. Beat-to-beat repolarization variability in ventricular myocytes and its suppression by electrical coupling. *American journal of physiology. Heart and circulatory physiology*, 278(3), pp.H677–87.

Zaugg, C.E. et al., 1997. Intracellular Ca2+ handling and vulnerability to ventricular fibrillation in spontaneously hypertensive rats. *Hypertension*, 30(3 Pt 1), pp.461–7.

Zhang, W. et al., 2014. Aliskiren-attenuated myocardium apoptosis via regulation of autophagy and connexin-43 in aged spontaneously hypertensive rats. *Journal of cellular and molecular medicine*, 18(7), pp.1247–56.

Zhao, L. et al., 2008. Losartan reduced connexin43 expression in left ventricular myocardium of spontaneously hypertensive rats. *Journal of Zhejiang University. Science. B*, 9(6), pp.448–54.

Zygmunt, A.C. et al., 2001. Larger late sodium conductance in M cells contributes to electrical heterogeneity in canine ventricle. *American journal of physiology. Heart and circulatory physiology*, 281(2), pp.H689–97.

Zygmunt, A.C., Goodrow, R.J. & Antzelevitch, C., 2000. I(NaCa) contributes to electrical heterogeneity within the canine ventricle. *American journal of physiology. Heart and circulatory physiology*, 278(5), pp.H1671–8.